UNIVERSITAT DE BARCELONA

Study of disseminated high-risk neuroblastoma in the bone marrow niche; from microenvironmental modelling to therapeutic targeting

Laura Garcia Gerique

Universitat de Barcelona

Facultat de Biologia

“Study of disseminated high-risk neuroblastoma in the bone marrow niche; From microenvironmental modelling to therapeutic targeting”

Memòria presentada per

Laura Garcia Gerique

per optar al títol de

Doctora per a la Universitat de Barcelona

Programa de Biomedicina

Biologia molecular i cel·lular del càncer

Tesi dirigida per la Dra Cinzia Lavarino

realitzada al Institut de Recerca Sant Joan de Déu

departament de Càncer Pediàtric

Tesis tutoritzada per la Dra Gemma Marfany Nadal

Departament de Genètica, Microbiologia i Estadística

UNIVERSITAT DE BARCELONA

-2020-

Universitat de Barcelona
Facultat de Biologia

“Study of disseminated high-risk neuroblastoma in the bone marrow niche; From microenvironmental modelling to therapeutic targeting”

Memòria presentada per
Laura Garcia Gerique
per optar al títol de
Doctora per a la Universitat de Barcelona
Programa de Biomedicina
Biologia molecular i cel·lular del càncer

Tesi dirigida per la Dra Cinzia Lavarino
realitzada al departament de Càncer Pediàtric
Institut de Recerca Sant Joan de Déu

Directora
Dra Cinzia Lavarino

Tutora
Dra Gemma Marfany

Doctoranda
Laura Garcia Gerique

Para Adrián González Lanza,
a quien no conocí, pero le debo esta tesis
...
Dra Carmen de Torres
quien me guió en comisiones y lab meetings
...
y Gemma Garcia Zapata
por todos los *Adestes Fideles* cantados

ACKNOWLEGMENTS:

Amb aquest llibre començo a enfilar l'última etapa d'un camí que vaig començar fa més de cinc anys al laboratori de Càncer de Desenvolupament de l'Hospital de Sant Joan de Deu. Com tots els camins que hom pot emprendre, ens hem trobat una mica de tot! Toca fer balanç del recorregut; un camí amb pujades costerudes i travessies pel desert, ple d'inesperats companys de viatge i també de comiats dolorosos. M'agradaria agrair a totes les persones que d'una manera o altre m'han acompanyat fins el cap del camí.

En primer lloc, agrair a les famílies de l'Adrián González i de l'Erika Prieto. Els mecenes que han aportat els diners pel meu sou però també l'*actitud positiva* i llum ✯ per seguir caminant, mai els hi estaré prou agraïda per tot el seu compromís i lluita, sou pura inspiració.

Agrair a la Dra. Cinzia Lavarino, qui em va donar l'oportunitat d'unir-me al seu equip. Sempre ha confiat en les meves capacitats, involucrant-me en projectes diversos, i a vegades arriscats, que m'han donat l'oportunitat de créixer com a una investigadora independent i a no tenir por de canviar i reinventar-me.

A totes les meves companyes de grup de Genòmica Translacional, en especial a l'Alicia Garrido, per ser sempre l'espatlla on recolzar-me.

Agrair la paciència i l'interès de la Dra. Montserrat Torrebadell i Sandra Pont del servei de Hematologia és un plaer treballar amb vosaltres.

A la resta de membres del laboratori de Càncer del Desenvolupament liderat pel Dr. Jaume Mora, qui sempre ens recorda la importància de tenir una veu pròpia.

A les Mandarines per totes les calçotades, *queimadas*, sushis, pizzes i cerveses compartides.

Agrair també, als companys del laboratori d'en Dr. Jordi Casanova de l'IRB, per fer-me sentir una més i acollir-me amb els braços oberts sense esperar res a canvi, i al Dr. Andreu Casali per seu guiatge.

Mencionar les companyes *outlayers*:

Dra. Noelia Salvador i Dra. Silvia Mateo, per proveir-me de noves perspectives i bons consells *ad libitum*.

Dra. Nagore Gené, Eliana Alves, Dra. Gaia Botteri i Estela Prada per la vostra autenticitat que ha estat abric i refugi.

Per últim acabar com he començat, agraint a les famílies, aquest cop la meva, que ha crescut significativament durant aquest anys.

Als meus pares per donar-me les eines i el suport per arribar fins aquí (i fins on calgui).

Als pares *in-law* pel assegurar-me els *descansos del guerrero*.

I per descomptat al meu company de viatge, Dr. Guillem Pascual, sense qui aquest camí no hagués estat tant divertit i enriquidor. T'estimo tronco.

ABSTRACT:

Neuroblastoma (NB) is the most common extracraneal solid tumor diagnosed in the first 5 years of childhood and accounts for approximately 15% of all pediatric cancer-related deaths. At the time of diagnosis, about half of NB patients present disseminated disease, being the bone marrow (BM) the most common site of dissemination. The persistence of infiltrated BM during treatment or relapse is predictive of patient poor outcome. The BM microenvironment has unique biologic properties that favor progression of disseminated NB tumor cells. In this environment, the receptor CXCR4 has a pivotal role for BM homeostasis and is involved in metastatic dissemination in several cancers. In NB, CXCR4 is expressed in tumor cells; however, its oncogenic role in relation with its ligand CXCL12 has shown contradictory results. Using an *in vitro* model that recapitulates low oxygen levels and chemokine signaling present in the BM environment, we explored whether CXCR4 together with MIF, a second ligand, is critical for NB survival and proliferation in the niche. We also evaluated MIF inhibition as a therapeutic option for NB.

To develop a BM-based *in vitro* model, NB cells were cultured in different conditioned media (CMs) derived from supernatants of patient-derived BM primary cells (CM-BM) and NB cell lines (CM-NB) cultured alone, or in combination (CM-BM/NB). To mimic BM oxygen levels, NB cells were cultured under hypoxia (1% O_2), as compared to cell culture normoxia (21% O_2). Expanded BM cultures used to generate CMs contained a heterogenic population with a predominant cellularity positive for mesenchymal stromal markers measured by flow cytometry. Cytokine arrays and ELISA assays of CMs revealed MIF as the highest NB released cytokine, whereas CXCL12 was not detected. The expression of MIF and CXCL12 signaling pathways was analyzed with different public NB databases. Among the analyzed genes, the high expression of CXCR4 and MIF was associated with patient poor outcome and high-risk disseminated staging. To further explore the role of CXCR4/MIF axis in high-risk disseminated NB, *in vitro* and *in vivo* functional studies were performed with or without the covalent MIF inhibitor 4-IPP and the CXCR4 antagonist AMD3100.

When exposed to BM-derived CMs and hypoxia, BM-derived NB cell lines showed increased surface expression of CXCR4 by flow cytometry. The same culture condition increased

phosphorylated levels of AKT/PI3K and ERK/MAPK measured by western blot. Cell viability assays showed that hypoxic conditions and BM-derived CMs enhanced NB cell proliferation at different time points. Similarly, *in vivo,* the co-injection of BM cells favored NB tumor progression by reducing engraftment times in contrast to NB injection alone. Using wound healing assays and Matrigel-coated Transwells, CM-BM/NB chemoattracted and enhanced migration and invasion of LAN-1 cells cultured under hypoxic conditions. These aggressive phenotypes promoted by the BM-based model were reverted by adding sub-lethal concentrations of the MIF inhibitor 4-IPP. We also explored whether MIF present in our CMs affected response to chemotherapy. After treatment with doxorubicin and etoposide at IC50 values LAN-1 cell viability increased in CM-BM/NB compared to control media. In both cases, chemo-sensitivity was restored when 4-IPP was added to CM-BM/NB. Finally, the administration of 4-IPP delayed the tumor progression and increased mice survival in a LAN-1 subcutaneous xenograft model.

In conclusion, our findings provide new understanding of the contribution of BM microenvironment to NB progression. Based on our BM-model, the relationship between the BM microenvironment and NB cells appears mediate, in part, by the autocrine CXCR4/MIF signaling axis. Furthermore, our results suggested that MIF could represent a therapeutic target for the treatment of patients with high-risk NB.

TABLE OF CONTENTS:

ABBREVIATIONS:

4-IPP	4-iodo-6-phenylpyrimidine
AC	Adrenal Cortex
ADCC	Antibody-Dependent Cell-Mediated Cytotoxicity
ADR	Adrenergic
ALK	Anaplastic Lymphoma Kinase
AM	Adrenal Medulla
AMP	Amplified
ANGPT1	Angiopoietin 1
ASCL1	Achaete-Scute Family BHLH Transcription Factor 1
ASCT	Autologous Stem Cell Transplantation
ATRX	ATRX Chromatin Remodeler
AURKA	Aurora Kinase A
B7H3	CD276 Molecule
BAD	BCL2 Associated Agonist Of Cell Death
BARD1	BRCA1 Associated RING Domain 1
BAX	BCL2 Associated X
BCL2	BCL2 Apoptosis Regulator
BDNF	Brain Derived Neurotrophic Factor
BETs	Bromodomain Containing genes
BM	Bone Marrow
BMCs	BM mononucleated cells
BMPs	Bone Morphogenetic Proteins
BRIC5	Survivin
CAF	Cancer Associated Fibroblast
CASP-3	Caspase 3
CASZ1	Castor Zinc Finger 1
CATA1	GATA Binding Protein 1
CD44	CD44 Molecule
CD74	CD74 Molecule

CgA	Chromogranin A
CHD5	Chromodomain Helicase DNA Binding Protein 5
CKIT	KIT Proto-Oncogene, Receptor Tyrosine Kinase
CM	Culture Media (CM)
CMC	Complement Mediated Cytotoxicity
CNS	Central Neuron System
CXCL1	C-X-C Motif Chemokine Ligand 1
CXCL10	C-X-C Motif Chemokine Ligand 10
CXCL12	C-X-C Motif Chemokine Ligand 12
CXCL13	C-X-C Motif Chemokine Ligand 13
CXCL16	C-X-C Motif Chemokine Ligand 16
CXCR2	C-X-C Motif Chemokine Receptor 2
CXCR3	C-X-C Motif Chemokine Receptor 3
CXCR4	C-X-C Motif Chemokine Receptor 4
CXCR5	C-X-C Motif Chemokine Receptor 5
CXCR6	C-X-C Motif Chemokine Receptor 6
CXCR7	C-X-C Motif Chemokine Receptor 7
D	Differentiated
DA	Dorsal Aorta
DAPI	4′,6-Diamidine-2′-phenylindole dihydrochloride
DC	Dendritic Cell
DEL	Deletion
DMSO	anhydrous Dimethyl Sulfoxide
DRG	Dorsal Root Ganglia
DX	Diagnostic
EGFR	Epidermal Growth Factor Receptor
ELISA	Enzyme-Linked Immunosorbent Assay
EMA	European Medicines Agency
EMT	Epithelial-to-Mesenchymal Transition
EPHRIN A/B	EPHRIN
FC	Flow Cytometry

FDA	US Food and Drug Administration
FGF	Fibroblast Growth Factor
FHG	Favorable Histology Group
FISH	Fluorescence *in situ* hybridization
FOXD3	Forkhead Box D3
GATA3	GATA Binding Protein 3
GLUT1	Solute Carrier Family 2 Member 1
GN	Ganglioneuroma
GNB-I	Gangioneuroblastoma Intermixed
GNB-N	Ganglioneuroblastoma Nodular
GPC2	Glypican 2
HIF-1A	Hypoxia Inducible Factor 1 Subunit Alpha
HIF1B	Egl-9 Family Hypoxia Inducible Factor
HIF-2A	Endothelial PAS Domain Protein 1
HRE	Hypoxia-Response Element
HSC	Hematopoietic Stem Cells
Hx	Hypoxia
IDRF	Image-Defined Risk Factors
iFBS	inactivated Fetal Bovine Serum
IL-15	Interleukin 15
IL-1ra	Interleukin 1 Receptor Antagonist
IL-2	Interleukin 2
IL-6	Interleukin 6
IL-6	Interleukin 6
IL-7	Interleukin 7
IL-8	Interleukin 8
I-MIBG	I-metaiodobenzylguanidine
IML	Intermediolateral Cell Column
INFG	Interferon Gamma
INPC	International Neuroblastoma Pathology Classification
INRGSS	International Neuroblastoma Risk Group Staging System

INSS	International Neuroblastoma Staging Systems
KIF1B	Kinesin Family Member 1B
LIN28B	Lin-28 Homolog B
LMO1	LIM Domain Only 1
LMO4	LIM Domain Only 4
mAb	Monoclonal Antibody
MCP-1	C-C Motif Chemokine Ligand 2
MDSC	Myeloid-Derived Suppressor Cells
MHC-I	Major Histocompatibility Complex, Class I, A
MHC-II	Major Histocompatibility Complex, Class II, DR Beta 1
MIF	Macrophage Migration Inhibitory Factor
mir-34A	MicroRNA 34a
MKI	Mitosis-Karyorrhexis Index
MM	Multiple Myeloma
MMP2	Matrix Metallopeptidase 2
MMP9	Matrix Metallopeptidase 9
MRD	Minimal Residual Disease
MSC	Mesenchymal Stem Cell
MUT	Mutated
MYCN	MYCN Proto-Oncogene, BHLH Transcription Factor
N	Notochord
NA	non-available
NB	Neuroblastoma
NC	Neural Crest
NCC	Neural Crest Cells
Neg	Negative
NES	Nestin
NF-KB	Nuclear Factor Kappa B Subunit 1
NGF	Nerve Growth Factor
NK	Natural killer
NM23A	NME/NM23 Nucleoside Diphosphate Kinase 1

NRG1	Neuregulin 1
NS	Non-Significant
NSCLC	Non-Small Cell Lung Cancer
NSE	Enolase 2
NT	Neural Tube
NTRK1	Neurotrophic Receptor Tyrosine Kinase 1
NTRK2	Neurotrophic Receptor Tyrosine Kinase 2
Nx	Normoxia
OCT4	POU Class 5 Homeobox 1
ODD	Oxygen-Dependent Degradation
OS	Overall Survival
P	Plasma
PAI-1	Serpin Family E Member 1
PD	Poorly Differentiated
PDX	Patient Derived Xenograft
PHD2	Prolyl Hydroxylase Domain-Containing Protein 2
PHOX2B	Paired Like Homeobox 2B
postTx	post-Treatment
PTHRP	Parathyroid Hormone 1 Receptor
PTPRC	Protein Tyrosine Phosphatase Receptor Type C
RANKL	TNF Superfamily Member 11
RT-qPCR	Real-Time Polymerase Chain Reaction
SA	Sympathoadrenal
SC	Schwann Cell
SEMAPHORINS	Semaphorin family
SG	Sympathetic Ganglia
SNAIL2	Snail Family Transcriptional Repressor 2
SNP	Single Nucleotide Polymorphisms
SNS	Sympathetic Nervous System
SOX10	SRY-Box Transcription Factor 10
SOX9	SRY-Box Transcription Factor 9

SPP1	Secreted Phosphoprotein 1
SRG	Suprarenal Sympathetic Ganglia
SYP	Synaptophysin
TAM	Tumor Associated Macrophage
TERT	Telomerase Reverse Transcriptase
TIL	Tumor Infiltrating Lymphocyte
TME	Tumor Microenvironment
Treg	Regulatory T cells
U	Undifferentiated
UHG	Unfavorable Histology Group
VCAM1	Vascular Cell Adhesion Molecule 1
VEGF	Vascular Endothelial Growth Factor A
VHL	Von Hippel-Lindau Tumor Suppressor
WNT	Wnt Family
WT	Wild-Type

INTRODUCTION:

1. Pediatric cancer:

Cancer is a group of diseases that are caused by an abnormal and uncontrollable cell division. In adults, cancer mainly originates as a result of accumulated alterations related with tissue self-renewal and environmental aggressions occurred during a life-course. Thus, adult cancer is principally an aging-related illness as its incidence increases in individuals above 70 years (*1*). Remarkably, 85% of adult cancers are carcinomas, which arise from epithelial cells that suffer a malignant transformation known as carcinogenesis (*2*). In contrast, only 9% of pediatric tumors are carcinomas while 50% arise from non-epithelial cells, mostly from hematologic and Central Neuron System (CNS) tissues (*3*). Thus, childhood cancers have their own entities such as, neuroblastoma (NB), medulloblastoma or different types of sarcomas, and these entities are virtually absent during adulthood.

Molecularly, pediatric cancers exhibit low mutation rates; instead, their oncogenic drivers are more related with genomic instability processes such as chromosomal rearrangements or epigenetic alterations (*4*). In contrast to the aging-related of adult tumors, the origin of pediatric entities occurs prenatally, during fetal development (*5*). On this account, the biology behind each childhood malignancy reflects their tissue ontogeny, resembling and behaving similar to the embryonic cell from which they arise.

Due to their low incidence and the lack of targetable mutations, childhood cancer cannot always benefit from discoveries from adult cancer research (*6*). Therefore, specific scientific advances must be attained to fight against pediatric tumors that affect still-developing individuals with a long-life expectancy (*7*). Pediatric malignancies are complex and differential diseases that require specific translational and clinical research, as well as improved knowledge of basic human development in order to better understand, treat and cure.

2. *Neuroblastoma:*

2.1. Prevalence and clinical presentation:

NB is the most common extracraneal solid tumor diagnosed during infancy and accounts for approximately 15% of all pediatric cancer-related death under 15 years (*8, 9*). NB is a highly heterogeneous disease, predominantly affecting children before the age of 5 years, being the median age at diagnosis 18 months. Worldwide, NB incidence is variable, being higher in countries with better medical surveillance, probably reflecting differences in diagnosis and registration practices among countries (*10*). In Spain, 66 NB cases are reported in infancy (< 5 years) annually, whereas only 1.7 cases between 10 to 15 years of age (*11*). NB tumors can arise anywhere along the Sympathetic Nervous System (SNS), mirroring its own origin during developmental stages in the sympathoadrenal (SA) lineage of the neural crest cells (NCC) (*12*). At diagnosis, tumors can arise as localized or disseminated disease. Primary lesions are localized in the adrenal glands (50%), abdomen (20%), mediastinum (16%) and different locations along the parasympathetic paravertebral chain (*13*) (**Figure 1**).

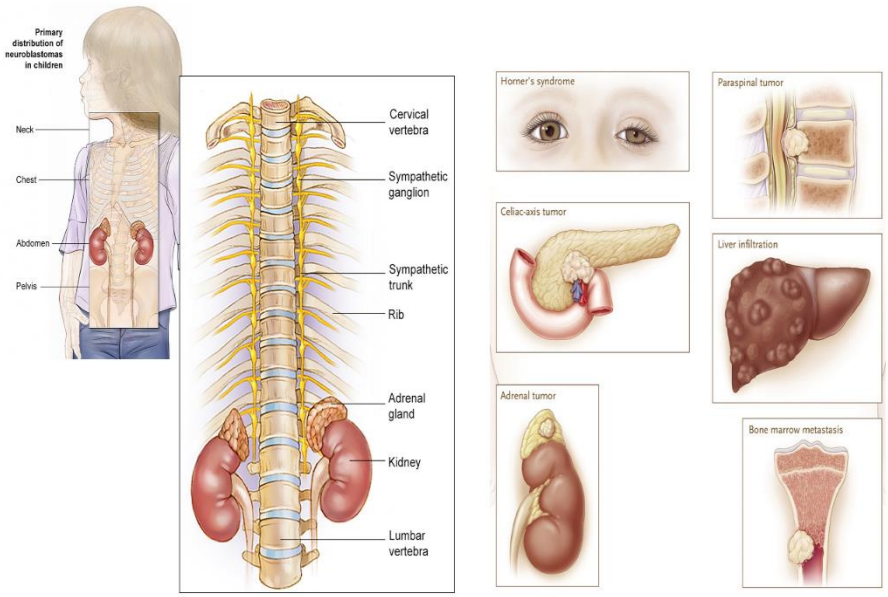

Figure 1: Clinical Presentations of NB. Tumors arise along the SNS, mainly in the adrenal medulla. Primary tumors could cause Horner's syndrome, cord compression and paralysis. Disseminated NBs often invade bone marrow, cortical bone and lymph nodes by means of the hematopoietic system. NBs can also metastasize to the liver, most notably in patients with stage 4S tumors (14).

2.1.1. Localized tumors:

Localized tumors are conformed by a unique primary focus mostly asymptomatic and usually found incidentally (*14*). However, in some cases localized tumors can also be present with symptoms, mainly due to tumor mass compression on adjacent organs and tissues. For instance, tumors located along the trunk can expand and invade the intervertebral foramina and induce transverse myelopathy due to epidural compression (*15*). Other NB-related paraneoplastic disorders are: The Opsoclonus-ataxia syndrome, characterized by an irregular eye and limbs movements, the Horner's syndrome, due to impaired function of cervical sympathetic ganglia, or treatment-resistant diarrhea and hypertension (*16-19*) (**Figure 1**).

2.1.2. Disseminated disease:

At the moment of diagnostic, 50% of NB patients show disseminated disease (*12*). The principal dissemination routes are hematogenous and lymphatic; homing in organs such as bone marrow (BM), cortical bone, liver, skin or lymph nodes. Unlike localized tumors, children with metastatic disease often suffer extensive and diverse systemic symptoms, mainly depending on primary tumor site or metastatic localization. Frequent symptomatology includes abdominal distension, bone pain and orbital ecchymosis or "raccoon eyes" (*13*).

2.1.3. 4S disease:

In 1971, a subset of disseminated NB with a good prognosis (5-year overall survival of 92%) was described as stage 4S (S calls for Special) (*20*). Stage 4S tumors represent 7-10% of all NB cases, with diagnosis restricted to patients younger than 18 months. These tumors normally present with a small primary tumor with disease dissemination restricted to the liver, skin, and minimal bone marrow spread (less than 10% BM involvement), although never affecting the cortical bone. The salient feature of Stage 4S is the possibility of spontaneously regression despite a large tumor burden, with little or no treatment.

2.2. Diagnosis:

NB diagnosis requires a histopathologic evaluation and laboratory tests together with diagnostic imaging techniques that are used to evaluate clinical assessment and posterior disease evolution during treatment. The diagnosis requires a representative tumor sample obtained from a biopsy or surgical resection. Samples can be obtained either from the primary site or a disseminated lesion (including infiltrated BM aspirates). Tumor samples must be evaluated for its histopathological features (confirming the expression of synaptophysin (SYP), chromogranin A (CgA) and neuron-specific enolase (NSE) according to neuroblastic tumor classification systems (*13*) (**Figure 2 A-B**). In addition to histologic evaluation, NB patients also show elevated levels of catecholamine metabolites within urine and plasma, biomarkers used in either diagnostic and progression (*21*).

2.3. Clinical assessment:

Currently, the assessment of primary lesions and disseminated status either at diagnosis or during patient evolution includes different imaging technics: computed tomography, bone scintigraphy and radiologic I-metaiodobenzylguanidine (I-MIBG). The I-MIBG is a potent tool due to NB high avidity; however, some matured phenotypes or relapsed clones could loss this property (*22-24*) (**Figure 2 E-H**). However, the assessment of minimal residual disease (MRD) state is performed by histologic and laboratory analysis, since these increase NB detection sensitivity one or two orders of magnitude in comparison with imaging system's (*12*). To this end, BM aspirate samples are evaluated periodically with standard histological protocols and Real-Time Polymerase Chain Reaction (RT-qPCR) in order to quantify the expression of NB high-specific marker such as Tyrosine Hydroxylase (*TH*), GD2 synthase (*B4GALNT1*), Cyclin D1 (*CCND1*) or Paired-like homeobox 2b (*PHOX2B*) (*25-27*).

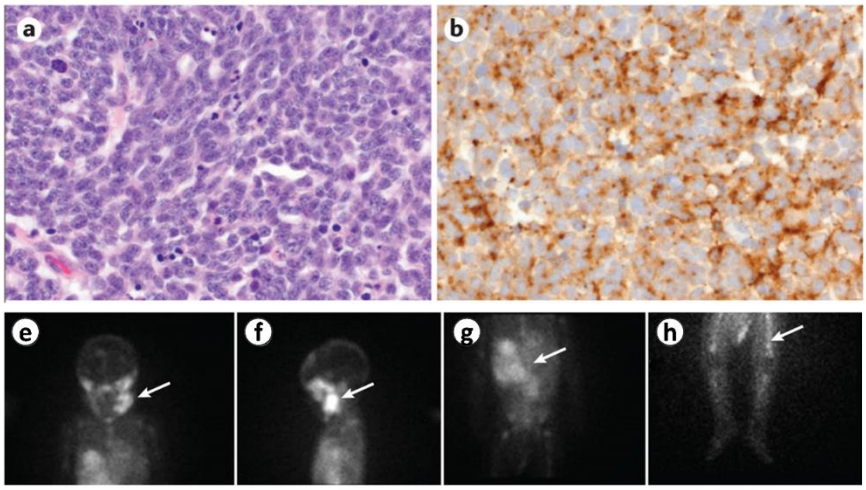

Figure 2: Diagnostic and clinical assessment. **a-b** Diagnostic biopsy from a patient 3 years of age with undifferentiated NB (400× magnification). **a** The biopsy is composed of small, round, monomorphic cells with hyperchromatic nuclei and scant cytoplasm, characteristic of malignant NB. **b** Immunohistochemistry positive for SYP. **e-h** I-MIBG imaging at diagnosis**.** Radiographic imaging of a boy 18 months of age. **e-f** Primary adrenal tumor and metastasis to multiple bones, including the mandible with an associated mass (arrows). **g** Right adrenal primary tumor (arrow) and **h** bilateral lower extremities (arrow). Adapted from (24).

2.4. Histology:

Historically, neuroblastic tumor classification rely on tumor cell histological differentiation grades in agreement to sample maturation traits. In 1984, Shimada H *et al.* proposed the first classification that correlated the histopathology traits with clinical behavior (*28*). A decade later, based on Shimada's classification, it was established the International Neuroblastoma Pathology Classification (INPC) (*29*). The INPC classification relies upon two main characteristics: the neuroblastic maturation grade and the presence of Schwannian stroma. Together they could distinguish four major entities: Neuroblastoma (NB) composed of immature neuroblasts and Schwannian stroma-poor; Ganglioneuroma (GN) composed of ganglion cells, Schwannian stroma-dominant; Gangioneuroblastoma intermixed (GNB-I) and Ganglioneuroblastoma Nodular (GNB-N) composed of mixture of immature neuroblasts and ganglion cells, Schwannian stroma-rich. The NB entity can be further classified in three different sub-groups, based on neuroblast differentiation grade: Undifferentiated (U), poorly differentiated (PD) and differentiated (D) (**Figure 3**).

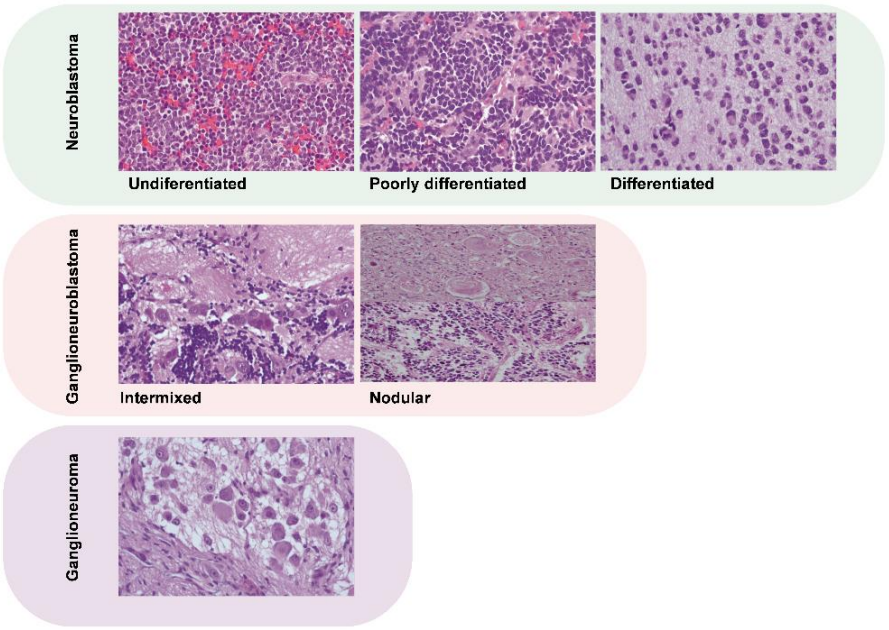

Figure 3: Histology examples of neuroblastic tumors in H&E staining (40x magnification): neuroblastoma (undifferentiated, poorly differentiated and differentiated), ganglioneuroblastoma (intermixed and nodular) and ganglioneuroma. Courtesy of HSJD Pathology service.

2.5. Risk stratification systems:

In order to add prognostic value to Shimada's histopathologic classification, two clinically relevant variables were included into the INPC system; patient age at diagnosis (divided by two age cut-offs, 18 and 60 months) and the Mitosis-Karyorrhexis Index (MKI) (categorized in low, intermediate and high) (*29, 30*). INPC differentiates two different prognostic groups: Favorable Histology Group (FHG) and Unfavorable Histology Group (UHG), with a low-risk and aggressive biology, respectively (*29, 30*) (**Table 1**).

In addition to the INPC system, in 1993 Brodeur GM *et al.* proposed a tumor classification system based on a combination of different clinical features mainly relying on surgical approaches, the International Neuroblastoma Staging Systems (INSS) (*31*) (**Table 2**). Since then, the INSS has been widely used. Note, the INSS classification system has been followed in the present thesis. However, a novel classification system has been recently proposed, the International Neuroblastoma Risk Group Staging System (INRGSS) (*32*).

Tumor	Diff.	Stroma	Charcteristics	Age at Diagnosis <18 18-60 >60	MKI
NB	UD	Poor	Primitive phenotype, neurites absent Prominent nucleol. Poor cytoplasma Ass. NMYC amp, diploidy and 1pLOH		L I H
	PD	Poor	Primitive phenotype Neurites < 5% Prominent nucleol. Poor cytoplasma		L I H
	D	Poor	Differenciated phenotype Neurites > 5% High cytoplasma/nuclei ratio		L I H
GNB-I		Rich (>50%)	Nested Neuroblast in differentation		
GN		Dominant	Stroma well differentited with, ganglion cells		
GNB-N		Rich/Poor	or GN	*	

Table 1: INPC Staging and prognostic system: Neuroblastoma (NB), Ganglioneuroblastoma Intermixed (GNB-I), ganglioneuroma (GN), ganglioneuroblastoma nodular (GNB-N). Undifferentiated (UD), partially differentiated (PD), differentiated (D). Favorable Histology Group (light purple) Unfavorable Histology Group (dark purple). Mitosis-Karyorrhexis Index (MKI): low (L) (<100/5000 cells), intermediate (I) (100-200/5000 cells) and high (H) (>200/5000 cells). *Nodular, depending on biopsy representation, I-MIBG, Catecholamine, BM metastasis (29,30).

The INRGSS is the result of an international cooperative effort to simplify NB classification. It focuses on risk classification considering clinical and biological features of pre-treated tumors together with Image-Defined Risk Factors (IDRFs). In INRGSS, tumors are divided in four different stages including other important prognostic factors; patient age at diagnosis, histology, DNA ploidy and chromosomal alterations (*v-myc avian myelocytomatosis viral oncogene (MYCN)* amplifications or the loss of chromosome 11q) (*32, 33*) (**Table 3**).

Stage	Definition
Stage 1	Localized tumor confined to the area of origin. Complete gross resection with or without microscopic residual disease; identifiable ipsilateral and contralateral lymph node negative for tumor. Adherent lymph nodes in direct continuity with and removed with the tumor may be positive for the tumor. A grossly resected midline tumors without ipsilateral (with: Stage 2A) or contralateral (with: Stage 2B) lymph node involvement is considered Stage 1
Stage 2A	Unilateral with incomplete gross resection; identifiable ipsilateral and contralateral lymph node negative for tumor
Stage 2B	Unilateral with complete or incomplete gross resection; with ipsilateral lymph node positive for tumor identifiable contralateral lymph node negative for tumor
Stage 3	Tumor infiltrating across midline with or without regional lymph node involvement; or unilateral tumor with contralateral lymph node involvement or midline tumor with bilateral lymph node involvement
Stage 4	Dissemination of tumor to distant lymph nodes, bone marrow, liver, or other organs except as defined in Stage 4S
Stage 4S	Localized primary tumor as defined for stage 1 o 2 with dissemination limited to liver, skin, and bone marrow (<10% of nucleated marrow cell are tumor cells)

Table 2: INSS International Neuroblastoma Staging System (31).

Stage	Age at Dx	Histology	Tumor diff. grade	MYCN status	Ploidy	Ch11q	Tx group
L1/L2		GN and GNB-I					L
L1		Any except GN and GNB-I		NA			L
				A			H
L2	< 18	Any except GN and GNB-I		NA		N	L
						Y	I
		GNB-N	Differentating	NA		N	L
						Y	I
			Poorly or Undifferentiaded	NA			
				A			H
M	< 18			NA	Hyperdiploid		L
	< 12			NA	Diploid		I
	12 to 18			NA	Diploid		I
	<18			A			H
	>18			NA/A			H
MS	<18			NA		N	VL
						Y	H
				A			H

Table 3: INRGSS classification. Neuroblastoma (NB), Ganglioneuroblastoma Intermixted (GNB-I), ganglioneuroma (GN), ganglioneuroblastoma nodular (GNB-N), amplified (A), non-amplified (NA), no (N), yes (Y), very low (VL), low (L), intermediate (I) and high (H). (33).

2.6.Biological factors:

Despite NB etiology remains unknown, some genetic factors, both at constitutional and somatic levels, are considered to play a major role in NB oncogenesis (*24, 34*). The vast majority of NB cases are considered to be sporadic and its oncogenesis depend on some recurrent genomic and genetic alterations (*35, 36*) (**Figure 4**).

2.6.1. MYCN

The genetic alteration most robustly associated with NB poor outcome is the amplification of the *MYCN* gene (chromosome 2p24.3) being a biomarker for risk stratification (*37*) (**Figure 4 A-B**). At diagnosis, 20% of NB cases harbor *MYCN* amplification (more than four-fold increase in the *MYCN* signal number compared to reference on chromosome 2 (*38*). This percentage increases up to 50% in patients with disseminated disease (*24, 39*). The *MYCN* amplification is associated with a high-risk stratification and poor outcome regardless of any other risk-associated factor such as NB staging or the age at the moment of diagnosis (*40, 41*). MYCN is considered a master regulator of transcription during development, particularly in neuroectodermal tissues (*42*). In fact, under SA promoters, ectopic expression of *MYCN* is sufficient to drive NB oncogenesis in zebrafish and mice (*43, 44*). However, despite being a recurrent NB driver, its potential as a therapeutic target is limited due to its natural functions as a transcription factor. In this context, alternative therapeutic approaches

are currently in consideration aiming to target MYCN pathways, such as AURKA (Aurora kinase A) or BET (bromodomain and extra-terminal motif) (*45, 46*).

2.6.2. ALK

Alterations of the *ALK* (*Anaplastic Lymphoma Kinase*) gene are present in ~7% of sporadic cases as mutations (10%) or amplifications (4%), while constitutional mutations have been shown to be the predominant genetic cause of familial NB (*47, 48*). Remarkably, amplification of *ALK* (2p23.2) occurs almost exclusively in NB with *MYCN* amplification. Tumors harboring both alterations are associated with a very poor outcome (*49*). This relation is mirrored in NB transgenic models, where *ALK* mutation boosted NB tumorigenesis when combined with *MYCN* amplification ectopic expression (*43, 50*). As a tyrosine kinase receptor, *ALK* alterations are targetable, which widens NB therapeutic options either at diagnosis or when *ALK* alterations are found in tumor relapses (*51, 52*).

2.6.3. LIN28B

The overexpression of the protein coding gene *LIN28B* (6q16.3) is frequently detected in high-risk NB (*53*). LIN28B regulates c (miRNA) biosynthesis, and its overexpression in tumors is linked to the repression of let-7 family miRNAs and derepression of let-7 targets. The repression of let-7 expression is required for normal development. LIN28B contributes to maintain the pluripotent state of embryonic stem cells by preventing let-7-mediated differentiation. In NB, this phenotype leads to an elevated expression of AURKA and MYCN proteins (*54*). In addition, ectopic overexpression of *Lin28B* drives NB tumorigenesis in a transgenic mouse model (*53*).

2.6.4. ATRX and TERT

About 10% of NB patients harbor loss-of-functions mutations or deletions in *ATRX* (Alpha Thalassemia/Mental Retardation Syndrome X-Linked) gene. This alteration is more frequent in older NB patients (44% of patients ≥ 12 years of age) (*55*). ATRX (Xq21.21) is a chromatin-remodeling helicase with an important role during neuronal development; however, its participation in SA differentiation remains unknown (*42*). Remarkably, no *ATRX* mutations have been reported simultaneously with *MYCN* amplification, and both are mutually exclusive with *TERT* (Telomerase Reverse Transcriptase) rearrangements (*47, 56*). TERT (5p15.33) expression is involved in telomere maintenance through telomerase

activity and alternative lengthening of telomeres (*57*). This phenotype facilitates the maintenances of telomere's length, a critical factor in cancer biology (*57*). At the moment of diagnosis, 30% of NBs have enhanced telomerase activity and 25% of tumors harbor TERT rearrangements, all of them associated with poor NB outcome (*56, 58*).

2.6.5. Chromosomal Alterations:

In NB, DNA index and the presence of specific recurrent chromosomal aberrations have a strong prognostic value (*55*). Specifically, DNA content with near-triploid genomes or whole-chromosome copy number changes, are associated with favorable clinical outcomes (*14*). Whereas, segmental chromosomal alterations, resulting from unbalanced translocations and *MYCN* amplification, are associated to poor outcomes (*59, 60*). Recurrent structural chromosomal alterations associated with NB poor outcome include deletions of arms 1p and 11q, and gain of 17q (**Figure 4 C**).

The loss of 1p is present in about 30-45% of cases and is highly associated with *MYCN* amplification (*12, 61*). The loss of specific chromosomal regions is usually related with the presence of tumor suppressor genes. In NB, different candidates among 1p segment are been studied: *CHD5, CAMTA1, KIF1B, CASZ1* and *mir-34A* (*62*). The loss of 11q is present in around 30% of NB cases, frequently observed in older patients and inversely associated *MYCN* amplification or loss of 1p (*59, 61*). This alteration confers more chromosomal instability (*59*). Also associated with aggressive phenotypes, the segmental gain of 17q (1-3 additional copies) is present in more than 50% of NB cases. This gain has been related with NB oncogenic gens including *NM23A* or *BRIC5* (*63, 64*).

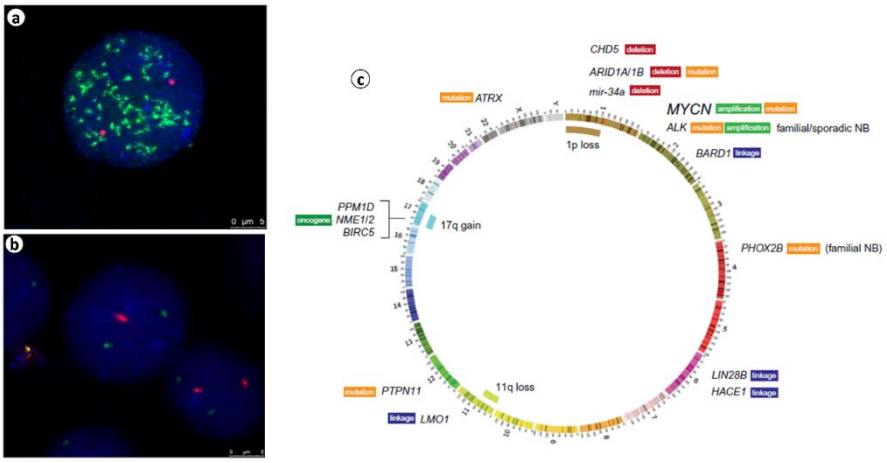

Figure 4: NB clinical assessment. **a-b** Representative images of NB cells infiltrated BM by Fluorescence *in situ* hybridization (FISH). **a** The status of *MYCN* amplification using a dual-color probe. *Green signals* represent the specific probe for *MYCN* and *red signals* stand for centromeric chromosome 2 probes. *MYCN* signals show more than 30 copies within the nuclei. **b** The status of 1p using a dual-color probe. *Green signals* represent the copy numbers at 1q21 and *red signals* are the specific DNA probe of 1p36. *Bars* 5 µm. **c** Summary of the major genomic features implicated in NB oncogenesis. Gene amplifications (pale green), mutations (orange), deletions (red) and oncogenes (dark green). Gene loci identified through linkage analyses for NB susceptibility genes (blue). Adapted from (35,36).

2.6.6. Familial NB:

Familial NB cases represent < 2% of total cases, are diagnosed at younger age than sporadic tumors and frequently with bilateral or multifocal disease presentation (*65, 66*). The vast majority are related with gain of functions mutations in *ALK* gene or with inactivating alterations in *PHOX2B* gene (*65, 67*). Both genes are important mediators during SA linage differentiation (*42*). In addition to these alterations, some common single nucleotide polymorphisms (SNPs) have been found to be related with NB oncogenesis such as *BARD1*, *LMO1*, *LIN28B* (*53, 68, 69*). These SNPs affect cell function at different levels (i.e. gene expression, epigenetic regulation or regulatory elements) and influence NB tumorigenesis, progression and maintenance (*24, 70*) (**Figure 5**).

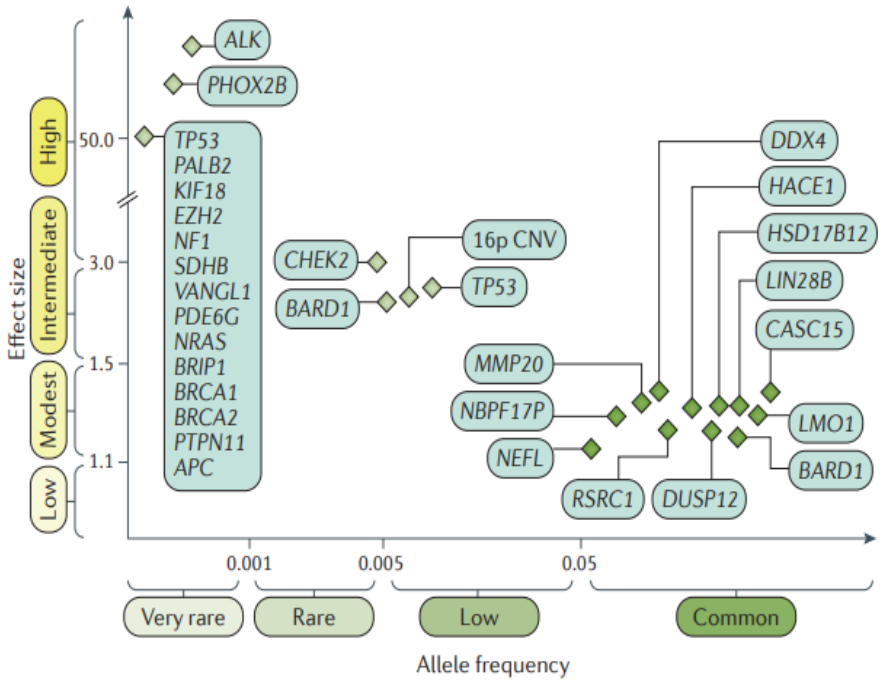

Figure 5: Model of Genetic Susceptibility to NB. The Y axis indicates the effect over NB susceptibility, and the X axis indicates the number of known and theoretical susceptibility alleles. Mutations in *ALK* or *PHOX2B* results in a single, highly penetrant risk allele that allows the development of malignant neuroblastic tissue and thus, related with familial cases of NB. Alternative, in sporadic cases, different polymorphisms are commonly found in a larger number of genes that cooperate to reach neuroblastic malignancy without *ALK* or *PHOX2B* mutations (24).

2.7. Treatment:

Treatment protocols for children with neuroblastic tumors are determined according to the predicted biological, histological and clinical features (patient age, tumor histology, *MYCN* status, DNA ploidy and chromosome aberrations) of the individual tumor. This is especially important for patients, since NB with low-risk features will undergo spontaneous regression (Stage 4S) or maturation (young children), whereas high-risk tumors will rapidly progress despite therapy. NB patients with favorable prognostic benefit from conservative protocols. In contrast, patients with unfavorable tumors require high-dose intensive multimodality treatments including surgery, chemo-, radio- and immune-therapy (*71, 72*) (**Figure 6**).

Patients with low- or intermediate- risk tumors frequently have locoregional lesions, being their preferential management clinical observation or surgery (*14*). However, for tumors with locoregional dissemination (satellite infiltrated lymph node) or infants with stage 4S with life-threatening complications (spinal cord compression or hepatic compromise), a moderate-intensity chemotherapy could be administrated to facilitate a posterior surgery (*73*). Survival rates for low- and intermediate-risk patients are above 90% and 70%, respectively (*24*). This excellent survival prognosis requires minimizing life-long treatment-derived toxicities.

One the other hand, patients with high-risk NB are currently treated with a multi-modal therapy protocol divided into three phases: induction (including chemotherapy and surgery), consolidation (including radiotherapy, myeloablative chemotherapy followed by a rescue with Autologous Stem Cell Transplantation (ASCT)) and maintenance (including retinoic treatment and immunotherapy).

The induction phase aims to reduce tumor burden, bulk lesions size and disseminated focus. During this therapy, patients receive an intense high-dose chemotherapy regiments including cisplatin, carboplatin, etoposide, vincristine, doxorubicin, and cyclophosphamide (*74*). Surgery could be performed at the middle or at the end of induction, with or without a complete resection (*25, 73*). In order to diminish local relapses due to surgery incomplete resection or chemotherapy-remaining lesions, patients are treated with localized radiotherapy during the consolidation phase (*75*). Importantly, at the end of the induction phase, disease response status correlates with patient outcomes (*76*). In that point, patients with poor or very poor response are considered to have a refractory or progressive disease and cannot proceed to consolidation phase. These patients are enrolled to alternative chemotherapy regiments that include different chemotherapy combinations and I-MIBG therapy (*24*). However, 50% of high-risk patients achieved very good or complete response after induction phase (*76*). The presence of MRD after induction is commonly present in the hematopoietic compartment (including BM). This reservoir is considered the main source for high-risk NB frequent relapses (*14, 77, 78*). Thus, in order to consolidate the induction response, some cooperative groups perform a myeloablative chemotherapy followed by a rescue with ASCT (*79, 80*). However, the benefits of this procedure are currently under debate and ASCT is not included in some treatment protocols (*25, 81, 82*).

After the first remission and during maintenance phase, treatment with isotretinoin (13-cisretinoic acid) is administrated to induce NB differentiation in order to reduce the risk of

relapse (*83, 84*). In addition to differentiation inducers, current gold-standard treatment for NB maintenance against MRD, includes anti-GD2 immunotherapy. The disialoganglioside (GD2) is a membrane marker expressed in a wide variety of embryonal tumors, including NB, and particularly in those derived from neuroectoderm (*85*). GD2 expression on NB cell membrane is ubiquitous, being expressed on all primary tumors regardless of stage. Importantly, GD2 is not modulated off cell membrane and persists on NB cell surface post-therapy. These characteristics makes it an excellent target for anti-GD2 immunotherapy (*86*). Although three different monoclonal antibodies have been clinically tested, the chimeric anti-GD2 IgG1 (Dinutuximab), was the first antibody to be approved against NB by the US Food and Drug Administration (FDA) and the European Medicines Agency (EMA) (*82*). This immunotherapy induces cellular cytotoxicity through innate immune system (Natural Killer (NK), macrophages and granulocytes) taking advantage of antibody-dependent cell-mediated cytotoxicity (ADCC) and complement mediated cytotoxicity (CMC) (*87*). The anti-GD2 treatment is usually administrated in combination with different immune stimulatory adjuvants such as IL-2 and GM-SCF that activate immune effector cells (*88, 89*). Future perspectives aiming to improve NB immunotherapy include novel targetable candidates (GPC2 and B7H3) and exploring alternative immuno-adjuvants (IL-15) (*90-92*).

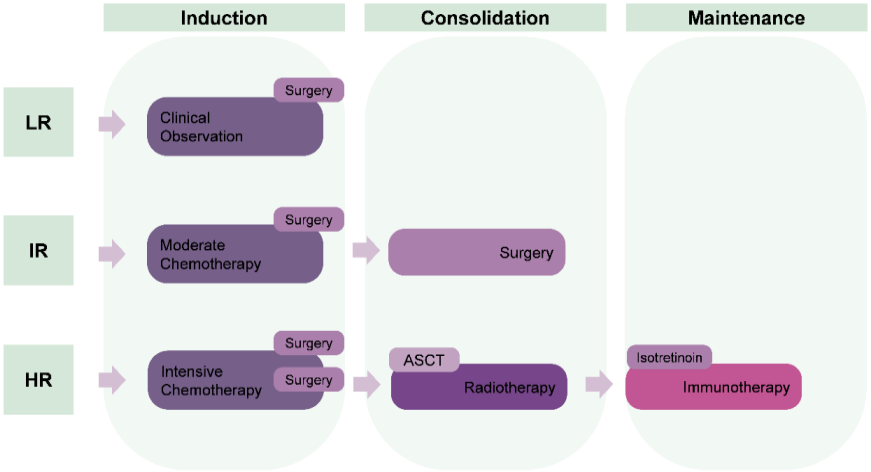

Figure 6: Treatment protocol overview for different NB Risk Classification: Low-risk (LR), Intermediate-risk (IR) and High-Risk (HR). LR disease usually managed with clinical observation alone or surgical resection, with asymptomatic tumors likely to spontaneously regress. IR patients are treated with moderate-dose chemotherapy and surgical resection of the primary tumor. Patient with HR disease requires intensive multimodal therapy divided into three treatment phases. Induction, that comprises intensive chemotherapy and primary tumor resection. Consolidation, with radiotherapy and high-dose ablation chemotherapy followed by ASCT. Maintenance or post-consolidation, based on anti–GD2 immunotherapy and differentiation agents. Adapted from (71,72).

3. The Neural Crest:

The neuroblastic tumors originate from embryonic cells, the NCCs, committed to the establishment of the SA tissues. The neural crest (NC) is a transitory organ that arises during gastrulation and neurulation of the dorsal edge of the neural tube (NT), as part of the neuroectoderm embryonic layer that lays along the entire rosto-caudal axis (*93*). The NC arises from the boundary region between the neural and the non-neural ectoderm in response to signaling gradients of transcription factors (i.e., BMP, WNT, FGF) released by the adjacent tissues, ectoderm, neural plate and axial mesoderm. In response to these secreted factors, resident cells of these border regions activate sequential transcriptional programs that define their identity as NCC (*94, 95*). Under the effect of complex gene regulatory networks, such as *SOX9/10*, *FOXD3* and *SNAIL2*, NCCs successively undergo

epithelial-to-mesenchymal transition (EMT), delamination of from the dorsal NT and migration following different embryonic routes towards target tissues, while differentiating into specific derivatives (**Figure 7 A**).

A common trait of NCCs is their high capacity to migrate throughout the developing embryo. During early migratory phases, NCCs preserve their multipotency, however as migration proceeds, NCCs are exposed to different environmental signals that initiates their specification (*96*). This NCCs linage-commitment is controlled along a cranio-caudal axis by both intrinsic and extrinsic signals that trigger ligand-specific programs: cranial, cardiac, trunk and sacral (*97*). Diverse migratory behaviors are observed during NCC development, ranging from individual cells to compact clusters (**Figure 7 B**). In addition, different migratory routes followed by NCCs are regulated by key guidance signaling axis such as CXCL12/CXCR4/CXCR7, Ephrin A/B or semaphorins (*98-101*). During this migration, NCCs differentiate towards a wide range of cell types that will conform different anatomic structures (*102*). From trunk NCC derivatives arise diverse cellular types including melanocyte, dorsal root ganglia (DRG), sympathetic neurons and ganglia, Schwann cells (SC) (the glia of the peripheral nervous system), adrenal medulla cells like chromaffin cells, neuroendocrine cells in the thyroid glands and the enteric nervous system (*103*).

3.1. Cell of origin:

The localization of NB primary tumors and the expression of lineage markers and the deregulation of critical NCC molecular factors in NB cells has defined the SA progenitors and SC precursors as the potential cells of origin of NB (30881286, 30740044, 30021854). Similarities between NCCs EMT and migration processes, and cancer stem cells has permitted to identify critical molecular players mediating NB tumor development and dissemination, such as LMO4, SNAIL2, FOXD3, MMPs, among others (*104-106*). Furthermore, NB tumor markers reflect this ontology; the disialoganglioside GD2 as a neuroectoderm marker, transcription factors *GATA3*, *ASCL1*, *PHOX2B*, *MYCN* as crucial gens for SA development program as well as the receptor anaplastic lymphoma kinase *ALK* or the enzyme tyrosine hydroxylase *TH* (*24, 107-109*) (**Figure 7 C**).

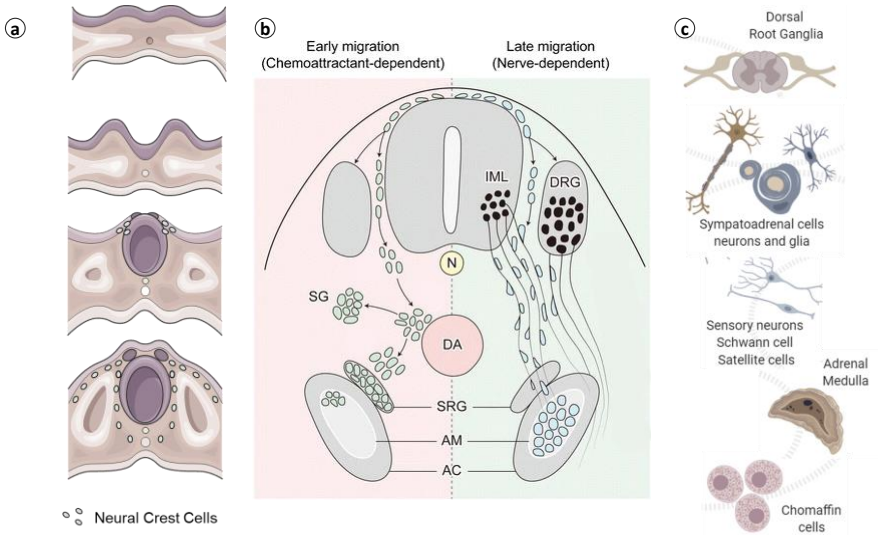

Figure 7: Development of neural crest and sympathoadrenal (SA) lineage **a** Development of the NCCs, with the specification of the neural plate border at the boundary of the neural plate. The neural plate closes to form the neural tube; the NCC progenitors are specified in the dorsal part of the neural folds. After specification, the NCCs undergo EMT and delaminate from the neural tube. Migratory NCCs follow stereotypical pathways to diverse destinations, where they will give rise to distinct derivatives. **b** Different developmental routes of SA lineages and adrenal chromaffin cells. SA lineage is derived from early-migrating NCCs that migrate ventrolaterally, following chemoattractant signals towards the dorsal aorta. NCCs are attracted by CXCL12 and NRG1 secreted by the para-aortic mesenchyme through their receptors CXCR4 and EGFR, respectively. Once NCCs reach the DA, they commit to SA lineage and start to express the lineage-specifying transcription factor gene *Phox2b* in response to BMP signaling from DA. These committed SA progenitors, migrate collectively to paravertebral sympathetic ganglia (SG), adrenal medulla or to suprarenal sympathetic ganglia (SRG). A small population of these migratory cells contribute to the formation of chromaffin cells in the AM. However, the vast majority of adrenal chromaffin cells are derived from SC precursors a late-migrating NCCs that move along nerves that innervate the adrenal gland. **c** Multiple trunk NCC-derived cell types and tissues which precursors could be the origin of NB cells. (AC) adrenal cortex; (AM) Adrenal medulla; (DA) dorsal aorta; (DRG) dorsal root ganglion; (IML) intermediolateral cell column; N, notochord; (SG) sympathetic ganglion; (SRG) suprarenal sympathetic ganglion. Adapted from (108, 109).

4. Tumor microenvironment:

Tumors are not exclusively constituted of cancer cells; they are complex masses of cells that include a heterogeneous population of cancer cells together with diverse non-tumor resident and recruited cell types (fibroblasts, endothelial cells, pericytes and immune cells), signaling molecules and extracellular matrix. Interactions between tumor and non-tumor cells are collectively known as the tumor microenvironment (TME) (*110*). In TME, non-tumor cells can have an active and often tumor-promoting role that greatly influences tumor evolution and progression, as well as tumor response and resistance to treatment. TME interactions are driven by complex networks of cytokines, chemokines, growth factors and inflammatory factors together with the inherent properties of the tissue.

4.1. Neuroblastoma microenvironment:

In NB, a major trait influencing primary lesion in TME is the absence or presence of Schwannian stroma that affects tumor growth and aggressiveness through different mechanisms and correlates with the maturation grade of neuroblastic tumors (*111, 112*). In addition, NB disseminated TME is also highly influenced by the presence of cancer associated fibroblast (CAF), pericytes and the presence or absence of tumor immunosuppressive components (*113-117*). A scheme of TME factors within NB primary tumors are summarized in the **extended Figure 8**.

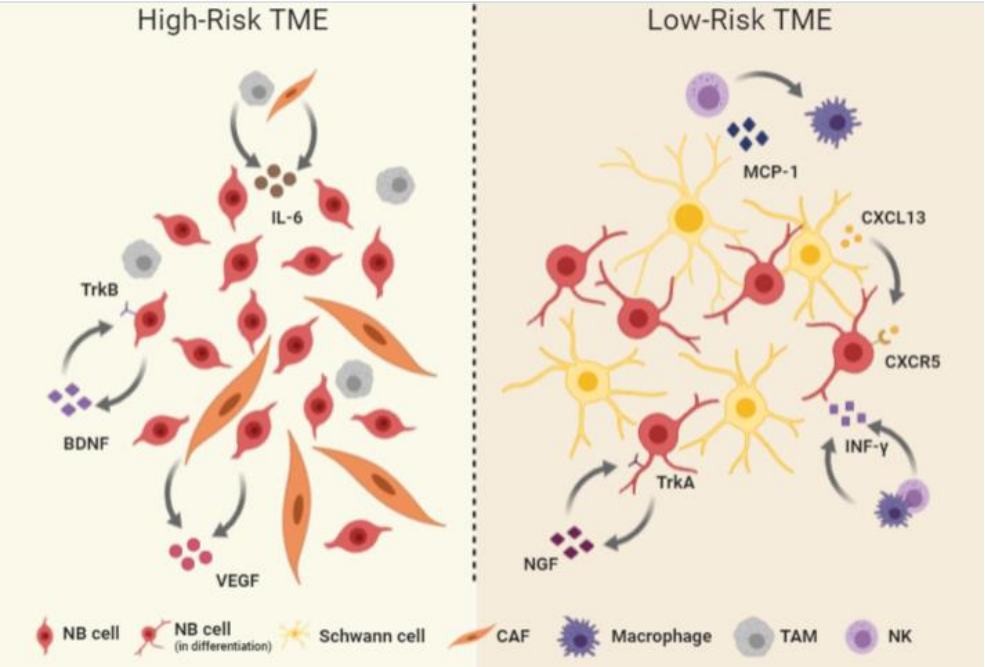

Extended Figure 8: Tumor microenvironment for different NB Risk Classification. (Left-panel) TME of high-risk tumors with undifferentiated neuroblast and lacking Schwannian stroma component (116). High-risk NB cells express TrkB (*NTRK2*) receptor that is activated by brain-derived neurotrophic factor BDNF promoting NB cell survival, drug resistance and angiogenesis by increasing different metalloproteases (MMPs) and serine proteases secretion that facilitate tumor dissemination (39,118,119). In response to hypoxic environment, high-risk NB cells promote neovascularization by releasing vascular endothelial cell growth factor (VEGF) to the TME (120). In response, TME components such as Cancer-Associated-Fibroblast (CAF) are attracted to the tumor and support angiogenesis by secreting additional VEGF, MMP-2 and MMP-9 in a positive feed-back loop (116,118, 121, 122). High-risk NB TME is depleted of anti-tumor immune effector cells but enriched by immunosuppressive mediators; regulatory T cells (Treg), myeloid-derived suppressor cells (MDSCs) and tumor associated macrophages (TAMs) (113-115, 123, 124). TAMs release high amounts of immunosuppressive cytokines, like IL-6, and suppresses MCP-1 release, promoting NB tumor growth, drug resistance and immune evasion (125-128). TAMs infiltration within tumor is associated with patient poor outcome (129). (Right-panel) Tumors with favorable biology are enriched for Schwannian stroma (111,112). Low-risk tumors express high levels of TrkA (*NTRK1*), this receptor is activated by NGF, highly released by the abundant Schwannian stroma. This cross-talk limits NB cellular proliferation and angiogenesis while promoting neuroblast differentiation (39,111,118). Similarly, Schwannian stroma releases CXCL13 that retains malignant NB clones through CXCR5 receptor impairing dissemination to distant sites (130). Low-risk TME has tumor infiltrating lymphocytes (TILs) including cytotoxic T-cell lymphocytes and activated NK cells that release INF-γ, reducing TAMs infiltration (131,132). The presence of INF-γ together with TrkA/NGF signaling up-regulates the expression of MHC-I that also increases adaptive immune response (133).

4.2.The bone marrow as neuroblastoma dissemination niche:

The BM is a complex organ that contains a wide range of cellular types that can be divided in two distinct populations: hematopoietic or non-hematopoietic (*134*). Being the major reservoir of hematopoietic and mesenchymal stem cells (HSCs and MSCs respectively), BM niche is the most common site of metastasis in NB, where this particular environment favors the progression and the survival of the tumor cells (*77*).

4.2.1. Anatomy:

Anatomically, BM is situated within the central cavities of bones. The inner bone surface that contacts with the marrow is the endosteal region, which is composed by thin bone trabecular layer and connective tissue (*135*). Within the cavity of the bone, blood flows from the center to the periphery and back to the center in a multitude of small arterioles and venous sinuses (*136*) (**Figure 9 A**). This vascular architecture assures an optimal delivery of nutrients and oxygen (*135, 137*). The HSC niches are situated closely to these small vessels in the perivascular zones where HSC are retained and supported by MSCs (*138*). This stroma synthesizes and release different factors promoting HSC maintenance and retention in the perivascular niche (*139-141*) (**Figure 9 B**).

4.2.2. The hematopoietic stem cell niche:

In the BM reservoir, MSCs are a wide heterogenic population with high plasticity and self-renewal capacity that supports hematopoiesis (*140, 142*). In fact, a particular population of MSCs ($Nestin^{+}$) situated around vessels, wrapping arterioles, are described as the stromal fraction conforming the HSC niche, as they co-localize with HSCs through the BM cavity (*143, 144*) (**Figure 9 C**). The perivascular stroma cells can be identified by their high expression of HSC niche factors -*Cxcl12*, *Scf*, *Angpt1*, *Il-7*, *Vcam1* and *Spp1*- (*141*). Among these, the principal mediators are the CXC-chemokine ligand 12 (CXCL12) and Stem Cell Factor (SCF) (*141, 143*). Upon their release, these ligands bind to CXC-chemokine receptor 4 (CXCR4) and c-KIT receptors respectively, being both highly expressed by HSCs (*145, 146*). Both signaling axis are essential to preserve the niche and retain HSC (*140*). In this

context, BM conditional depletion of *Scf* or *Cxcl12* in perivascular stromal cells resulted in a HSC depletion enhancing their mobilization into the blood circulation (*139, 147-149*) (**Figure 9 D**). However, components, function and location of HSC niches in the BM are variable since they are affected by different physiological conditions, such as hormone signaling, circadian rhythms, nutrition status or stress (*150, 151*).

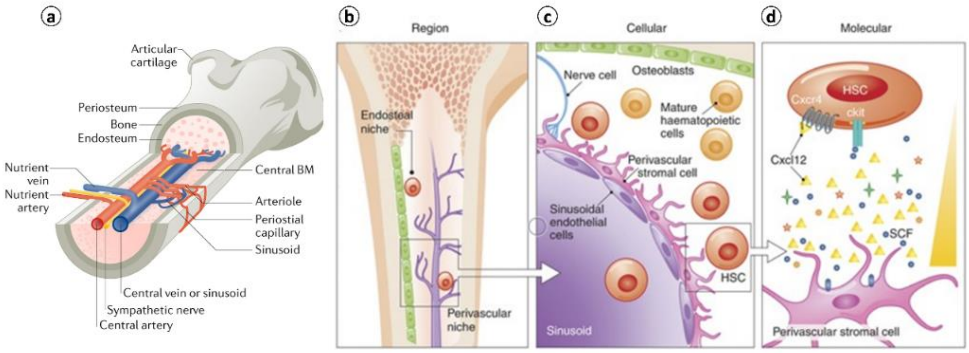

Figure 9: BM-HSC niche. **a** Longitudinal view of a femur illustrating BM anatomy. The periosteal layer covers the outer surface of the bone, and the endosteum layer is at the interface of bone and BM. Branching arteries run parallel along the marrow cavity feeding into the arteriole network often close to endosteum. This network is distributed evenly throughout the marrow cavity and then bend to form the venous circulation (blue). **b** The HSC niches reside in the BM cavity. **c** Within the niche, HSCs can be located in perivascular regions, where HSCs interact directly or indirectly with different types of cells that comprise their niches, mainly stromal cells. **d** These cells release factors (Cxcl12 and SCF) that maintain hematopoietic homeostasis by favoring HSC quiescence, while allowing self-renewal and differentiation upon demand. Adapted from (139,149).

4.2.3. Oxygen levels within hematopoietic stem cell niche:

Despite being highly vascularized; BM shows a particularly high hypoxic environment. Hypoxia - defined as a reduction of tissue oxygen tension levels – is a hallmark of cellular homeostasis. Physiologically, tissue normoxia or physioxia levels range from 3% to 10% of O_2, whereas hypoxia is considered at 0.5% to 3% and anoxia when levels are below 0.5% (*152*). Within the marrow cavity, oxygen tension ranges from 1% to 4% (*138*). Direct measures in mouse BM compartments showed oxygen levels of ~1.8% in the endosteal regions and even lower in perivascular areas (~1.3%). In fact, perivascular HSC niches are

localized in zones with lower oxygen availability, likely due to high oxygen consumption rates within HSC niche (*140, 153*). Principal cellular response mechanisms to hypoxic environments are further detailed in **extended Figure 10**.

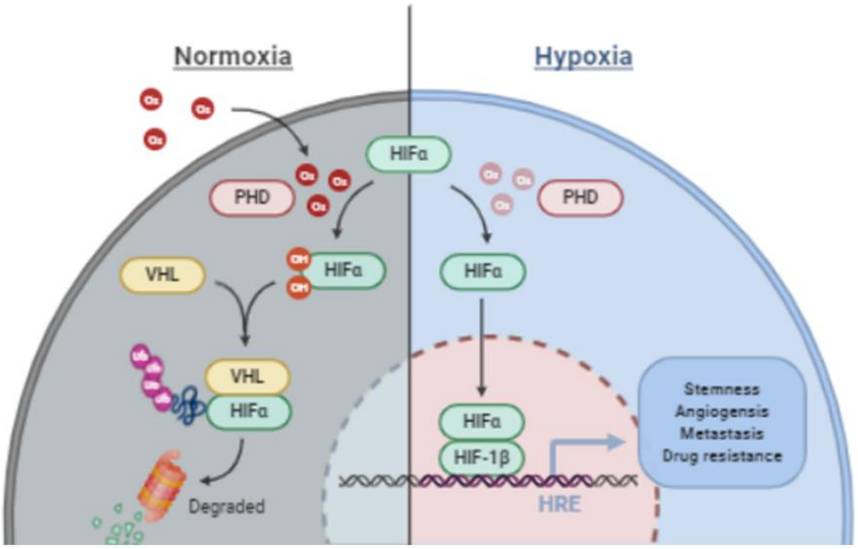

Extended Figure 10: Principal cellular adaptations in response to hypoxic environments are controlled by the hypoxia inducible factors (or HIFs), a broad family of transcription factors. HIF-1α and HIF-2α are some of the key components of HIFs family proteins and both are coupled to the constitutively expressed subunit HIF-1β to from an active heterodimer complex (154, 155). In response to hypoxia, the heterodimer is translocated to the nucleus and binds to promoter regions with hypoxic response element (HRE) domains that activate a hypoxia-induced gene expression program. Importantly, HIFs members cannot sense oxygen levels. This role is performed by the prolyl hydroxylase domain proteins (PHDs), a family of oxygen-sensitive proteins. The best characterized is PHD2 protein, which hydroxylates two proline residues within oxygen-dependent degradation (ODD) domains of HIFα subunits (156) under physioxic conditions. These modifications are recognized by Von Hippel-Lindau (VHL), a subunit of the ubiquitin E3 ligase complex that polyubiquitylates proline hydroxylated HIFα units, enabling their degradation via proteosome. Therefore, under physioxic conditions, HIFα are constitutively degraded by the PHD-pVHL-HIF axis (157). On the contrary, when oxygen levels are low, HIFα hydroxylation is reduced, enabling a rapid protein accumulation and dimerization with HIF-1β to activate the hypoxia response program (158). In NB, hypoxia has an important impact on tumorigenesis, progression, dissemination and drug response (155,158).

4.3.Microenvironment of disseminated neuroblastoma:

The BM environment particularly rich in cytokines, growth factors and highly hypoxic are known to influence over high-risk NB biology as a refuge against the cytotoxic effects of chemotherapy (*77*). The invasion ability of disseminated disease in bone and BM (> 10%) is associated with patient poor outcome (*159*).

4.3.1. Homing and invasion:

Disseminated NB cells express a broad range of chemokine receptors, although their role in metastatic progression is poorly described (*160, 161*). The CXCR6/CXCL16 axis promotes NB retention, whereas the axis CXCR3/CXCL10 may inhibit NB progression within the marrow (*162, 163*). Since CXCR4/CXCL12 retain and preserve HSC cells within BM niche, this axis has been widely studied in cancer dissemination, including NB (*114, 139, 161, 164*) (**Figure 11**). CXCR4 is highly expressed by NCCs, NB tumors and NB cell lines (*165*). In fact, CXCR4 overexpression alone clearly promotes NB cell proliferation and tumor growth (*166, 167*). Moreover, NB cells transfected with CXCR4 express higher stem cell markers such as *c-KIT* and release higher amounts of IL-8 and VEGF when compared to wild-type NB cells (*168*). CXCL12 is expressed but not released by NB cells, thus tumors respond to paracrine CXCL12 released by TME (*169, 170*). However, whether CXCR4/CXCL12 axis induces high-risk NB dissemination to the BM is still under debate (*171-173*).

In recent studies, NB cells overexpressing CXCR4 showed migration and chemo-attraction to recombinant human CXCL12 in a dose-dependent manner, although this phenotype was not observed in cells expressing native CXCR4 levels (*174*). In other *in vitro* studies CXCR4 promoted NB migration and invasion phenotypes in response to MSC-derived CXCL12 (*167, 171*). However, a study with native-CXCR4 expressing NB cells did not observe migration, invasion or chemo-attraction phenotypes when exposed to ectopic CXCL12, even under hypoxic conditions that up-regulate CXCR4 expression (*175*). In summary, CXCR4 signaling favors NB proliferation, however, whether the CXCR4/CXCL12 axis promotes NB dissemination and facilitates NB homing to BM is still controversial.

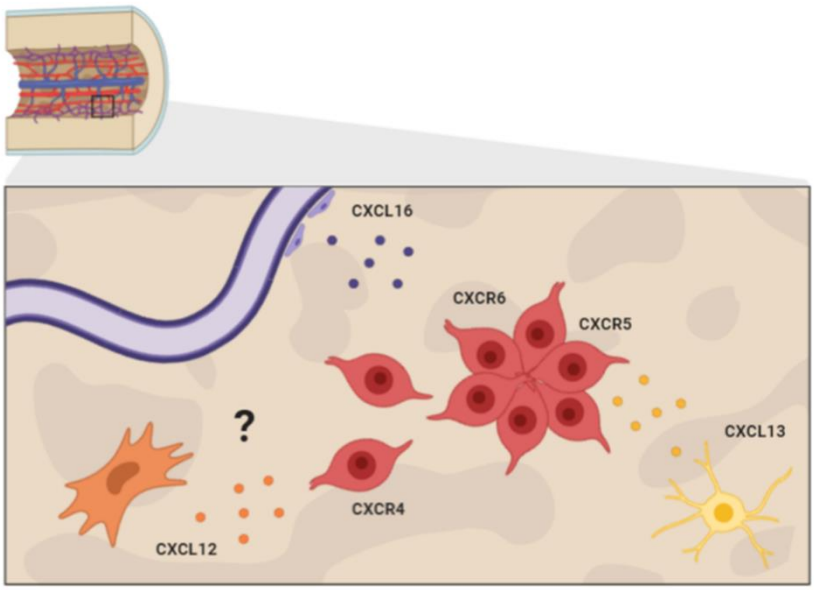

Figure 11: Role of chemokine signaling in NB invasion. NB cells express different chemokine receptors including CXCR4, CXCR5 and CXCR6. Invasion and/or retention of NB cells in the BM may be mediated by the respective ligands, either secreted (CXCL12, CXCL13) by or expressed on the cell surface (CXCL16) of BM resident cells. The CXCR4/CXCL12 axis is a major candidate to mediate bone marrow NB invasion but its role is controversial. Endothelial cells (purple), stromal cells (orange), Schwann cells (yellow) and NB. Adapted from (161).

Alternative mediators to CXCR4/CXCL12 axis have also been considered. CXCL12 also activates CXCR7; however, in contrast to CXCR4, CXCR7 expression in NB has been associated with more differentiated NB phenotypes (*170, 176*). In xenograft models, the single overexpression of CXCR7 promoted NB dissemination towards the adrenal gland and liver, whereas when overexpressed together with CXCR4 NB cells showed preferential BM invasion (*166, 167*). Thus, these studies suggest that different mechanisms control NB dissemination tropisms.

In addition to CXCL12, the receptors CXCR4 and CXCR7 have a second ligand, the Macrophage Migratory Inhibitory Factor (MIF) (more detailed is **section 5**) (*177, 178*). MIF is highly secreted by several cancers and its role in tumor progression is linked to autocrine signaling through CXCR4 and CXCR7. In this context, CXCR4/MIF interaction promoted

metastasis-related behavior by increasing cell proliferation, adhesion, migration and invasion in colon cancer, non-small cell lung cancer (NSCLC), glioblastoma and rhabdomyosarcoma (*179-183*). Additionally, the axis MIF/CXCR7/AKT pathway drives tumor growth and metastasis independently of the CXCR4/CXCL12 axis in metastatic prostate cancer (*184*). The role of MIF within BM disseminated TME in NB has never been studied.

4.3.2. Progression and osteolysis:

Once the BM niche is infiltrated by NB cells, malignant cells take advantage of BM signaling molecules to sustain tumor proliferation and progression (*185*). NB and TME components interact promoting pro-inflammatory and pro-activation signals that stimulate osteoclastogenesis responsible of the osteolytic lesions found in bone metastasis of high-risk NB patients (*186*). As result of bone lysis, important amounts of growth factors are released from the bone matrix into the BM niche, providing additional pro-tumor signals for NB cells (*185*). NB progression within the BM is further detailed in the **extended Figure 12**.

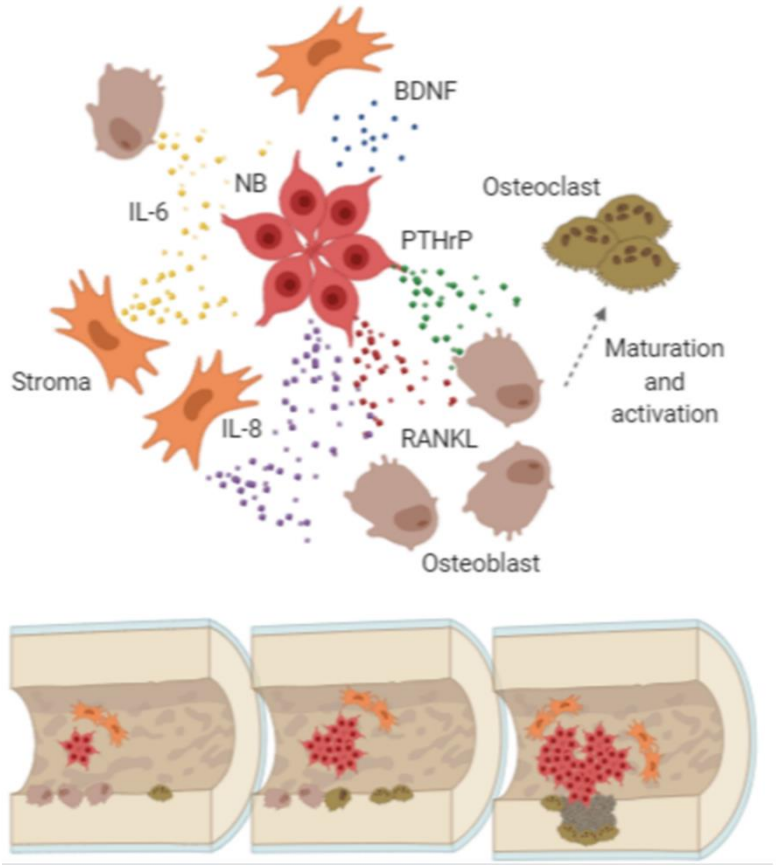

Extended Figure 12: Disseminated NB progression within the BM. Once BM niche is infiltrated by NB cells, malignant proliferation takes advantage of BM signaling to sustain tumor progression. BM-stromal cells release high amount of IL-6 under hypoxic conditions, NB cells express IL-6R witch supports tumor progression (125,187,188). As NB progress within the marrow, the adjacent bone suffers osteolytic lesions as results of osteoclast maturation and activation (188). In a positive feed-back loop, BM-resident osteoblasts release BDNF that activates NB cells through TRKB receptor, promoting NB cell progression within the niche (189). Tumor progression and BM-stroma cells release IL-8 to the environment, this signaling initiates osteoblast ($CXCR1^{+}$) maturation into osteoclast precursors (190). Then, osteoclast precursors are activated by NB-derived signaling RANKL, PTHrP and IL-8 and BM-stroma signaling IL-6. (191, 192, 193). Together, signaling derived from NB and BM-resident cells collaborates to promote NB progression within the bone and BM (186).

5. Macrophage Migratory Inhibitor Factor (MIF):

Human MIF (22p11.2) is a highly conserved, multifunctional cytokine expressed in various cell types including hematopoietic, epithelial, endothelial, mesenchymal and neuronal cells. MIF participates in inflammatory and immune responses through autocrine and paracrine mechanisms via binding and activating the receptors CD74/CD44, CXCR2, CXCR4 and CXCR7. Upon receptor binding, several downstream signaling pathways are activated, including MAPK/ERK, AMPK and AKT (*194*). The expression of MIF receptors is not uniform across the different cell types, resulting in differential responses to MIF in the diverse tissues. Intracellularly, MIF is stored in cytoplasmic vesicle-like structures and is secreted to the extracellular media in response to a number of stimuli including lipopolysaccharide (LPS), TNF-α, or hypoxia stimulus, since MIF promoter region has an HRE domain (*195-200*) (see **extended Figure 10**).

Thus, MIF stimulates the production of tumor necrosis factor TNF-α, interferon IFN-γ, IL-1β, IL-2, IL-6 and IL-8 and other effector cytokines (*201*). In addition to its cytokine function, MIF harbors an enzymatic activity with phenylpyruvate tautomerase activity, although its function in vertebrates it still unclear and probably vestigial (*202, 203*). The MIF protein (114 amino acids; 12.5kDa) functions as a symmetrical homotrimer complex (*197, 204*). During its biosynthesis, MIF can suffer different post-transcriptional modifications, although their biologic significance remains to be established (*194, 205*). Altered expression of MIF has been associated with different pathologies such as auto-immune disease, infections and cancer, mainly due to its pro-inflammatory role (*206-209*).

5.1. MIF signaling:

MIF has four described receptors; CD74/CD44, CXCR2, CXCR4, and CXCR7 (*177, 178, 210, 211*) (**Figure 13**). Among them, CD74 was the first identified (*210*). CD74 is a chaperone coupled to major histocompatibility complex II (MHC II), highly expressed by antigen-presenting cells (*212, 213*). In addition to its chaperone role, CD74 can function as cell membrane receptor. Upon MIF binding, CD74 forms complexes with CD44 or CXCRs

receptors to activate MIF downstream signaling pathways (*211*). As a complex, CD74/CD44/MIF activate the MAPK/ERK signaling pathway (*211, 214*).

In addition to CD74/CD44, other members of the CXC chemokine receptor family are known to interact with MIF; CXCR2, -4 and -7. CXCR2 is mainly expressed by neutrophils and endothelium cells, while CXCR- 4 and 7 are expressed by hematopoietic linages and neuronal cells. both recognize also the CXCL12 ligand (*194*). MIF binding to CXCR4 induces activation of MAPK and PI3K signaling (*194, 215*). Additionally, all three CXCR receptors can oligomerize with CD74 and act as co-receptors. These heterogenic complexes activate the PI3K pathway and *IL-8* expression in response to MIF (*216-220*).

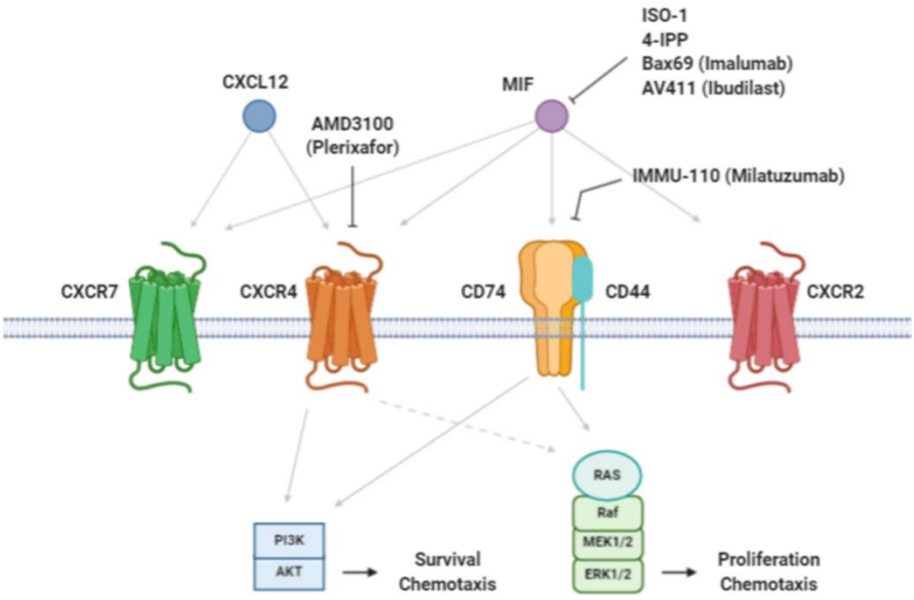

Figure 13: Signaling axis of MIF and CXCL12, and targeted drugs. MIF binds to CXCR2, CXCR4, and CD74 receptors, whereas CXCL12 binds to CXCR4 and CXCR7. CXCR2 and CXCR4 induce G protein-coupled signaling and effect survival, proliferation, and chemotaxis. CD74/CD44 mediates similar effects in a G protein-independent manner. CXCR7 is not a G protein-coupled receptor but can induce β -arrestin signaling to induce CXCR4 endocytosis. Targeting drugs with pre-clinical or clinical data are available. MIF: macrophage migration inhibitory factor, PI3K: phosphatidylinositide 3-kinase. Adapted from (218-220).

5.2.MIF in neuroblastoma:

MIF is frequently overexpressed in cancer, including carcinomas and developmental tumors (*221-225*). As a result of its pleiotropic roles, MIF can support cancer progression through diverse mechanism; promoting cell proliferation, angiogenesis, impairing apoptosis, regulating cell migration and differentiation or favoring tumor immune evasion (*209*). MIF is secreted both by tumor and immune cells, thereby it can critically influence the TME.

MIF is highly expressed by NB cell lines and tumor tissues (*226, 227*). Among neuroblastic tumors, undifferentiated high-risk NB showed higher MIF protein expression than more differentiated, low-risk entities such GN (*227, 228*).

Beyond its relation with tumor differentiation, several studies have demonstrated the oncogenic effects of ectopic MIF over NB cell lines. MIF induces a dose dependent increase of *MYCN* and the release of VEGF and IL-8, suggesting a potential role of MIF over angiogenesis (*227*). Moreover, two different studies described MIF as an anti-apoptotic and proliferation inducer since NB cell line SH-SY5Y exposed to MIF increased release and expression of BDNF, Bcl2 and down-regulated Casp-3 and Bax protein levels, while increasing Bad and AKT phosphorylation (*229, 230*). In agreement with these studies, the down-regulation of MIF expression in NB cell line SK-N-DZ with a MIF antisense sequence (AS-MIF) down-regulated the expression of *MYCN*, *c-MET*, *TRKB* and *IL-8*. As a result, AS-MIF cells were less proliferative and migratory *in vitro* and showed impaired tumor growth and reduced metastatic events in a nude mice model (*225, 231*).

In addition, MIF inhibition by iRNA was able to revert vincristine resistance in NKF-NB-3 cell line, suggesting a potential role in chemoresistance (*228*). Recently, MIF-mediated NB cell proliferation and migration has been related to the tumor suppressor miR-451 (*232*).

Finally, several *in vivo* studies in syngeneic models suggested the immunomodulatory effects of MIF over NB environment, as *Mif* is also overexpressed by Neuro2a and AGN2a mouse-derived cell lines. Neuro2a-derived MIF reverted T-cell activation and proliferation, suggesting a potential role over NB immune evasion (*233*). Inhibition of *Mif* expression in

AGN2a by siRNA, showed less engraftment ratios with a TME enriched in lymphocytes T $CD8^+$, $CD4^+$, macrophages and dendritic cells in *in vivo* syngeneic models (*234*).

5.3. Targeting MIF pathways:

MIF has an important effect over immune response in multiple diseases, thus its potential as a druggable target is gaining relevance (*219*). Despite the diverse reported inhibitors of MIF activity, few of these have been tested either *in vitro* and/or *in vivo* studies (*235*) (**Figure 13**).

Among them, the best characterized is the MIF antagonist (S,R)-3-(4-hydroxyphenyl)-4,5-dihydro-5-isoxazole acetic acid methyl ester (ISO-1) (*236*). ISO-1 is an isoxazoline inhibits the tautomerase activity and MIF-dependent arachidonic acid release from macrophages by binding to the MIF monomers without altering the tertiary structure (*237*). Despite ISO-1 has a low MIF inhibitor activity, *in vitro* or *in vivo* studies shown anti-MIF activity in lung cancer, pancreatic cancer, rhabdomyosarcoma and NB (*183, 229, 238-240*).

Recently, the novel MIF inhibitor 4-iodo-6-phenylpyrimidine (4-IPP) is gaining interest as an anti-cancer agent. 4-IPP is an irreversible MIF inhibitor that forms a covalent bond with the catalytically active NH2-terminal proline to inhibit its biologic activity. In comparison to ISO-1, 4-IPP is 5–10 times more potent inhibitory effect at blocking MIF-dependent catalysis (*241*). In cancer, 4-IPP has been shown to induce apoptosis and mitotic cell death growth of thyroid cancer cells, inhibit head and neck squamous cell carcinomas proliferation and invasiveness, and impair lung adenocarcinoma cell migration (*241-243*). In Multiple Myeloma (MM), a cancer involving BM dissemination, 4-IPP treatment modulates MM cells stemness, invasion and sensitizes tumor cells to chemotherapy (*244, 245*). In rhabdomyosarcoma, a pediatric malignant soft tissue sarcoma, ISO-1 and 4-IPP reduced cell migration and restored immune sensitivity *in vitro* (*239*). To our knowledge 4-IPP has never been tested NB.

Phase I/II clinical trials are evaluating different anti-MIF therapies for cancer treatment. Particularly, the anti-MIF monoclonal antibody (mAb) Imalumab (Bax69) has been studied in malignant solid tumors, ovarian cancer and metastatic colorectal cancer and resulted to be well-tolerated (NCT01765790, NCT02540356, NCT02448810, respectively).

Ibudilast (AV411) is a non-selective phosphodiesterase inhibitor that also impairs pro-inflammatory signaling by inhibiting MIF, TNF-α, IL-6, and IL-1β (*246, 247*). Recently, Ibudilast treatment was shown to delay progression of multiple sclerosis in a phase II clinical trial (NCT01982942). In cancer, preclinical *in vivo* studies in patient derived xenograft (PDX) models treated with ibudilast in combination with temozolamide showed significant overall survival. An early phase clinical trial is currently evaluating ibudilast and temozolamide treatment combination for patients with newly diagnosed and recurrent glioblastoma (*248*) (NCT03782415).

The CXCR4 receptor antagonist Plerixafor (AMD3100) has been considered as an indirect targeting strategy for MIF inhibition. AMD3100 has been approved by the US FDA for mobilization of normal HSC from the BM into the blood stream of patients in high-dose chemotherapy regimens with autologous transplantation (*249*). Disruption of the CXCR4/CXCL12 interaction with the AMD3100 agent has been evaluated for HSC mobilization in diverse malignancies, including NB where it was found to be effective and safe to improve ASCT (*250*).

Milatuzumab (hLL1), a mAb anti-CD74 and anti-MIF, is being evaluated against hematologic malignancies (NCT01101594, NCT00421525, NCT00603668, NCT00868478, NCT00504972, and NCT00989586). Milatuzumab is well-tolerated although further studies are needed to demonstrate the clinical benefits in solid tumors.

HYPOTHESIS AND OBJECTIVES:

Treatment of high-risk NB and particularly of disseminated tumors remains a therapeutic challenge greatly due to recurrent disease relapse. Despite aggressive multimodality therapy, the overall survival of patients after relapse remains poor. Novel targeted treatment approaches such as immunotherapy have demonstrated effectiveness in a MRD setting, improving outcome of these patients. However, significant efforts are still needed for more effective treatment strategies to improve cure rates of high-risk patients.

In this thesis, we focused on the most common site of NB dissemination, the BM, and its role as an oncogenic environment. The BM is a complex organ with heterogeneous cell populations, multiple secreted components and diverse physical features. Evidence shows that this complex microenvironment is critical for the survival and invasion of NB tumor cells to the BM. However, little is known about the biology underlying the aggressive behavior of NB disseminated to this niche.

Our hypothesis is that BM microenvironment features such as low oxygen levels and cytokine signaling play a critical role for NB survival, invasion and proliferation. Thus, a comprehensive understanding of the interactions between NB cells and the BM niche and how these interactions are altered in pathological states can aid the development of new therapeutic strategies.

The objective of this thesis was to investigate the biology underlying the malignant behavior of NB cells present in the BM of patients with aggressive, disseminated NB tumors, and identify potential new targets against these malignant cells.

To accomplish our general objective, the specific aims were:

1. To establish a BM microenviroment model in vitro that enabled the identification of factors critical for the interactions between NB cells and the BM niche. Our purpose was to generate a model that recapitulated important features of the niche (cytokine signaling and low oxygen tension) of patients with disseminated disease. We used conditioned media generated from patient-derived BM cells and NB cells cultured

under diverse oxygen levels. The secretome of the BM, in the form of CM, was tested and characterized to identify cytokines of interest.

2. To study in vitro and in vivo the effects of our BM-based model on the malignant behavior of NB (viability, migration, invasion and drug resistance). We explored cell signaling pathways that may contribute to the malignant behavior of NB cells in the BM niche.

3. To explore novel therapeutic strategies aimed at reducing aggressiveness and invasiveness of NB cells present in the BM niche. To this end, we tested the potential antitumor effects of molecules that inhibit selected critical mediators (point 1) in our BM model in vitro as well as in NB tumor xenografts in vivo.

MATERIALS AND METHODS:

1. Cell culture:

Commercial cell lines and primary cell cultures were maintained in regular medium conditions consisting of RPMI-1640 high glucose medium supplemented with 10% of inactivated Fetal Bovine Serum (iFBS), 2 mM L-glutamine and Penicillin/ Streptomycin (100 u/mL and 100 µg/mL, respectively) (Gibco-Life technologies). During culture maintenance, cell medium was changed every 3-4 days in a controlled atmosphere at 37ºC and 5% CO_2.

Cell passages were performed by enzymatic dissociation with Trypsin EDTA (Gibco, Thermo Fisher) before cell cultures reached 80% of confluence. After dissociation, cells were washed with fresh regular media and plated in a new T-75 flask (Corning) or counted and cultured in appropriate plates in order to proceed with an experiment.

For long-term storage, cells were kept frozen in liquid nitrogen. To this end, dissociated cellular pellets were re-suspended in 1 mL of iFBS with 10% of Anhydrous Dimethyl Sulfoxide (DMSO; Sigma-Aldrich) and aliquoted in cryovials (Corning). Cells were kept frozen at -80ºC for 2-3 days and then transferred to nitrogen tanks for cellular cryopreservation. When needed, cryopreserved cells were thawed at 37ºC, re-suspended in tempered regular media and washed by centrifugation in order to dismiss remaining DMSO. Thawed cells were plated in a new T-75 flask with regular medium and kept in regular culture conditions.

1.1. Neuroblastoma cell lines:

Neuroblastoma (NB) commercial cell lines (LAN-1, SH-SY5Y, IMR5) were obtained from the repository of the Laboratory of Developmental Tumors, Hospital Sant Joan de Deu (HSJD, Barcelona). **Table 4** summarizes clinical and biological features of each NB culture used in this thesis (*251*).

NB cells	Biopsy	MYCN status	ALK	P53	1p del	State	Dtatus
LAN-1	BM	amp	mut	mut	del	ADR	post Tx
SH-SY5Y	BM	non amp	mut	wt	no	ADR	post Tx
IMR5	Abdominal	amp	wt	wt	del	ADR	Dx

Table 4: Neuroblastoma cell lines features. Bone marrow (BM), amplified (amp), mutated (mut), wild-type (wt), deletion (del), ADR (adrenergic), non-available (na), post-treatment (postTx), diagnostic (Dx) (251).

1.2. Primary patient-derived bone marrow cultures:

Fresh BM aspirates were obtained from 43 NB patients at different stages of the disease treated in our institution. Each established cell culture was named after the code BMNB_XX followed by a correlative number. Samples were obtained from different anatomical regions as bilateral anterior and posterior iliac crests.

To stablish primary cell cultures, four BM aspirates *per* patient were collected in 3 mL EDTA 3K tubes (SARSTEDT AG & Co) and centrifuged in a density gradient Histopaque®-1077 (Sigma-Aldrich, USA) at 2000 g for 20 minutes to obtain BM mononucleated cells. After three washes with regular media, BMCs were plated in T75 flasks and expanded in regular culture conditions up to 15 days (passage zero), renewing media every 3-4 days. During all the study, 31 BM from NB patient were used to produce Conditioned Media (CMs) and 11 discarded due to low cellular expansion (n=9) or bacterial contamination (n=2). The presence of NB dissemination within BM aspirates was determined by the molecular diagnostic service at our institution using RT-PCR. This technique determines NB infiltration by quantification of mRNA levels of the paired-like homeobox 2b gene (*PHOX2B*), a regulator of the development of neural crest derivatives that is not expressed by BM cells, enabling a sensitive quantification of minimal residual disease (MRD) (**Table 5**).

In addition, BM-derived MSC primary culture obtained from a non-oncologic patient was purified and cultured in specific media: Isove's modified Dulbecco's medium (IMDM), 10% of calf bovine serum, 2 mM L-glutamine, Penicillin/ Streptomycin (Gibco-Life technologies) and 10 ng/mL platelet-derived growth factor BB (Peprotech, UK). Parents and/or tutors sign informed consent before collection of samples. The study was approved by the Institutional Review Boards.

ID	MRD	INNS	Use
BMNB_25	neg	4	P
BMNB_26	neg	3	P
BMNB_27	neg	na	P
BMNB_28	neg	na	P
BMNB_29	neg	na	P
BMNB_30	neg	4	P
BMNB_31	<1:177	4	P
BMNB_32	neg	na	CM
BMNB_33	neg	na	P
BMNB_34	neg	4	P
BMNB_35	neg	4	CM
BMNB_37	<1:66	4	aplasic
BMNB_38	neg	na	CM
BMNB_39	neg	na	CM
BMNB_41	neg	4	CM
BMNB_42	<1:30000	na	CM
BMNB_43	neg	4	CM
BMNB_44	<1:42	na	aplasic
BMNB_45	neg	3	CM
BMNB_46	neg	4	CM - FC
BMNB_47	<1:18000	na	CM - FC
BMNB_48	neg	na	contamination
BMNB_49	neg	4	FC
BMNB_50	<1:10000	4	aplasic
BMNB_51	neg	4	CM - FC
BMNB_52	neg	na	CM - FC
BMNB_53	neg	4	IC50 - FC
BMNB_54	neg	na	aplasic
BMNB_55	neg	na	CM
BMNB_55	neg	na	contamination
BMNB_56	<1:100000	na	CM
BMNB_57	neg	4	CM
BMNB_58	neg	na	P
BMNB_59	neg	na	FC
BMNB_60	neg	na	aplasic
BMNB_61	neg	3	FC
BMNB_62	neg	4	FC
BMNB_63	neg	na	aplasic
BMNB_64	neg	4	aplasic
BMNB_65	neg	na	CM
BMNB_66	neg	na	aplasic
BMNB_67	neg	na	aplasic
BMNB_68	neg	na	CM
BMNB_70	neg	4	FC
BMNB_71	neg	na	FC
BMNB_72	neg	na	FC
BMNB_73	neg	na	IC50
BMNB_74	neg	na	FC
BMNB_75	neg	na	CM
BMNB_76	neg	na	FC
BMNB_77	neg	4	FC
BMNB_81	neg	4	CM
BMNB_83	neg	4	CM

Table 5: List of BM samples used in this thesis. Clinical data available: NB minimal residual disease (MRD) expressed as a ratio of tumor cell to non-tumor cell. International Neuroblastoma Staging System (INSS) and its use. Negative (neg), non-available (na), conditioned media (CM), plasma (P), flow cytometry (FC).

1.3. Conditioned cell culture media:

In order to study NB tumor dissemination in the BM, we generated BM cell culture CMs to enable us to model the BM microenvironment *in vitro*. Together with CMs, different oxygen concentration gradients were applied to cell culture to better recapitulate relevant features of the studied niche.

In order to generate CMs, we used fresh *in vitro* expanded BM cells ($2x10^6$; CM-BM), BM cells co-cultured with NB cells in a ratio of 1:1 ($1x10^6$ each; CM-BM/NB) or NB cells cultured alone ($2x10^6$; CM-NB). After 48 hours, CMs were collected, centrifuged at 1000 x g for 10 minutes and kept at -80ºC for future assays (**Figure 1**). Previous to each experiment, CMs were thawed and diluted 1:1 with regular RPMI without iFBS. As a control condition, CM-CNT was generated previous to each experiment and was composed of complete RPMI with 5% of iFBS.

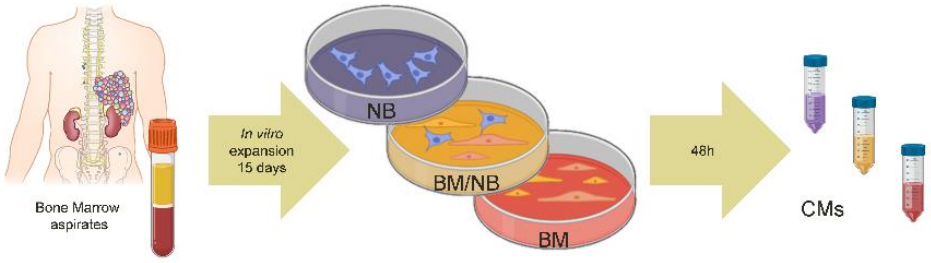

Figure 1: Graphical scheme describing generation of conditioned media.

1.4. In vitro hypoxia:

This project includes different oxygen tension levels as a relevant variable to model the BM niche *in vitro*. Experiments were carried out either in atmospheric oxygen levels [21% O_2; normoxic conditions (Nx)] or 1% O_2 [hypoxic conditions (Hx)]. Oxygen levels were controlled with a modular incubator chamber, MIC-101 (Billups-Rothenberg, Inc), where hypoxic experiments were sealed and atmospheric air replaced by a mixed air (95% N_2, 5% CO_2 and 1% O_2) (Linde SA) fluxed at 1 (L/min) during 5 minutes. Experiments longer than 72 h

were refluxed every 3 days. As a positive control for hypoxic environment we used Cobalt(II) chloride (Sigma Aldrich).

2. Cytokine Profile Arrays:

To explore the potential activation of cell signaling in our CMs, we used Cytokine Protein arrays (R&D Systems), which enable simultaneous detection of multiple cytokines in a single sample. We assessed the presence of cytokines in CM-CNT, CM-NB, CM-BM, CM-BM/NB as well as BM plasma samples from patients with or without NB infiltration, following manufacturer's protocol. The chemiluminiscent signal of each membrane was detected with iBright Imagine System (Thermo Fisher) and quantified with QuickSpots Software (R&D Systems). Results obtained from cytokine profile arrays were validated by ELISA.

3. Phospho-Kinase Array:

In order to detect phosphorylation changes in multiple intracellular cell signaling pathways, we used the Phospho-Kinase Array Kit (R&D Systems). Similar to cytokine profile array, this kit consists of a membrane-based antibody array that allows parallel determination of relative levels of protein kinase phosphorylation in cell lysates. We interrogated phosphorylation levels in the following conditions: LAN-1 cells cultured 48 h under normoxia and hypoxia. Chemiluminiscent signal of each membrane was detected with iBright Imagine System (Thermo Fisher) and quantified with QuickSpots Software (R&D Systems) as previously described.

4. Enzyme-linked immunosorbent assay (ELISA):

Levels of CXCL12 and MIF were measured in conditioned media and cell media supernatants using Human CXCL12/SDF-1 DuoSet ELISA and MIF Quantikine ELISA Kit (R&D systems) following manufacturer's protocols. Supernatants were collected from

cultured cells, centrifuged 1000 g 10 minutes at 4ºC in order to discard cellular debris and stored at -80ºC until ELISA procedure was performed.

5. Genomic data:

Four different gene expression data sets were used to select potentially relevant targets in our BM-based model. The first dataset (Gene expression Omnibus repository ID: GSE94035) comprised RNA-seq data (HiSeq 2000, Illumina) from 16 primary tumors, 42 bone marrow-derived disseminated tumor cells and corresponding 28 bone marrow-derived non-tumor cells of stage M patients (*78*). The second dataset (GSE54720) comprised gene expression array data (U219, Affymetrix) from 21 primary NB biopsies obtained at the moment of diagnosis (*252*). The third data set (GSE62564) was a RNA-seq dataset from 498 primary NB diagnostic biopsies (*253*). The last dataset (ArrayExpress ID: E-MTAB-6814) contains RNA-seq data from a study performed across different mammalian species during development and aging stages (4-week post-conception until elderly >60 years old) (*254*).

6. Survival analysis:

In order to preform survival analysis, we used data from the gene expression data set GSE62564. Overall Survival (OS) probabilities were calculated with the Kaplan-Meier Method and compared by means of log-rank test. These analyses were performed with GraphPad Prsim 8 (La Jolla, Ca).

7. Western Blot analysis:

To obtain whole cell protein extracts, samples were lysed with RIPA 1X buffer (50 mM Tris pH 8.8, 150 mM NaCl, 0.1% SDS, 0.5% Sodium deoxycholate and 1% NP40) plus complete Proteases Inhibitor Cocktail Tablets (Roche). Protein extracts were quantified with Bradford Reagent (BioRad). Samples were separated by electrophoresis in polyacrylamide gels (8-

12%) and transferred to nitrocellulose membranes (Invitrogen). Immunoblot detection was performed with near-infrared labeled secondary antibodies (Oddyssey CLs, LI-COR Inc). Relative protein levels were measured by Image J software. Used antibodies are reported in (**Table 6**).

Antibody	Ref	Company	Use	Working dilution
Phospho ERK1/2	4370	Cell Signaling Technology	WB	1:1000
ERK1/2	4695	Cell Signaling Technology	WB	1:1000
Phospho-AKT	4060	Cell Signaling Technology	WB	1:1000
AKT	9272	Cell Signaling Technology	WB	1:1000
gamma-Tubulin	T6557	Sigma	WB	1:30000
IRDye® 680RD α-Rabbit	926-68071	Li-COR	WB	1:5000
IRDye® 800CW α-Rabbit	926-32211	Li-COR	WB	1:5000
IRDye® 680RD α-Mouse	926-68070	Li-COR	WB	1:5000
IRDye® 800RD α-Mouse	926-32210	Li-COR	WB	1:5000
CXCR4-PE	FAB170P	R&D Systems	FC	1:10
CD74-Alexa467	FAB35901R	R&D Systems	FC	0.2 µg/mL
CD45-PE	130-110-632	Milteny Biotech	FC	1:50
CD45-V500	655873	Becton Dickinson	FC	2.5 µg/mL
CD11b-PE	333142	Becton Dickinson	FC	5 µg/mL
CD34 PerCP	345803	Becton Dickinson	FC	1.25 µg/mL
HLA-DR PerCP	347402	Becton Dickinson	FC	2.5 µg/mL
CD19-PeCy7	341113	Becton Dickinson	FC	2.5 µg/mL
CD123-APC	658171	Becton Dickinson	FC	2.5 µg/mL
CD117-APC	333233	Becton Dickinson	FC	2.5 µg/mL
CD90-PE	130-097-932	Milteny Biotech	FC	1:20
CD105-FITC	130-098-778	Milteny Biotech	FC	1:20

Table 6: List of antibodies used in this thesis. Western blot (WB) and flow cytometry (FC).

8. Cell viability assays:

In order to test CM-driven cell viability, NB cells were counted with Trypan blue (Sigma-Aldrich) in a Neubauer chamber. Next, cells were plated in 96-well plates (Costar, Cambridge, MA) at 2000 cells *per* well (LAN-1 and SH-SY5Y) or 8000 cells *per* well (IMR5) in 100 µL of regular media and kept in standard conditions for 24 h enabling cellular attachment. Then, regular media was replaced by different conditioned media CM-NB, CM-BM, CM-BM/NB or CM-CNT and cultured under normoxic or hypoxic conditions (n=6 *per* condition). Cell viability was measured with MTS assay (Promega, Fitchburg, WI, USA) at 0, 24, 48, 72, 96 hours at 490nm with Infinitive Mano + plate reader (Tecan). At each time point, cell viability was measured as fold change compared relative to the initial MTS signal at time 0 h. These experiments were repeated at least with two different batches of CM. In

order to assess whether selected treatments could affect NB viability, the same protocol was performed adding to each CMs, 4-IPP (5 µM), AMD3100 (10 nM) or vehicle.

9. RNA transcript quantification:

Real-time qPCR assays were performed to quantify gene expression levels of hypoxia-related genes after the exposure to hypoxic conditions. First, samples were washed with PBS previous to be lysed in TRI Reagent (Sigma-Aldrich). Purified RNA was obtained following an organic extraction protocol, a phenol containing solution that enables RNA isolation from proteins and genomic DNA. Then, RNA was precipitated with alcohol and rehydrated in diethylpyrocarbonate (DEPC) water. Nanodrop one C (Thermo Fisher) was used for quantification and quantity control. RNA quality thresholds were set above 1.7 (260/280 ratio) and above 2 (260/230 ratio). RNA conversion to cDNA was perform with 1 µg of total RNA reverse-transcribed using Random Primers, RNasin® Plus Ribonuclease Inhibitor, M-MLV Reverse Transcriptase (200 u/µL) all of them from (Promega, Fitchburg, WI, USA). Gene expression was quantified with Taqman Gene Expression Assays or Syber Green on Applied Biosystems QuantStudio 6 Real-Time PCR system (Thermo Fisher), using the ΔΔCT relative quantification method. Primers used in this project are listed in **Table 7**.

Gene	Fw (5'→3')	Rv (5'→3')
HIF-1 α	TTCCAGTTACGTTCCTTCGATCA	TTTGAGGACTTGCGCTTTCA
HIF-2 α	GTGCTCCCACGGCCTGTA	TTGTCACACCTATGGCATATCACA
VEGF	AGGAGGAGGGCAGAATCATCA	CTCGATTGGATGGCAGTAGCT
GLUT1	GCCATACTCATGACCATCGC	AGCTCCTCGGGTGTCTTATC
YWHAZ	ACTTTTGGTACATTGTGTGGCTTCAA	CCGCCAGGACAAACCAGTAT

Table 7: List of primers used in this thesis. From (255, 256).

10. Colony-forming assay:

NB cell lines were plated in 6-well plate at 500 cells *per* well (LAN-1) or 1000 cells *per* well (SH-SY5Y) in 3 mL of regular media and kept in standard conditions for 24h enabling cellular attachment. Then, regular media was replaced by different conditioned media CM-NB, CM-BM, CM-BM/NB or CM-CNT and cultured under normoxic or hypoxic conditions (n=3). After

15 days, colonies were fixed with 4% paraformaldehyde for 30 minutes and stained with a mix of 2% crystal violet and 20% methanol for 10 minutes. Colonies were photographed (10x) to evaluate their number, morphology and size by using the software GraphPad Prsim 8 (La Jolla, Ca).

11. Drug activity assays:

11.1. Cytotoxicity (IC50):

The cytotoxicity of AMD-3100 (Selleckchem), ISO-1 (Selleckchem) and 4-IPP (Merck) was assessed at different concentration ranges using MTS assay (Promega). All drugs were diluted with ethanol at a stock concentration of 10 mM. Cell lines and primary cultures were plated at 2000 cells *per* well (LAN-1 and SH-SY5Y), 8000 cells *per* well (IMR5) or 50000 cells *per* well (BM) in 100 µL of regular media in 96-well plates for 24 h. Then, each drug was added at a specific concentration range: AMD-3100 (50-0.0001 µM), ISO-1 (50-0.2 µM), 4-IPP (50-0.2 µM) (n=6 *per* each concentration). After 72 hours, the percentage of viable cells for each treatment was compared to control wells (drug vehicle), which were considered as 100% viable. The half maximal inhibitory concentration of tumor cell viability (IC50) was calculated with nonlinear regression log (inhibition) vs. response Variable slope (four parameters) using the software GraphPad Prsim 8 (La Jolla, Ca).

11.2. Drug response to conditioned media:

Here, we evaluated whether our BM-based model could modify *in vitro* NB response to different chemotherapy agents including SN-38, doxorubicin and etoposide. Cells were plated at 2000 cells *per* well directly in CM-CNT or CM-BM/NB and exposed to normoxia or hypoxia. After 24 h, drugs were added at different concentration ranges: SN38 (500-0.076 nM) doxorubicin (2500-0.381 nM) and etoposide (3750-0.572 nM). After 72 h, a MTS assay was performed and IC50 concentrations determined for each different drug and culture condition.

12. Cell migration analysis:

To explore if our BM-based cell culture conditions could promote NB cell migration, we performed wound healing assays. NB cells were plated into 6 well plates until they reached total confluence. Then, a mechanically disruption (or wound) was performed by scratching the monolayer cell surface with a pipette tip. Non-adhered cells were washed with PBS and regular media was replaced by each CMs and incubated in normoxic or hypoxic conditions. In order to quantify cellular migration towards the wound, pictures were taken right after the insult and 24 h later.

In a second set of experiments, cells were treated with 5 µM of 4-IPP or 10 nM of AMD3100 together with CM-BM/NB to test the effect of the drug over pro-migratory phenotype in the selected culture conditions. The percentage of wound surface reoccupied by cellular migration was measured with Image J Plugin Wound Healing Tool by RIO Imaging.

13. Invasion Assay:

To test how our BM-based model could promote cell invasion in NB cells, we utilized an 8.0 µM pore membrane Cell Culture Inserts Transwells (Falcon). These Transwells were pre-coated with Matrigel (10% in RPMI media) and allowed to polymerize up to 2 hours at 37ºC. Upper chambers were then filled with $2x10^5$ cells *per* well in 200 µL of regular media with 1% iFBS, whereas lower chambers were filled with 500 µL of each CMs. Cells were incubated in normoxic and hypoxic conditions for 96 h. Each Transwell condition was performed in triplicates.

In a second set of experiments using inhibitors, cells were pre-treated overnight with 10 nM AMD3100 or 5 µM 4-IPP and then plated in Transwell's upper-chambers at the same drug concentration in regular media with 1% iFBS under hypoxia. Lower-chambers contained CM-BM/NB. These experiments were repeated at least with two different batches of CMs.

Finally, the medium with non-invaded cells was aspirated and the underside of Transwell membrane carefully washed with PBS, fixed with 4% paraformaldehyde for 30 minutes and stained with a mix of 2% Crystal violet and 20% methanol for 10 minutes. Invasion was

assessed measuring three representative areas *per* membrane using light microscopy (20x; DM 5000 B Leica).

14. Flow Cytometry:

14.1. Bone marrow characterization:

We interrogated our BM primary cell cultures for surface expression of markers present in BM population stromal cell populations. At day 15 of BM expansion, BM cells (n=6) were de-attached and washed with blocking-PBS. A total of $5x10^5$ cells *per* tube were stained with two panels of fluorochrome conjugated antibodies (Becton Dickinson Bioscience). Panel 1 included CD11b-PE, CD105-FITC, CD45-V500, CD34-PerCP, CD19-PeCy7, CD123-APC and panel 2 included CD90-PE, CD45-V500, HLA-DR-PerCP, CD19-PeCy7, CD117-APC (**Table 3**). A primary culture of BM-derived mesenchymal stem cells (MSCs) isolated from a non-oncologic patient was used as a control sample for mesenchymal markers (CD90, CD105 and HLA-DR). A non-stained tube was used as negative control to detect unspecific signals. Percentages of cell population were calculated as the ratio of positive stained cells for each marker over the total population. Sample acquisition was performed in a FACSCanto II (BD Biosciences) and all channels were previously compensated for fluorescence spillover. Data analysis was performed with Novoflow software (Acea Bioscience).

14.2. Membrane receptor detection:

To evaluate membrane receptor levels in response to our BM-based model, we performed flow cytometry relative quantification. NB cells were plated at $5x10^4$ cells *per* well in a 6 well plate. After 24 h at regular culture conditions, floating cells were removed and regular media was replaced with each different CM; CM-CNT, CM-NB, CM-BM, CM-BM/NB, under normoxic or hypoxic conditions up to 72 h. Flow cytometry studies were performed at sub-confluent culture conditions. Then, cells were washed with PBS previous to being collected non-enzymatically with Versene (Thermo Fisher Scientific) incubation for 10 minutes at room

temperature. De-attached cells were washed once with blocking-PBS previous to being stained with fluorescent conjugated primary antibodies for 30 minutes at room temperature and protected from light exposure. Primary antibodies include CXCR4-PE (1:10; R&D Systems; FAB170P), CD74-Alexa647 (1:10; R&D Systems; FAB35901R) (**Table 3**). After incubation, samples were washed with blocking-PBS and stained with 4′,6-Diamidine-2′-phenylindole dihydrochloride (DAPI) (Sigma-Aldrich) at a non-toxic concentration of 0.2 µg/mL to dismiss dead cells from the analysis. Samples were analyzed with the flow cytometer ACEA Novocyte 3000 (Acea Bioscience Inc.) and results processed with NovoExpress Software (Acea Bioscience Inc.).

14.3. Neuroblastoma and bone marrow co-cultures:

We performed co-cultures combining NB and BM cells in order to evaluate the specific vulnerability of tumor but not BM cells to MIF inhibition. Thus, NB cells were plated at $5x10^4$ cells *per* well in regular media and allowed to attach for 24 h. Then, right after gradient density selection, BM cells were counted and pleated in a ratio of 10:1 (BM:NB) together with 30 µM of 4-IPP or vehicle. NB and BM cells cultured alone were used as positive and negative controls, respectively. After 72 h, floating and attached cells were collected together and washed with blocking-PBS. Then, samples were stained with CD45-PE antibody for 30 minutes at room temperature avoiding light exposure (**Table 3**). After incubation, samples were washed with blocking-PBS. In order to quantify dead cells, samples were stained with 0.2 µg/mL DAPI and then analyzed with ACEA Novocyte 3000 Flow Cytometer (Acea Bioscience Inc.). Sample acquisition and results analyses were performed with NovoExpress Software (Acea Bioscience Inc.)

14.4. Gating protocol:

Flow cytometry gating examples applied to analyze cell samples are depicted in **Figure 2**. First population (P1) was selected with a dot plot facing SSC-H to FSC-H (**Figure 2 A**). Next (P1) population was gated to select singlet events in a dot plot facing FSC-H to FSC-A creating a singlet population (**Figure 2 B**). Finally, singlet population was gated to discard

dead cells, samples were stained with DAPI and selected by facing Pacific Blue signaling to Count in a histogram plot (**Figure 2 C**). This gating protocol was applied to each analyzed sample to select a population composed of alive singlet cells for further comparisons.

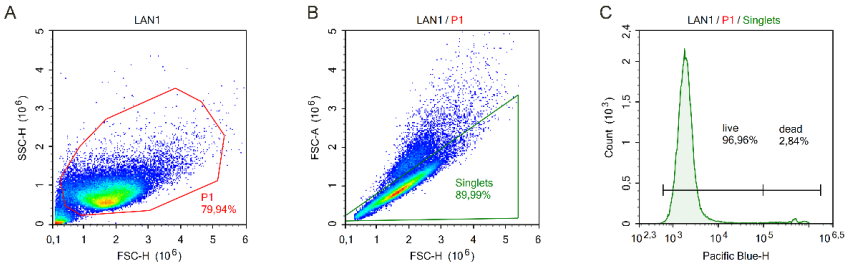

Figure 2: Example of flow cytometry gating applied to each sample in this project. **A** Main population selection (P1). **B** Singlet population selection from P1 **C** DAPI negative population as live events in P1>Singlets.

15. In vivo assays:

In vivo experiments were performed at the animal facility at our institution according to European directive (EU Directive 2010/63/EU) and local animal ethics committee (CEA9330). Xenograft models were generated by injecting NB cells subcutaneously into female athymic nude mice (Envigo). Each animal was injected in both flanks with $5x10^5$ to $1.5x10^6$ LAN-1 cells diluted in 100 µL of Matrigel : RPMI mixture (vol : vol) depending on the experiment protocol. Animal follow-up was carried out every 3-4 days by weight control and measuring tumor volumes with a caliper. To calculate tumor size (mm^3), we used the following formula: $1/2(length \times width^2)$ (*257*). Endpoint criteria for any animal procedure was set when tumor size reached 2000 mm^3 in a single flank or animal lost 20% of weight. Mice were ethically euthanized by cervical dislocation. Samples including tumors and healthy tissues of the animals were collected in formaldehyde solution or snap-frozen at -80Cº for posterior experiments.

15.1. Neuroblastoma and bone marrow co-injection:

Here, we studied whether subcutaneous injection of NB cells together with BM cells affected tumor engraftment and development. We compared LAN-1 engraftment, growth and survival after implantation alone or co-injected with BM cells in a 1:1 ratio. Briefly, mice were subcutaneously injected as follows:

- NB group; injected with 5 x 10^5 LAN-1 cells *per* animal *per* flank (n=18)
- BM/NB group; injected with 5 x 10^5 LAN-1 cells plus 5 x 10^5 of *in vitro* expanded BM primary cells (n=22)
- BM group; injected with 5 x 10^5 of *in vitro* expanded BM primary cells (n=4)

Tumor follow-up was performed as described above. Data from two different *in vivo* experiments are represented together. Engraftment and survival analyses were calculated by Kaplan-Meier Method performed with GraphPad Prism 8 software.

15.2. 4-IPP and Dinutuximab treatment

We interrogated the antitumor efficacy of the MIF inhibitor 4-Iodo-6-phenylpyrimidine (4-IPP) (Merck) in a model of NB minimal residue disease. For *in vivo* treatment studies, 4-IPP was diluted in corn oil (Sigma-Aldrich) as previously described (*241*). For tumor generation, LAN-1 cells were injected subcutaneously into athymic nude mice (1.5 x 10^6 cells *per* flank) as described above. Seven days post-injection mice were randomly distributed in four different groups:

- Control; vehicle via intraperitoneal route (n=14)
- 4-IPP; 80 mg/kg via intraperitoneal route; 3 days a week every 2 days for 4 weeks (n=10)
- Dinutuximab; 2.85 mg/m^2 (20 µg *per* mice) via intravenous route; 2 days a week every 3 days (n=10)
- Combination; same dosages as single-agent regiments (n=10)

16. Statistics:

Statistical analysis was performed with Graphpad Prism 8 software (La Jolla, USA). Detailed information for each analysis is specified in figure captions.

RESULTS:

1. Neuroblastoma bone marrow microenvironment model

1.1. *Generation of conditioned media to recapitulate the bone marrow niche*

The aim of the present study was to develop and establish an *in vitro* model that recapitulated BM microenvironment of patients with NB. For this purpose, we needed to recapitulate some of the major features of the BM microenvironment such as the secretome of the highly heterogenic cellular population that characterizes this niche.

Here, we aimed to reproduce *in vitro* the heterogeneity of the BM of NB patients. To this end, we established primary cultures from 20 BM aspirates obtained from 14 different high-risk NB patients collected at different time points of the clinical evolution of the disease. BM primary cells were directly plated in culture after performing a density gradient isolation, which allows to preserve mononuclear cells and remove erythrocytes and granulocytes (**Figure 1 A**). After 15 days, BM cultures showed a heterogenic phenotype under the microscope. The main expanded cell population had an adhesive fibroblast-like morphology; however, additional cells resembling macrophages and lymphocytes were also identified (**Figure 1 A**). In order to characterize these different cell populations, we stained BM cultures with different lineage-specific markers for flow cytometry analysis (BM cultures n=6, each one from a different patient). A predominant cell population was positive for mesenchymal markers including CD90, CD105 and HLA-DR (51.3±22.7%, 35.0±18.2%, 16.0±4.2%, respectively). As a positive control for mesenchymal markers, we used a previously generated BM-MSC cell culture derived from a non-oncologic patient. This purified and characterized cell culture was also positive of CD90, CD105 and HLA-DR (99.8%, 99.4% and 71.52% respectively). In addition to the mesenchymal population, BM cultures also stained for the myeloid-linage marker CD11b (16.9±6.5%), lymphoid-lineage marker CD19 (13.9±7.7%) and dendritic cell marker CD123 (6.0±8.2%). Residual cell populations stained for the endothelial cell marker CD34 (0.2±0.06%) and hematopoietic stem cell marker CD117 (1.1±0.5%) (**Figure 1 B-C**).

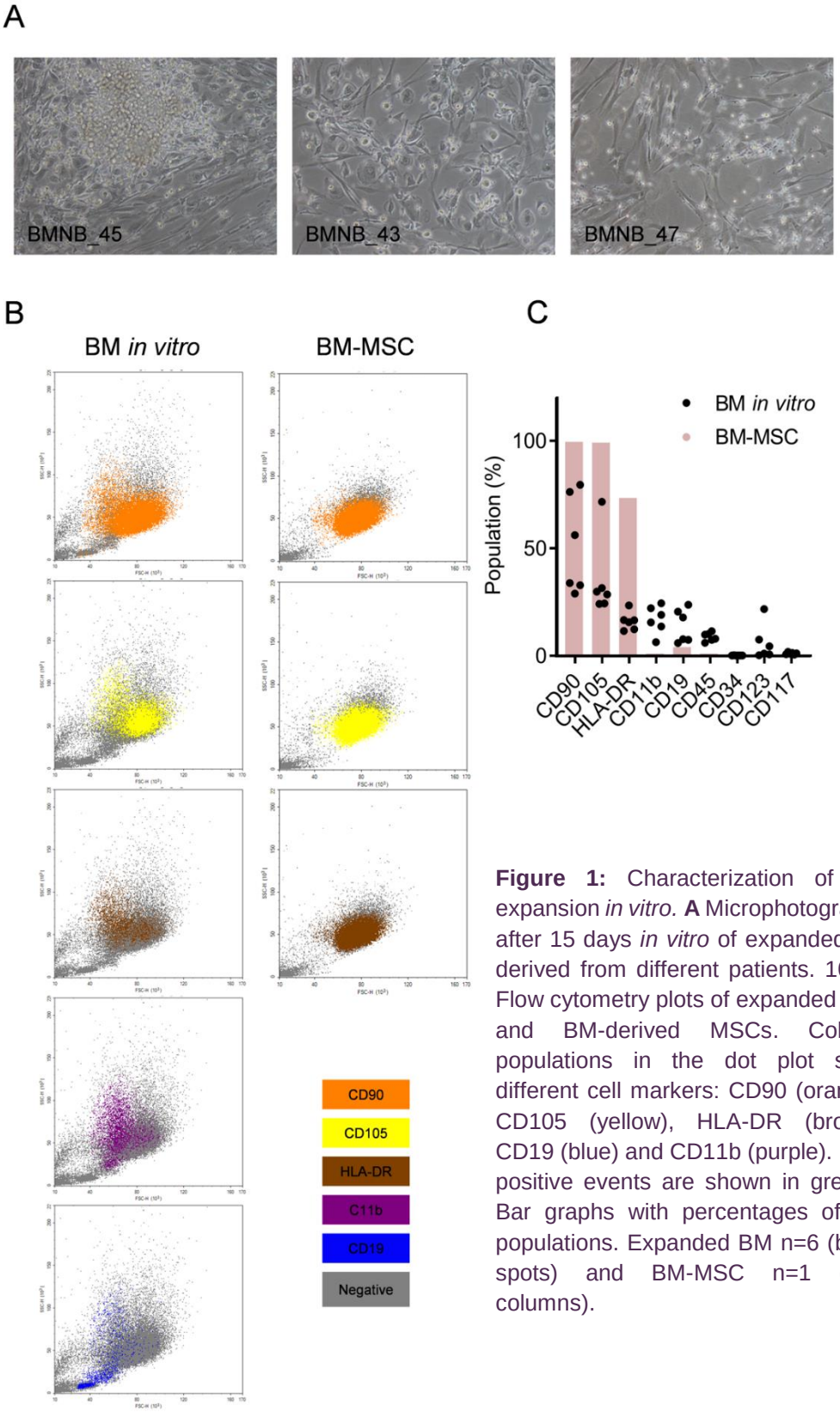

Figure 1: Characterization of BM expansion *in vitro.* **A** Microphotography after 15 days *in vitro* of expanded BM derived from different patients. 10x **B** Flow cytometry plots of expanded BMs and BM-derived MSCs. Colored populations in the dot plot show different cell markers: CD90 (orange), CD105 (yellow), HLA-DR (brown), CD19 (blue) and CD11b (purple). Non-positive events are shown in grey. **C** Bar graphs with percentages of cell populations. Expanded BM n=6 (black spots) and BM-MSC n=1 (pink columns).

After expansion, BM cells were incubated alone or in combination with NB cell lines in order to obtain CMs from different sources. After 48 h in standard conditions, supernatants were collected, centrifuged and kept at -80ºC for future procedures. With this approach, we generated three different types of CM: BM primary cells cultured alone (CM-BM) or co-cultured with NB cells (CM-BM/NB), and NB cells cultured alone (CM-NB).

In order to characterize the secretome, in the form of CMs, we used a Cytokine Profile Array that permitted to detect released cytokines (**Figure 2 A**). Seven out of 36 cytokines (MCP-1, CXCL1, IL-1ra, IL-6, IL-8, MIF and PAI-1) were present in CM-BM and CM-BM/NB, but not in CM-NB. Remarkably, MIF was the only cytokine detected in CM-NB and was detected at similar levels in CM-BM/NB. In addition, secretion of the pro-inflammatory protein MCP-1 was found to be lower in CM-BM/NB compared to CM-BM alone. IL-1ra and PAI-1 levels were higher in CM-BM/NB compared to CM-BM, despite being negative in CM-NB. On the other hand, no evidence of CXCL12 was observed in the CMs (**Figure 2 B**).

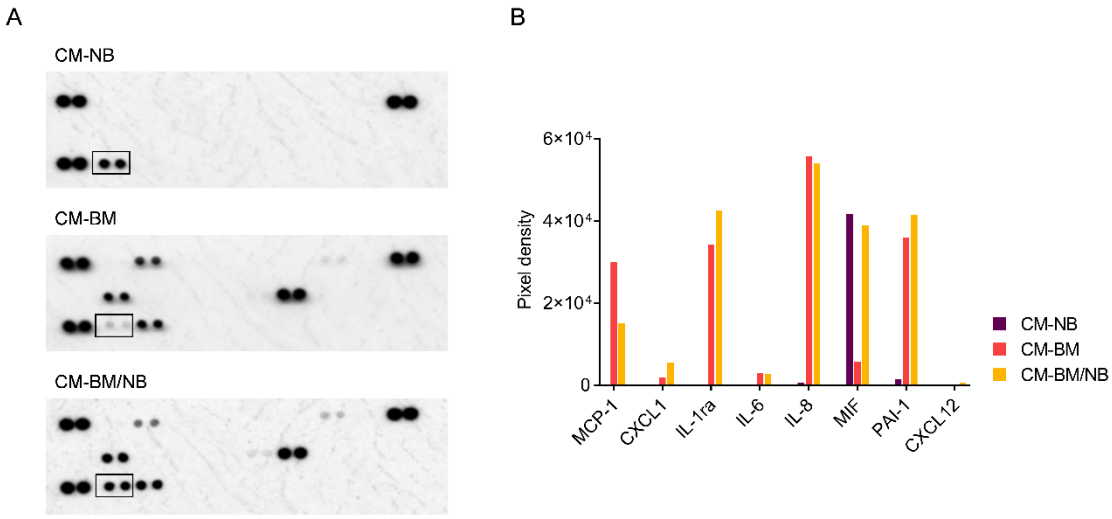

Figure 2: Characterization of CMs. **A** Membranes of CM-NB, CM-BM, CM-BM/NB 36-Cytokine Profile Array, MIF spots are framed. **B** Quantification of cytokines present in CMs; each column represents mean pixel density of duplicate spots.

Cytokine arrays results were validated by ELISA. Secreted MIF was quantified in different batches of CM-NB, CM-BM and CM-BM/NB, obtaining protein concentrations of 7.47±3.52, 3.32±1.76 and 6.07±2.40 ng/mL, respectively. MIF levels diverged among CM-NBs obtained from different NB cells lines and ranged from 14.45 ng/mL in LAN-1 cells to 3.8 ng/mL in IMR5 cells (**Figure 3 A**). These findings suggested that NB cells secreted MIF when cultured either alone or in the presence of BM cells. Additionally, in agreement with the cytokine profile array, no detection of CXCL12 was observed in any CM by ELISA as all signals were below the detection limit of the technique; 31.2 pg/mL (**Figure 3 B**).

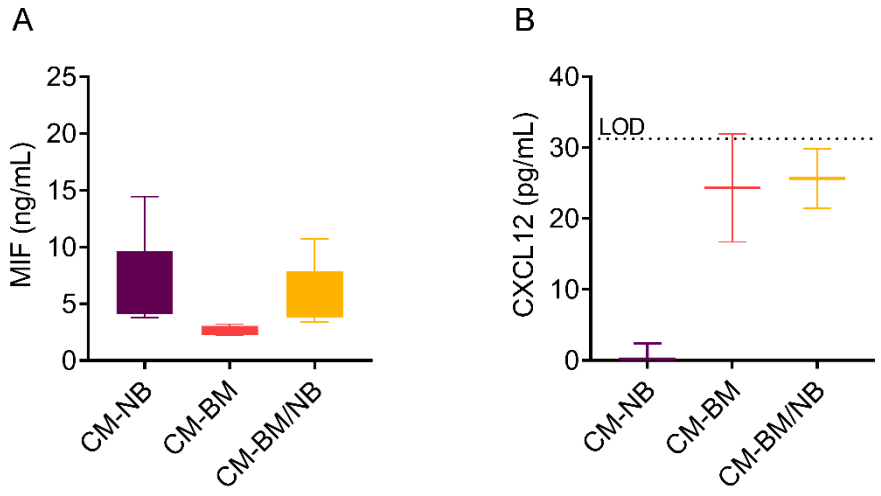

Figure 3: ELISAs from CMs **A** Box plot with quantification of secreted MIF, measured in different CMs batches (CM-NB n=6, CM-BM n=5 and CM-BM/NB n=6). **B** Box plot quantification of secreted CXCL12 measured in different CMs batches (CM-NB n=2, CM-BM n=2 and CM-BM/NB n=2) detected signals were below ELISA kit's Limit of Detection (LOD).

In order to verify the secretome of our CMs, we performed additional cytokine arrays directly on plasma samples obtained from patients' BM aspirates (**Figure 4**). This enabled us to identify matched cytokines between CMs and patient BM samples, suggesting similar properties, and thus validate our experimental approach. Matched cytokines also permitted to identify factors potentially relevant for tumor maintenance/invasion in the BM niche. To this end, we interrogated 105 cytokines using the same technology of Cytokine Profile Arrays in two BM-derived plasmas. These samples were obtained from a patient with NB

(INSS stage 4) disease disseminated to the BM at the moment of relapse (one *PHOX2B*-positive cell among 177 BM cells).

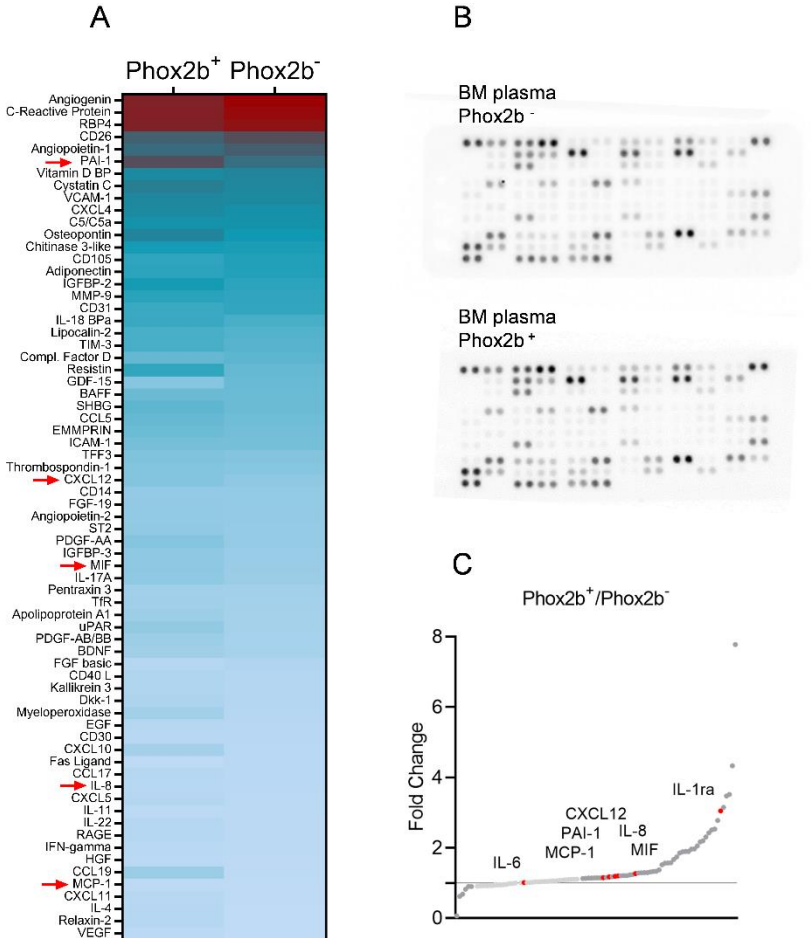

Figure 4: CM's cytokines in correlation with BM plasma. **A** Heat map of pixel densities for 105 cytokine analysis between infiltrated (Phox2b$^+$) and non-infiltrated (Phox2b$^-$) BM plasma **B**. Membranes of 105-Cytokine Profile Array. **C** Paired analysis of BM plasma, infiltrated normalize with no infiltrated. Cytokines highlighted in red are present in CMs, light gray cytokines did not show differences between samples.

Membrane analysis revealed differences between the cytokine profiles (**Figure 4 A-B**). Of the 105 evaluated cytokines, 53 showed increased release in the infiltrated plasma, among these IL-1ra, MIF, IL-8, PAI-1 and MCP-1 were also present in our CM's. Twelve cytokines were found to be negative in non-infiltrated sample but present in the infiltrated one, being CXCL1 one of them. No differences were found in IL-6 levels between the two studied samples. IL-1ra, IL-6, PAI-1 and MIF cytokines showed a similar expression profile between patient-derived BM plasmas and CM-BM and CM-BM/NB, particularly for MIF secreted profiles (**Figure 4 C**).

In summary, after a period of *in vitro* expansion, BM cultures preserved a heterogenic population that partly mimicked the BM cellular complexity. Cytokine secretion profiling showed strong similarities between CMs and patients' BM-derived plasmas, with the presence of MIF but not CXCL12 being common to all the analyzed samples. These finding suggested that the nature of the secretome of CMs was dependent on the BM cells and not on individuality of the BM donor (patient). Moreover, our preliminary results highlighted MIF as a relevant cytokine potentially involved in the interaction between NB cells and the BM-niche. Our CM's recapitulated thus part of the BM cellular heterogeneity and cytokine signaling profile, and enabled us to further explore MIF in the context of NB disease in the BM niche.

1.2. Generation of hypoxic cell culture to mimic bone marrow environment

In addition to cytokine signaling, BM microenvironment is characterized by low oxygen tension, particularly in the HSC niches (*258*). These hypoxic niches were mimicked in our BM-like model by combining CMs (CM-NB, CM-BM, CM-BM/NB or CM-CNT) and different oxygen levels; high oxygen (atmospheric oxygen 21%; herein named normoxia) or low oxygen (physiological BM 1% O_2, 5% CO_2 and 94% N_2; herein hypoxia) levels. Hypoxic conditions were confirmed by analyzing the expression of hypoxic-inducible transcription factor HIF-1α by western blot. We compared LAN-1 cells cultured under normoxia (Nx), hypoxia (Hx) or after treatment with cobalt(II) chloride ($CoCl_2$; 30 and 150 µM), a chemical inducer of hypoxia response (*259*) (**Figure 5 A**).

Response to hypoxia was also confirmed by RT-qPCR. We observed up-regulation of the hypoxia transcription factors *HIF-1A* and *HIF-2A,* as well as the hypoxia response genes *VEGF*, *GLUT1* and *OCT4* in LAN-1, SH-SY5Y and IMR5 at 48 h after cell culture in 1% of oxygen, confirming primary response to reduced oxygen levels. (**Figure 5 B**). Finally, we explored the effects of hypoxia on the activity of the principal signaling pathways using the Proteome Profiler Phospho-Kinase Array. The results showed increased phosphorylation in several intracellular pathways such as cyclic-AMP, PI3K and MAPK at 48 h after hypoxia exposure (**Figure 5 C**). These results confirmed the activation of hypoxic response in NB cells cultured under 1% of O_2.

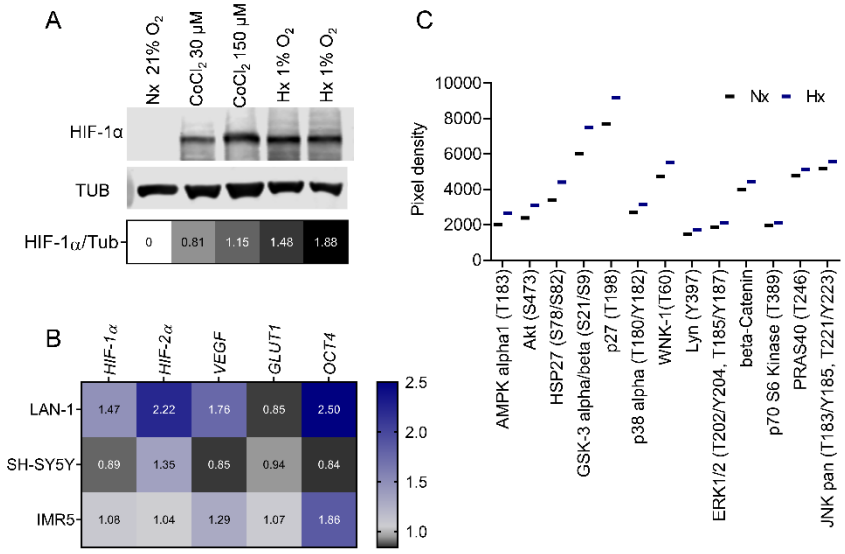

Figure 5: Validation of hypoxia culture. **A** Western blot and head map quantification of HIF-1α on LAN-1 cells after 4 h of each treatment. **B** RT-qPCR results represented as a fold change of normoxia expression levels $2^{(-\Delta\Delta CT)}$. **C** Phosphorylation levels increased after 48 h of LAN-1 culture under normoxia or hypoxia conditions.

2. *Gene expression analysis of the CXCR4/MIF pathway in neuroblastoma tumors and developmental tissues*.

To explore the CXCR4/MIF pathway in NB tumors, we first analyzed expression profiles of genes of interest during dissemination to the BM and then compared them with primary tumors. Firstly, we analyzed a publicly available dataset (Gene Expression Omnibus repository ID: GSE94035) of gene expression obtained by high throughput sequencing (RNAseq). This expression profiling dataset included 16 primary high-risk NB tumors obtained at diagnosis, 42 samples of enriched BM-derived disseminated tumor cells (DTCs; n=22 at diagnosis and n=20 at relapse), as well as 28 BM non-tumor mononuclear cell (MNCs) samples. The DTC enrichment ranged from 18 to 96%.

Our analyses revealed that expression levels of MIF correlated with DTCs-enrichment percentage, being higher in highly enriched samples. This result supported NB cell as the main source of MIF within the BM niche, as previously observed in the CM's. DTCs enrichment levels were consistent with expression levels of the NB marker *PHOX2B*. MIF expression levels were similar between primary tumor samples and DTC samples at diagnostic (data not show). Altogether, these results suggested a stable expression of MIF among primary and disseminated NB cells while supporting NB cells as the principal source of MIF within the BM environment (**Figure 6**).

On the contrary, the receptors CXCR4, CD74, CXCR7, CD44 and CXCR2 were highly expressed in BM-MNCs, whereas showed an inverse correlation with DTC-enrichment percentage. Similar correlation was observed when the expression of PTPRC (CD45) was compared with DTC-enrichment, consistent with NB cells being $CD45^-$ (*260*).

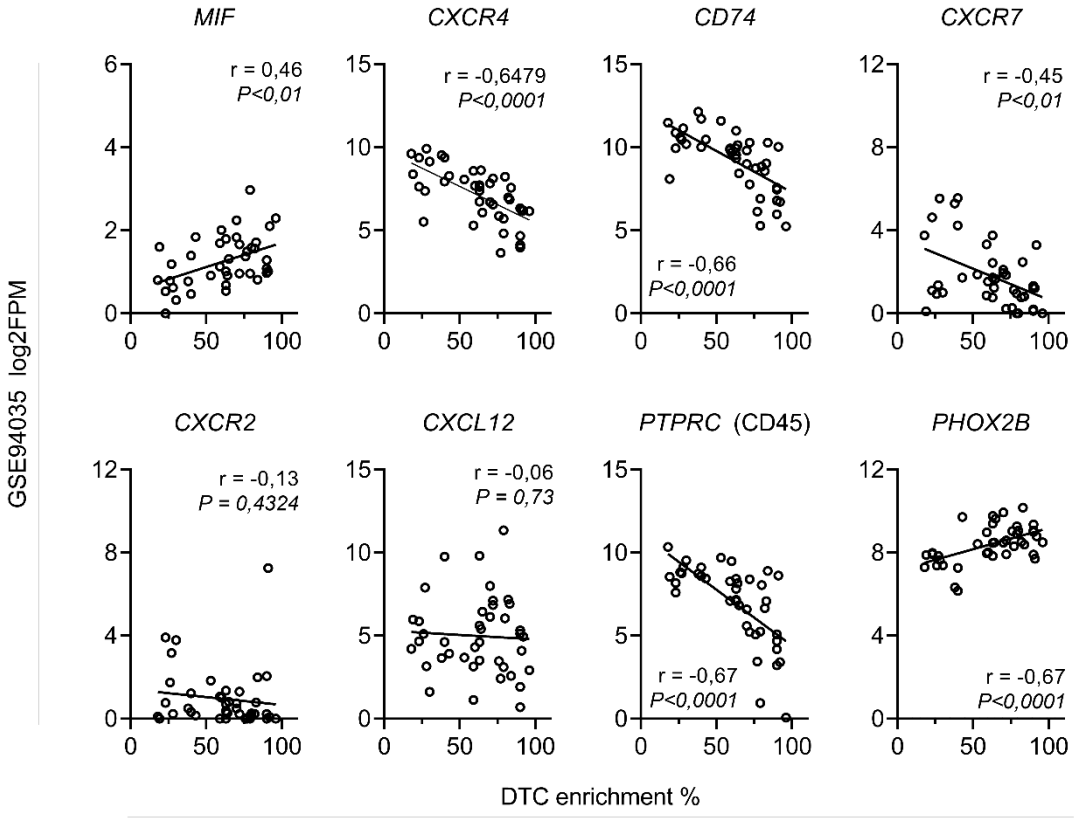

Figure 6: Correlation analysis from GSE94035. Gene expression levels were correlated with disseminated tumor cells (DTC) percentage.

Next, we then focused our analysis on two gene expression datasets obtained from primary NB tumor biopsies obtained at diagnosis (GSE54720 and GSE62564). GSE54720 was a microarray gene expression dataset generated by our group (GSE54720, HSJD, Barcelona). From a total of 21 cases staged following INSS criteria; n=5 stage 1, n=3 stage 3, n=10 stage 4 and n=3 stage 4s. GSE62564 was a publicly available RNAseq dataset of 498 primary NB samples (INSS criteria; n=121 stage 1, n=78 stage 2, n=63 stage 3, n=183 stage 4 and n=53 stage 4s). Clinical data was available for all cases except nine samples, which were excluded from the study. Genes of interest (**Introduction; Figure 13**) were expressed in all tumor samples with similar trends in both datasets; except for the receptors *CXCR2* and *CXCR7* that showed lower expression (GSE62564, mean log2RPM of 1.18±1.49 and 3.0±1.23 respectively) compared to *CXCR4*, *CD74* and *CD44* (GSE62564, mean log2RPM of 5.39±1.07, 8.15±1.31 and 7.71±1.66 respectively) (**Figure 7 A-B**).

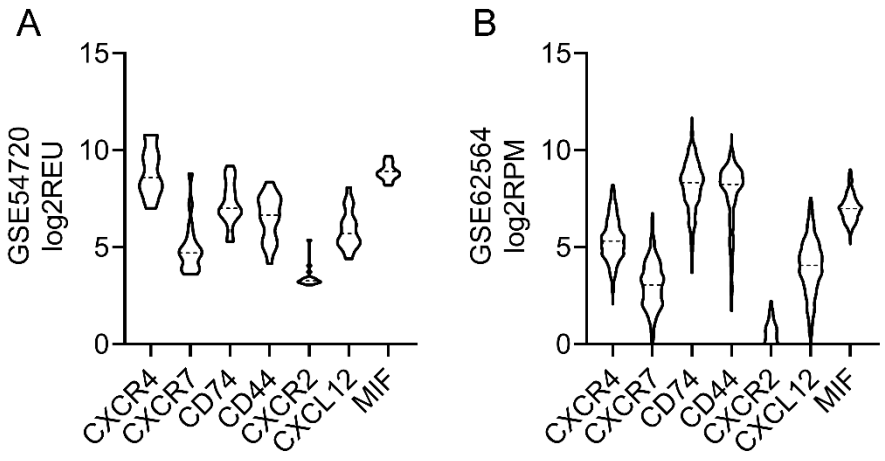

Figure 7: MIF-related genes expression in NB primary tumors in **A** GSE547020 and **B** GSE62564.

We then proceeded to evaluate the association between gene expression levels and NB patient's overall survival. Survival analyses were performed with the GSE62564 for which more than 15 years follow-up data were available (**Figure 8**). We used the Contal-O'Quigley method to determine the optimal cut point to discern two gene expression groups named "high" and "low" (*261*). Survival estimation was then performed using Kaplan-Meier method. Differential gene expression levels of *CXCR4, MIF, CD74, CD44 and CXCL12* were all significantly associated with patient outcome (*P<0.001*). High expression of CXCR4 and MIF were associated with unfavorable overall survival of patients (*P<0.001* and *P<0.0001*, respectively) (**Figure 8 A-B**). In contrast, high expression levels of *CD74*, *CD44* and *CXCL12* were associated with more favorable outcomes (*P<0.0001* each of them) (**Figure 8 C-D**).

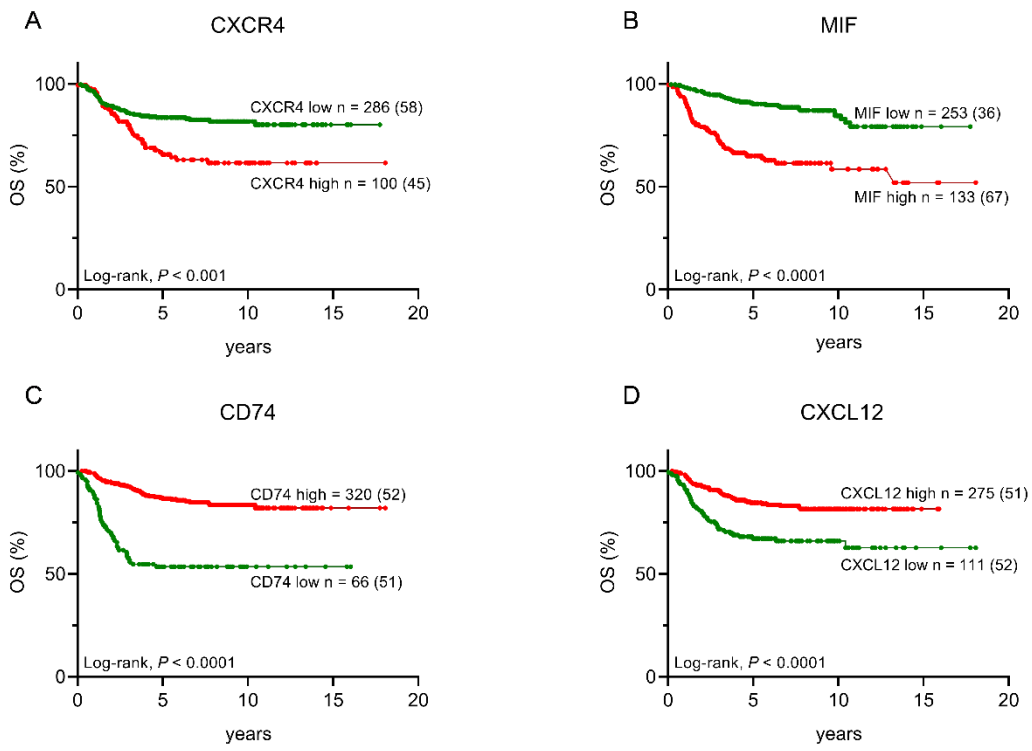

Figure 8: Kaplan Meyers curves representing overall survival analysis of GSE62564 in relation to **A** *CXCR4*, **B** *CD74*, **C** *CXCL12* and **D** *MIF* expression data. High expression is colored in red and low expression in green. (n) number of patients per group while events per group are shown within parenthesis. Overall survival (OS).

Next, we focused on NB tumors which show dissemination to distant sites, INSS stage 4 and Stage 4S NB. Both stages are clinically defined by disseminated disease at diagnosis; however, patients with NB stage 4S show BM infiltration below 10% and are associated with a favorable prognosis, whereas patients with stage 4 show high tumor invasion within BM niche and are associated with unfavorable prognosis (**see Introduction Section 2.1.**). Around 35% of stage 4 NB tumors have *MYCN* gene amplification (*262-264*). Thus, stage 4 samples were also grouped accordingly to these features; non-*MYCN* amplified (na) and *MYCN* amplified (a). Altogether, GSE54720 compiled 3 stage 4S, 5 stage 4 (na) and 5 stage 4 (a), whereas GSE62564 contained 48 stage 4S, 116 stage 4 (na) and 65 stage 4 (a) NB patients.

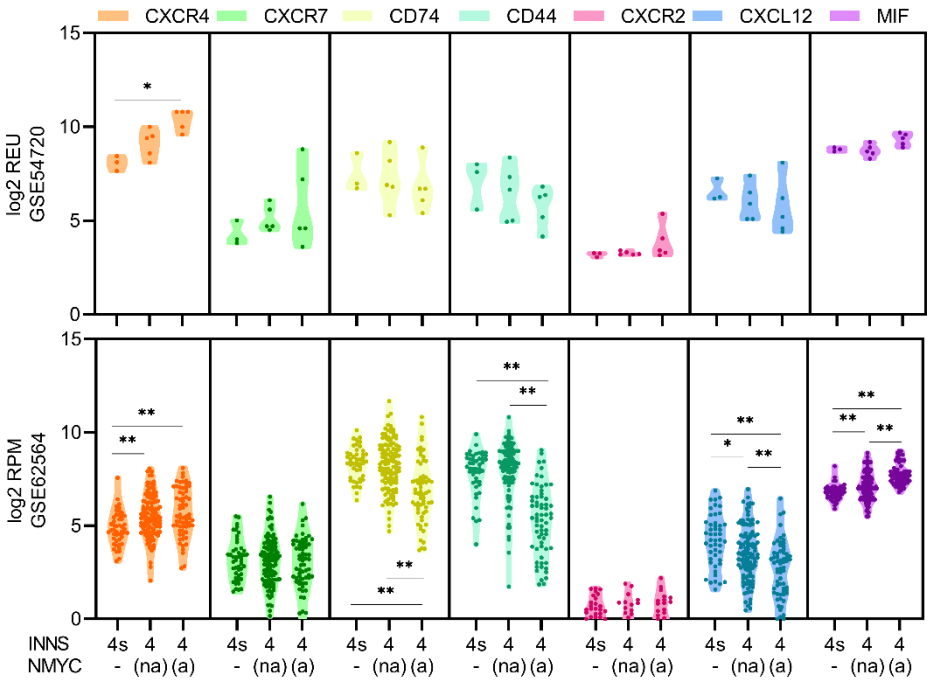

Figure 9: Analysis of studied genes in relation to disseminated neuroblastoma stages in GSE54720 (up) and GSE62564 (down). Violin plot showing gene expression in relation to each neuroblastoma subgroup. (an) non-amplified (a) amplified. One-way Anova Kruskal Wallis test * *P<0.05* and ** *P<0.01*.

The expression of *CXCR4* was enhanced in patients with stage 4 (a) when compared to stage 4S (GSE54720 *P<0.05*; GSE62564 *P<0.01*) or compared to stage 4 (na) (GSE62564 *P<0.01*). In contrast, *CD74* and its co-receptor *CD44* showed lower expression in stage 4 (a) than in stage 4S or stage 4 (na) (GSE62564 *P<0.01* in both), even though there were no differences between stage 4S and 4 (na). *CD74* and *CD44* only achieved significant differences in the GSE62564; however, GSE54720 results showed similar trends despite the smaller sampler size. *CXCR7* and *CXCR2* expression did not show statistical differences among disseminated NB groups (**Figure 9**). Regarding ligands, *CXCL12* expression was higher in stage 4S when compared to stage 4 (both, (na) and (a); *P<0.05* and *P<0.01* respectively; GSE62564). Moreover, stage 4 (na) had increased *CXCL12* levels compared to stage 4 (a) (GSE62564 *P<0.01)*. In contrast, MIF showed the opposite results, being increased in stage 4 (a) compared to stage 4 (na) and stage 4S (GSE62564 *P<0.01* for both*),* as well as increased in stage 4 (na) compared to stage 4S (GSE62564 *P<0.01)*

(**Figure 9**). Results obtained from our analyses emphasized that, besides sharing same the receptors, expression of *CXCR4* and *MIF* was associated with high-risk disseminated NB, whereas *CD74-CD44* and *CXCL12* expression was associated with *MYCN* non-amplified NB tumors.

Next, we interrogated the expression levels of our genes of interest across human development using a dataset derived from tissue-specific biopsies obtained during fetal and post-natal ages (*254*). This database is available at ArrayExpress repository under the code E-MTAB-6814. We analyzed gene expression of *CXCR4*, *CD74*, *CXCL12* and *MIF* during the development of 3 different tissues: brain mesencephalon, n=53 (fetal n=32, pediatric n=12, adult n=9), liver n=49 (fetal n=37, pediatric n=6, adult n=6) and kidney (fetal n=27, pediatric n=9, adult no data) (**Figure 10**). Unfortunately, no data from neural crest or bone marrow was available. For receptors, differential expression was found during brain development, being *CXCR4* highly expressed during fetal period until infancy (6-9 month) and less expressed during childhood and adulthood. On the contrary, *CD74* had low expression levels during fetal development and its expression progressively increased from newborn until childhood (up to 9 years), remaining highly expressed during adulthood. In brain, no clear pattern was found for ligands during development or aging; however, increased *MIF* expression was reported after birth. In liver, *CD74* was homogeneously expressed during pre-natal and post-natal periods, and *CXCL12* tended to increase at post-natal stages and during adulthood. In kidney, a prominent increase of *CD74* occurred after birth and during all pediatric ages. No data were available for adult stages (**Figure 10 A-B**).

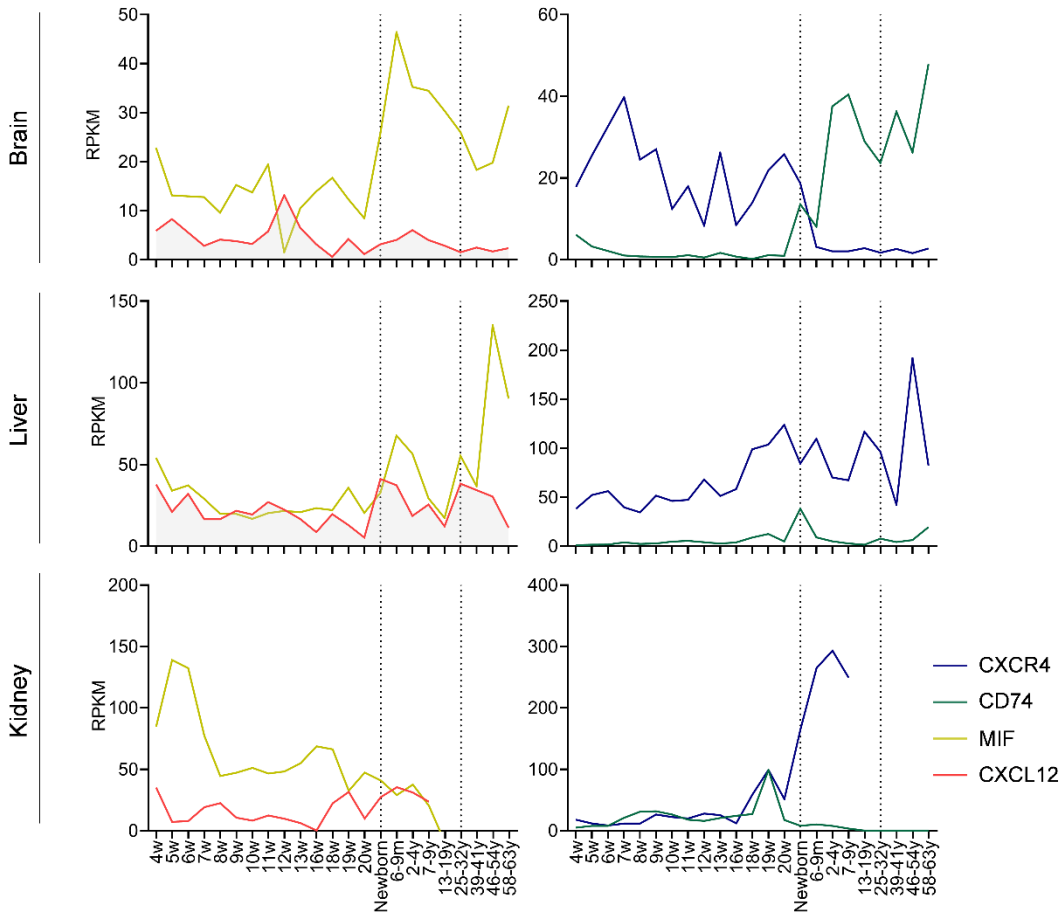

Figure 10: Gene expression data of brain, liver and kidney development and aging. Time-course histogram for receptors (*CXCR4* and *CD74)* and ligands (*MIF* and *CXCL12*).

In summary, high gene expression levels of *CXCR4* and MIF were associated with a more unfavorable outcome of patients with NB, whereas *CD74*, *CD44* and *CXCL12* were associated with less aggressive disease. In addition, *CXCR4* expression in neuroectodermal-derived tissues was higher at embryonal stages, whereas MIF showed increased expression mostly in brain during childhood. This is of interest since NB is an embryonal tumor of neural lineage origin.

2.1. Bone marrow-based in vitro model promotes neuroblastoma viability in bone marrow derived cell lines while increasing CXCR4 membrane expression and activating PI3K and MAPK signaling pathways

Here, we explored the impact of our previously characterized CMs on NB cells i*n vitro*. Together with CMs, NB cells were also cultured under low oxygen levels to better recapitulate the BM niche (*265*). We cultured NB cells in the presence of each CMs (CM-NB, CM-BM, CM-BM/NB or CM-CNT) at both normoxia (Nx; atmospheric oxygen 21%) or hypoxia levels (Hx; 1% O_2, 5% CO_2 and 94% N_2). Cell proliferation and activity of relevant oncogenic pathways were analyzed.

To study the effects of our BM-based model, we measured cell viability as a surrogate marker of NB proliferation using the MTS assay. Fold change of cell viability in a time-course setting (0, 24, 48, 72 and 96 h) was assessed relative to initial values (0 h). Significance was determined comparing each experimental condition to CM-CNT at normoxia (**Figure 11 A**). LAN-1 cells showed a time-dependent increase in cell viability when cultured under BM-derived CM's (CM-BM and CM-BM/NB), this effect was further enhanced under hypoxic conditions. Despite SH-SY5Y cells showed a similar increase upon adding BM-derived CMs, oxygen levels did not affect cell viability over time. In contrast, IMR5 cells, we observed that none of the evaluated CMs increased cell viability and only hypoxia at CM-CNT increased significantly their proliferative capacity (**Figure 11 B**). Studied NB cell lines showed different responses to BM-based model in terms of cell viability. Interestingly, response to BM-derived CM's was mainly observed in NB cell lines obtained in origin from BM infiltration such as LAN-1 and SH-SY5Y. These cell lines were selected for posterior experiments.

A

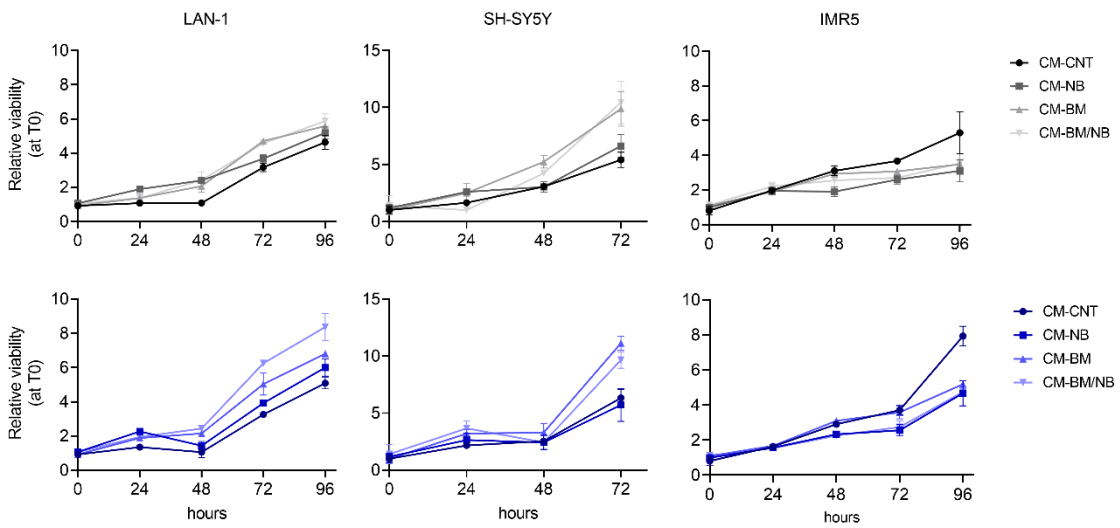

B

P adj. values	LAN-1			SH-SY5Y			IMR5		
	48h	72h	96h	48h	72h	96h	48h	72h	96h
CM-NB	0.002	ns	ns	ns	ns	na	0.0001	0.0008	0.0034
CM-BM	0.0036	<0.0001	ns	0.0004	0.0013	na	ns	ns	0.0152
CM-BM/NB	0.0002	<0.0001	0.0211	ns	0.0004	na	ns	0.0022	0.0181
CM-CNT	ns	ns	ns	ns	ns	na	ns	ns	0.006
CM-NB	ns	0.0287	0.0099	ns	ns	na	0.008	0.0006	ns
CM-BM	0.0017	<0.0001	0.0009	ns	0.0001	na	ns	ns	ns
CM-BM/NB	0.0001	<0.0001	<0.0001	ns	0.0021	na	0.0038	0.0032	ns

FIGURE 11: Viability assays. **A.** LAN-1, SH-SY5Y and IMR5 cell lines cultured in CMs under normoxic and hypoxic conditions performed over 4 days. Data were represented as a fold change viability to time 0 h (n=6). **B.** Table with significances obtained in viability assays. Adjusted P-values were obtained by performing Two-way ANOVA Dunnett's multiple comparisons test, comparing each culture condition to control group Normoxia CM-CNT. Normoxia conditions were represented in shades of grey color, hypoxia conditions in blue color code. Non-significant (ns), non-applicable (na).

No differences in basal CXCR4 or CD74 membrane levels were found among the different cell lines (data not shown). Thus, we next investigated whether the BM *in vitro* model could modulate the amount of MIF receptors on NB cell membrane. To this end, we measured membrane levels of CXCR4 and CD74, which showed in our microarray analysis differential gene expression associated with NB patient outcome (**Figure 8 A-B**). We performed flow cytometry analysis on LAN-1 and SH-SY5Y cell lines at 72 h after exposure to all experimental conditions. Under normoxia, no difference in membrane levels of CXCR4 was

observed in LAN-1 cells, whereas SH-SY5Y increased CXCR4 in all CM's (CM-NB; *P<0.0001*, CM-BM*; P<0.001* and CM-BM/NB; *P<0.0001*) (**Figure 12 A-B**). When hypoxia was added, LAN-1 cells showed a trend, even if not statistically significant, to increase CXCR4 membrane levels particularly in CM-BM and CM-BM/NB (*P =0.11* and *P =0.29* respectively). Similar results were obtained for SH-SY5Y under hypoxia, as an increase of CXCR4 was observed in CM-NB; *P<0.0001*, CM-BM; P<*0.05* and CM-BM/NB; *P<0.001.* Suggesting no effects of hypoxia on this cell line in terms of CXCR4 membrane levels.

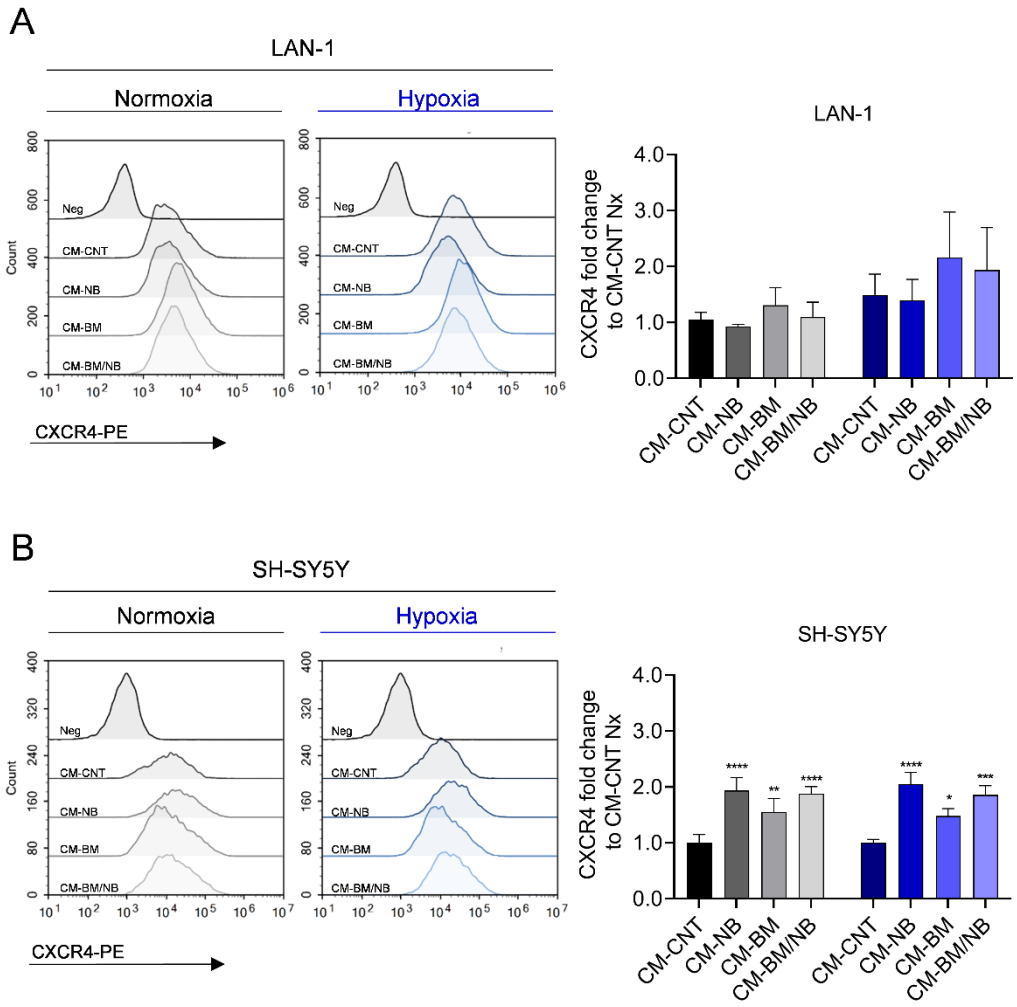

Figure 12: Membrane CXCR4 levels by flow cytometry. **A** Histograms showing CXCR4 membrane levels in LAN-1 cultured under BM-based model at 72 h. **B** Bar graphs with CXCR4 quantification. Data was represented as a fold change to CM-CNT Normoxia (n=3). **C** Histograms showing CXCR4 membrane levels in SH-SY5Y cultured under BM-based model at 72 h. **D** Bar graphs with CXCR4 quantification. Data was represented as a fold change to CM-CNT Normoxia (n=3). Histograms were generated with NovoFlow Software (Acea Bioscience). Normoxia results were represented in a black-grey color code and hypoxia in blue color code. Significances (*) *P<0.05*, (**) *P<0.01*, (***) *P<0.001* and (****) *P<0.0001*.

Regarding CD74, no increase in levels of this receptor was observed under any experimental condition in both cell lines. On the contrary, SH-SY5Y cells showed decreased levels of CD74 in normoxia (CM-NB; *P<0.0001*, CM-BM; *P<0.01* and CM-BM/NB; *P<0.0001*), being even more pronounced under hypoxia (CM-CNT; *P<0.0001*, CM-BM; *P<0.05* and CM-BM/NB; *P<0.001*) (**Figure 13 C-D**).

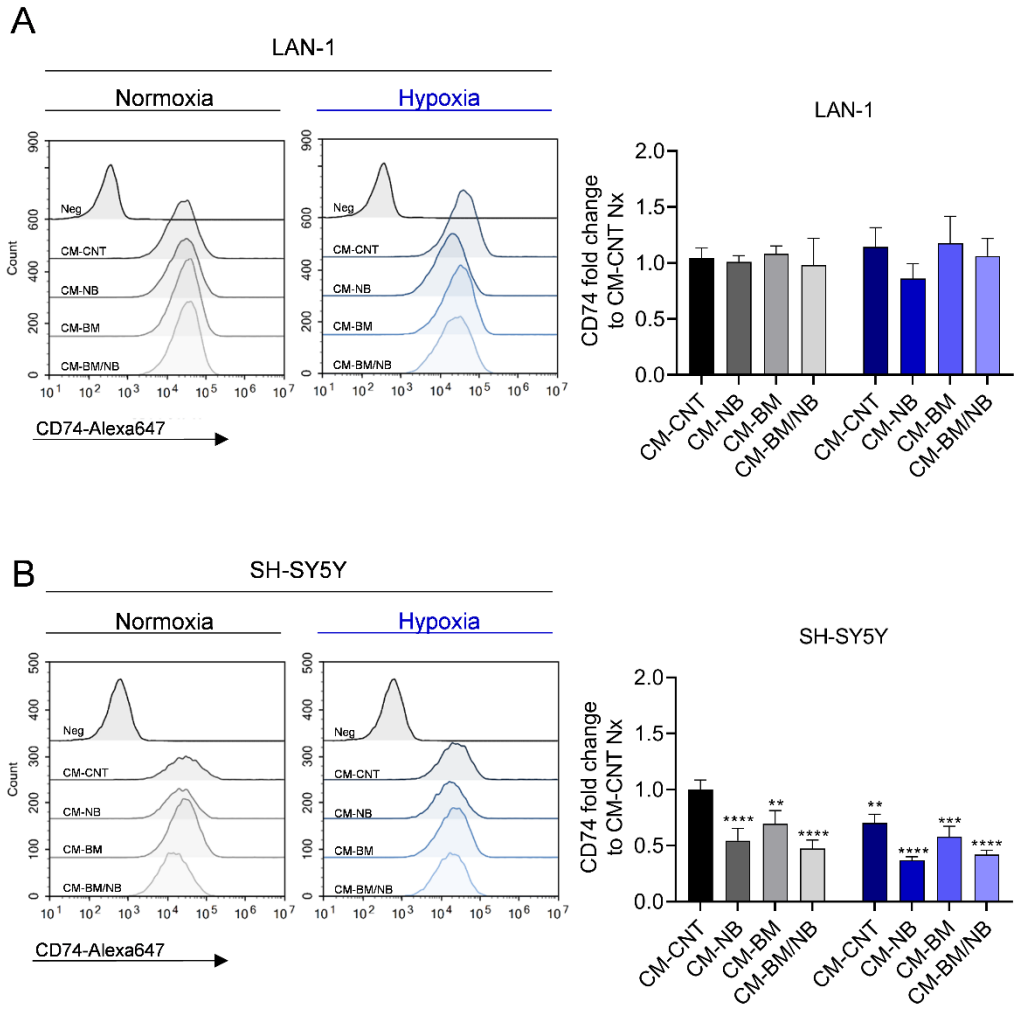

Figure 13: Membrane CD74 by flow cytometry. **A** Histograms showing CD74 membrane levels in LAN-1 cultured under BM-based *in vitro* model for 72 h. **B** LAN-1 CD74 quantification represented as a fold change to CM-CNT Normoxia (n=3). **C** Histograms showing CD74 membrane levels in SH-SY5Y cultured under BM-based *in vitro* model for 72 h. **D** SH-SY5Y CD74 quantification represented as a fold change to CM-CNT Normoxia (n=3). Histograms were generated with NovoFlow Software (Acea Bioscience). Normoxia results were represented in a grey color code and hypoxia in blue color code. Significances (*) *P<0.05*, (**) *P<0.01*, (***) *P<0.001* and (****) *P<0.0001*.

Endorsed by previous studies that linked CXCR4 with the activation of PI3K and MAPK signaling pathways (*215*), we sought to study whether these pathways could be modulated

by our BM-based *in vitro* model. Thus, we preformed western blot assays to quantify phosphorylation levels on AKT(S473) (PI3K pathway) and ERK1/2(T202/Y204 and T185/Y187) (MAPK pathway) after exposure of NB cells to all the experimental conditions. NB cell lines LAN-1 and SH-SY5Y were cultured under the same conditions as in viability assays. After 48h, samples were collected to proceed with protein extraction, quantification and immunoblot detection (**Figure 14**). In normoxia, LAN-1 showed higher pAKT/AKT ratios after exposure to CM-BM and CM-BM/NB, conditions with increased cell viability. Hypoxia increased pAKT/AKT ratios in CM-BM and CM-BM/NB. All conditions showed an increment of pAKT/AKT ratios when compared to their respective normoxia counterparts. Regarding the MAPK pathway, LAN-1 showed higher pERK/ERK ratios in CM-BM and CM-BM/NB, but exclusively when cultured under hypoxic conditions. The increment of pAKT and pERK in LAN-1 exposed to low oxygen levels was previously observed during hypoxia characterization (**Figure 5 C**). SH-SY5Y showed high pAKT/AKT and pERK/ERK ratios in all CM's, particularly in CM-BM. Similar to cell viability results, minor phosphorylation changes were observed between CMs when cultured under hypoxia (**Figure 14 B**).

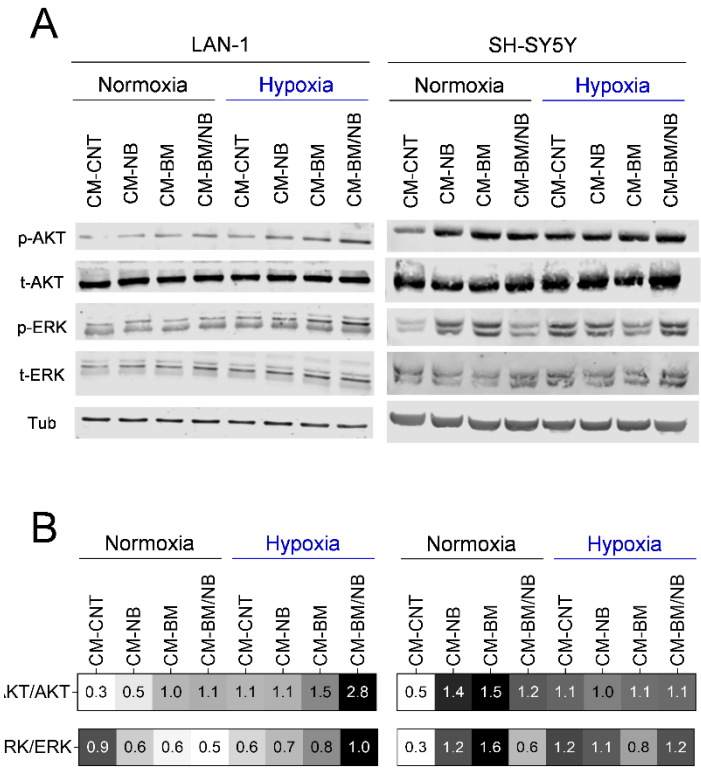

Figure 14: Western blot quantification **A** Images of immunoblots obtained from LAN-1 and SH-SY5Y cells cultured under BM-based *in vitro* model for 48 h. P-AKT (S473) and P-ERK (T202/Y204 T185/Y187). Gamma Tubulin was quantified as a loading control. **B** Heat map with phosphorylation ratios (phosphorylated band / total band). Band intensity levels was calculated with Fiji Software.

Overall, CM-BM, CM-BM/NB and hypoxia increased CXCR4 membrane levels in both BM derived cell lines –LAN-1 and SH-SY5Y-. In addition, western blot results showed an activation of PI3K/AKT and MAPK/ERK signaling pathways in these particular conditions. Altogether, these result suggested a relationship between elevated CXCR4 receptor, cell signaling activation and cell viability observed under in the context of our BM-based model.

The distinct activation of cell signaling pathways and phenotypes that we observed *in vitro* prompted us to explore the effect of our BM-model conditions on the tumorigenic capacity of NB cells. To this end, we performed an *in vitro* colony formation assay (**Figure 15**). LAN-1 cells enhanced colony formation capacity when cultured under hypoxic conditions, across all the CMs applied, as compared to normoxia (**Figure 15 A**). A similar trend was observed for SH-SY5Y cells (**Figure 15 B**). Both cell lines showed a clear phenotype change in colony architecture. Under hypoxic conditions, both LAN-1 and SH-SY5Y showed larger, outspread colonies, with cells less aggregated to each. This was particularly evident for CM-BM and CM-BM/NB conditions. To further explore this phenotype, we performed migration, invasion assays.

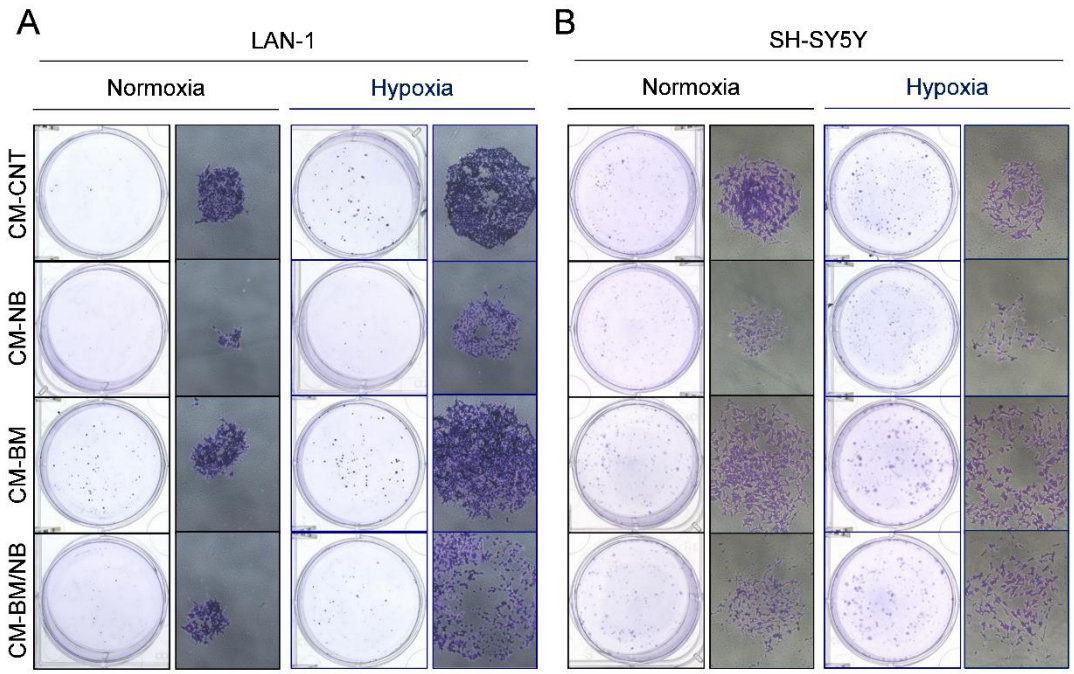

Figure 15: Colony formation assay. **A)** Pictures of LAN-1 fixed colonies stained with crystal violet. Detail of a developed colony aspect (10x). (n=3) **B)** Pictures of SH-SY5Y fixed colonies stained with crystal violet. Detail of a developed colony aspect (10x). (n=3)

2.2. Bone marrow-based in vitro model promotes neuroblastoma aggressive phenotype and favors tumor engraftment in vivo

MIF and CXCR4 signaling has been described to promoted cell migration and invasion in adult carcinomas as well as in pediatric tumors such as rhabdomyosarcomas (*239*). To test the migration capacity of NB cells, we examined monolayer cell migration in response to a mechanical scratch wound after 24 h in the presence and absence of our experimental cell culture conditions. The percentage of open wound area was quantified with Fiji Software.

LAN-1 has been previously described as a low migratory cell line compared to other NB cell lines (*266*). Interestingly, LAN-1 cells showed enhanced migration capacity when exposed to CM, being significant after 24 h exposure to CM-BM and CM-BM/NB under hypoxic conditions (both, *P<0.001*) when compared to control conditions (**Figure 16 A-B**).

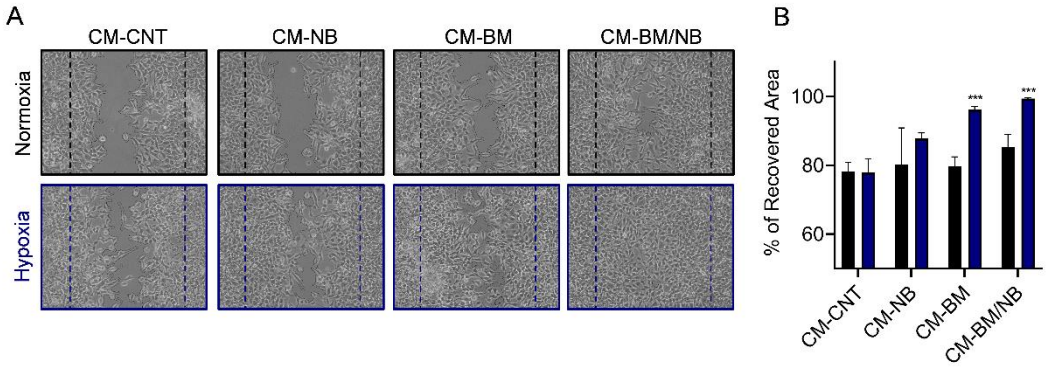

FIGURE 16: Wound healing assay in LAN-1. **A** Wound closure after 24 h, hyphen lines delimitate initial wound edge. **B** Bar graph with recovery quantification. Normoxia results represented in black-grey colors and hypoxia in blue range colors. Statistic differences calculated comparing each experimental condition to control (CM-CNT in normoxia) with Two-way Anova Dunnett's multiple comparison test, (n=3). (***) *P<0,001*.

Next, we tested the ability of our BM-based model to stimulate cell motility and invasion in LAN-1 cells by performing chemotaxis and chemoinvasion experiments (transwell assays). To this end, NB cells were placed in the upper-chamber of matrigel-coated transwells while different CM's were added in the lower-chamber (**Figure 17 A**). After 96h, we assessed the ability of cells to migrate towards the chemoattractant and cross the tissue barrier (Matrigel-

coated membrane). The peak stimulatory effect was observed when LAN-1 cells were cultured under hypoxia and chemo-attracted by CM-BM/NB (*P<0.001*), and to a less extent CM-BM (*P=0.71)* (**Figure 17 B**). These findings demonstrate that the secretome of the CM-BM/NB has a clear chemo-attractant effect on LAN-1 cells, inducing cell migration and invasion across the 3-D matrix barrier toward it. These observations are in agreement with the results of the wound healing assays.

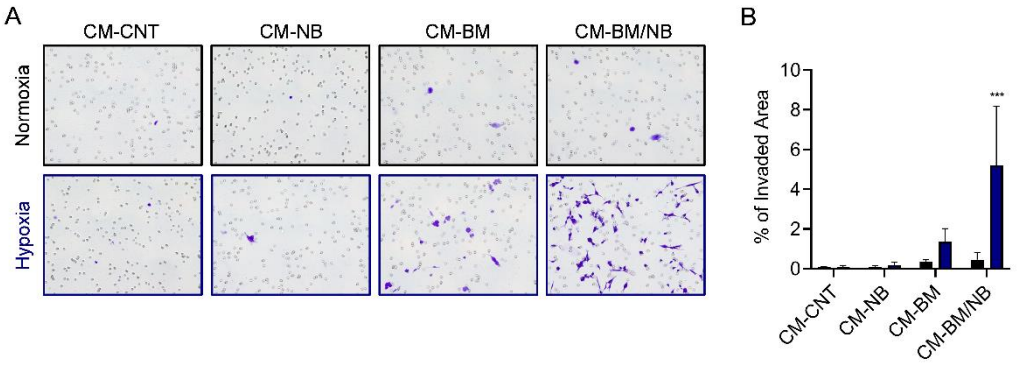

FIGURE 17: Transwell invasion assay in LAN-1 cells. **A** Pictures of migrated cells (Crystal Violet stained) after 96 h of culture. (20x magnification) **B** Quantification of invaded area of membranes. Normoxia (black-grey) and hypoxia (blue-range). Differences were calculated comparing each experimental condition to control (CM-CNT in normoxia) with Two-way Anova, Dunnett's multiple comparison test. (n=3). (***) *P<0.001*.

Altogether, NB exposure to *in vitro* BM-based model reported enhanced cell viability, activation of PI3K/AKT and MAPK/ERK signaling pathways, increased cell migration, invasion and chemo-attraction particularly with CM-BM/NB in hypoxic conditions.

To further explore the effect of BM microenvironment on NB tumor cells, we injected subcutaneously into each flank of athymic nude mice LAN-1 cells either alone (NB group, 5 x 10^5 *per* flank) or mixed with expanded BM cells (1:1 ratio; group BM/NB). As negative control, a small group of mice were injected with BM cells alone (group BM). Time to tumor cell engraftment, tumor growth rate, morphology, invasion capacity, metastasis incidence and recipient mouse survival were assessed until tumors reached the end-point criteria (1500 mm^3) (**Figure 18**).

Both groups –NB and BM/NB group- showed an engraftment of 100%. Interestingly, the median engraftment time was significantly shorter in BM/NB compared to NB group (16 vs 43.5 days) (*P<0.05*). As expected, no engraftment or evidence of disease was observed in

the BM group, where BM cells progressively disappeared (**Figure 18 A**). Macroscopic aspect of tumors was similar, being all highly vascularized. The BM/NB group showed a shorter, albeit not significant, survival time when compared to NB group (95 vs 106 days) (**Figure 18 B**). In addition to the subcutaneous masses, both groups developed macroscopic disseminated disease to distant lymphoid ganglia. The incidence of metastasis was similar in both groups, as 6 out of 12 in BM/NB group and 4 out 8 in NB group were observed (data not show).

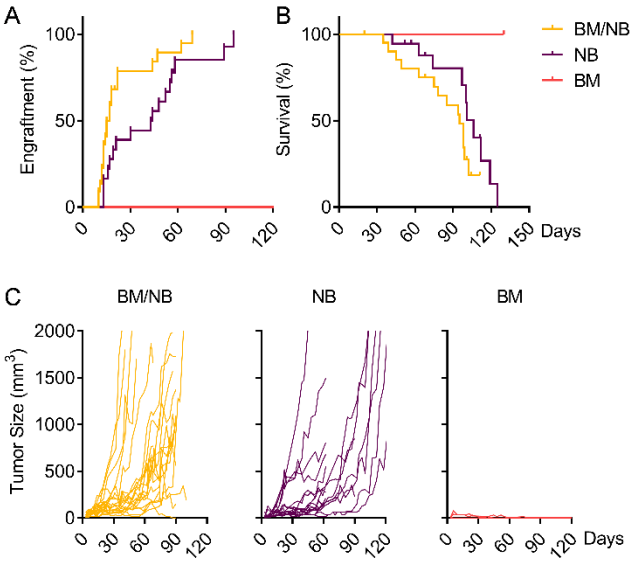

FIGURE 18: Effects of BM cells in LAN-1 xenograft. **A)** Engraftment curves for each group. Engraftment event was reported at 100 mm^3 tumor size. **B)** Survival curves for each group. Survival event was reported at 1500 mm^3 tumor size. **C)** Plot of individual tumor size for each group.

These results suggested that BM cells contribute to generate a favorable microenvironment that promoted a more rapid engraftment of NB cells (LAN-1). However, the beneficial effect on NB cells was restricted to the first few weeks of tumor growth, probably due to the short survival of BM cells within the model. This further supports the importance of BM microenvironment for NB growth.

2.3. Bone marrow-based in vitro model stimulates neuroblastoma chemotherapy resistance

Here, we studied whether the BM-based model affected NB response to chemotherapy. We tested LAN-1 response to drugs included in chemotherapy protocols of patients with high-risk NB tumors, specifically SN-38 (irinotecan) (500-0.08 nM), doxorubicin (2500-0.38 nM) and etoposide (11250-1.7 nM) (**Figure 19**).

Under control conditions (CM-CNT and normoxia), IC50 values were 1.49 nM (1.34-1.65 nM) for SN-38, 27.43 nM (22.17-34.3 nM) for doxorubicin and 491.3 (447.4-546.8 nM) for etoposide (**Figure 19 A**). Our BM-based model affected LAN-1 sensitivity in a drug-specific manner. SN-38, a topoisomerase I inhibitor, showed less cytotoxicity when LAN-1 cells were cultured in hypoxic conditions in both CM-CNT and CM-BM/NB ($P<0.01$ and $P<0.05$); whereas, CM-BM/NB in normoxia did not increase SN-38 resistance (**Figure 19 B**). In contrast, the DNA intercalant agent doxorubicin showed higher IC50 values and corresponding less cytotoxicity in cells cultured with CM-BM/NB regardless of oxygen levels (**Figure 19 D**). Finally, etoposide, a topoisomerase II inhibitor, showed higher IC50 values in all culture conditions compared to CM-CNT at normoxia ($P<0.05$) (**Figure 19 E-F**). The high IC50 values observed for etoposide at basal levels suggested intrinsic LAN-1 resistance to this drug, independent of the BM cell culture conditions. Taken together, CM-BM/NB increased LAN-1 resistance to doxorubicin and etoposide whereas SN-38 resistance seemed to be related with a hypoxic environment.

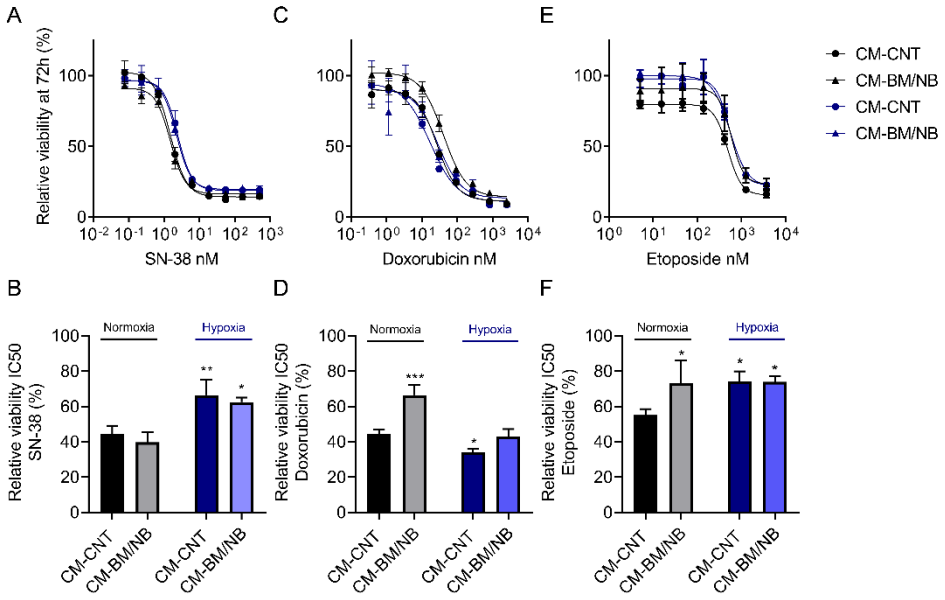

FIGURE 19: Cytotoxic activity of chemotherapy compounds on LAN-1 cells cultured with BM-based model at 72 h. **A** SN-38 cytotoxicity at different BM-based model culture conditions. **B** Relative LAN-1 cell viability at SN-38 IC50. **C** Doxorubicin cytotoxicity at different BM-based model culture conditions. **D** Relative viability at doxorubicin IC50. **E** Etoposide cytotoxicity at different BM-based model culture conditions. **F** Relative viability at etoposide IC50. Normoxia (black-grey) and hypoxia (blue-range). Differences were calculated comparing each experimental condition to control (CM-CNT under normoxia) with Two-way Anova, Dunnett's multiple comparison test. (n=3) (*) *P<0.05*, (**) *P<0.01* and (***) *P<0.001*.

3. Therapeutic targeting of MIF induces tumor-specific cell cytotoxicity in neuroblastoma

One of the specific objectives of our study was to identify novel therapeutic strategies to reduce aggressiveness and invasiveness of NB cells present in the BM niche. To this end, we explored different pharmacological approaches to target MIF and CXCR4 as potential critical mediators for NB progression within BM niche (**Introduction; Figure 13**).

First, we explored the potential antitumor effect of the CXCR4 antagonist AMD3100 (Plerixafor), a drug that impairs CXCR4/CXCL12 interactions and CXCR4 signaling (*249*). We performed MTS assays in order to evaluate whether AMD3100 at a concentration range of 50 µM to 0.0001 µM could affect NB cell viability. In regular culture conditions (RPMI supplemented with 10% iFBS, L-glutamine and Penicillin/Streptomycin), concentrations

below 1 µM of AMD3100 did not affect cell viability; however, at concentrations above 1 µM, the drug stimulated NB cellular viability in all tested cell lines. Although in contrast with what we expected, similar results of AMD3100 have been previously described by Berning P. *et al*. in Ewing sarcoma and NB cell lines, where authors suggest a compensatory feedback interaction between CXCR4 and other tyrosine kinase receptors (*267*).

No differences in drug response were observed when cultured under different oxygen levels (**Figure 20 A**). In addition, we also confirmed a dose-dependence down-regulation of CXCR4 by flow cytometry when LAN-1 cells where treated with AMD3100 at regular conditions (**Figure 20 B)**.

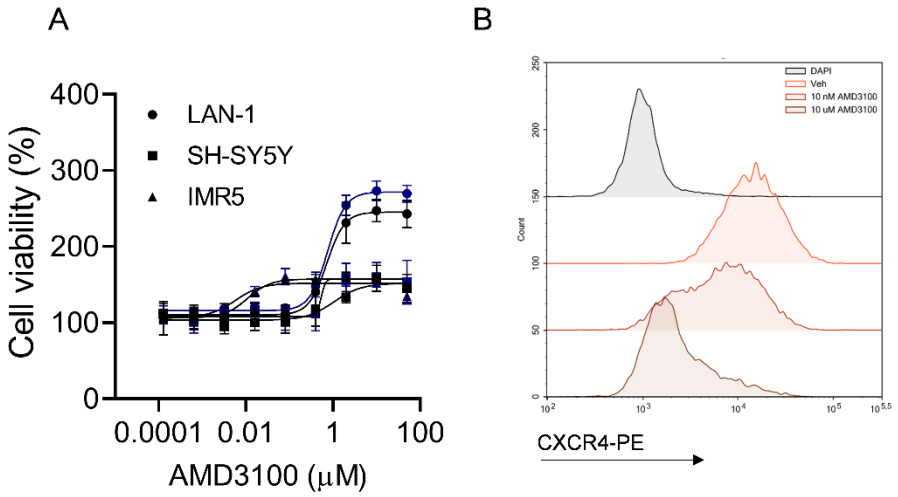

Figure 20: Activity of CXCR4 inhibitor on neuroblastoma cell lines **A** Non cytotoxic activity of AMD3100 in LAN-1, SH-SY5Y and IMR5 under normoxia (black) or hypoxia (blue) (n=6). **B** Flow cytometry histogram of membrane CXCR4 in LAN-1 treated with 10 µM and 10 nM of AMD3100 for 24 h.

We next focused on the inhibition of MIF as a potential therapeutic strategy. We evaluated two pharmacological compounds, ISO-1 and 4-IPP. The first, considered the reference drug for MIF inhibition, impairs the tautomerase activity as well as the binding capacity of MIF with CD74 (*194*). The second, 4-IPP, is a covalent MIF inhibitor with higher affinity for the protein and capacity to inhibit at lower drug concentrations as compared to ISO-1 (*241*). Treatment with ISO-1 (concentration range of 50-0.2 µM) showed limited NB cytotoxicity (**Figure 21 A**). In contrast, treatment with 4-IPP (concentration range of 50-0.2 µM) showed

a concentration-dependent cytotoxicity against NB cell lines: LAN-1 IC50 in normoxia 30.0 µM (21.4-226.1 µM) and hypoxia 30.5 µM (25.9-59.8 µM), SH-SY5Y IC50 in normoxia 17.3 µM (15.3-19.9 µM) and hypoxia (na) and IMR5 IC50 in normoxia 0.17 µM (na -0.76 µM) and hypoxia 1.49 µM (1.2 -1.8 µM) (**Figures 21 B**). Since MIF ligand was also detected in the secretome of bone marrow cells, in the form of CM-BM, we also explored whether 4-IPP was cytotoxic against primary BM-derived cells. Importantly, no cytotoxicity was observed below 50 µM, suggesting that 4-IPP acts specifically on NB tumor cells and no potential treatment-related toxicities would be expected on patients' BM cells (**Figure 21 C**).

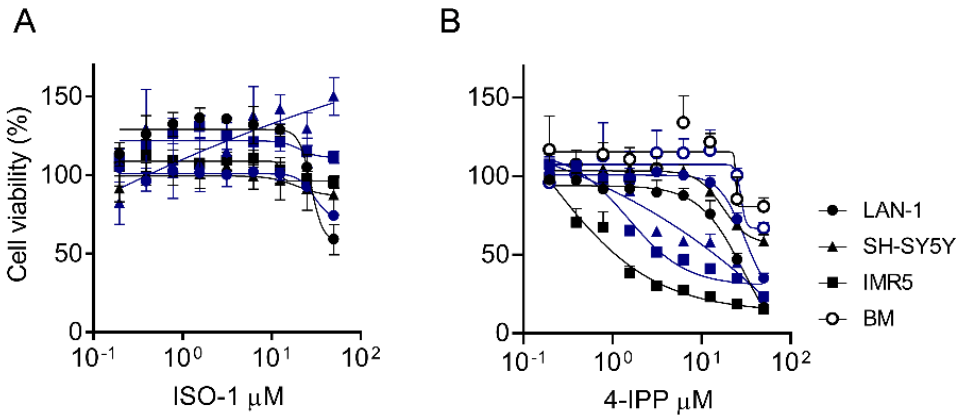

C

	4-IPP IC50 µM (95% Confidence Interval)	
	Normoxia	Hypoxia
LAN-1	30,05 (21,52-226,1)	30,51 (25.85-59.83)
SH-SY5Y	17,27 (15,25-19,86)	na
IMR5	0,17 (na -0,76)	1,49 (1,15-1,82)
BM	> 50	>50

Figure 21: Activity of MIF inhibitors on neuroblastoma cell lines and BM primary cultures **A** Cytotoxic activity of ISO-1 in a panel neuroblastoma cell lines under normoxia (black) or hypoxia (blue) conditions (n=6). **B** Cytotoxic activity of 4-IPP in a panel neuroblastoma cell lines and BM primary culture under normoxia (black) or hypoxia (blue) conditions (n=6). **C** Table with IC50 values of 4-IPP activity in µM. Non-applicable (na).

Next, we tested whether 4-IPP cytotoxicity was selective against NB cells (LAN-1) when cultured together with BM-derived cells in a 1:10 ratio (**Figure 22**). To this end, LAN-1 cells were plated 24 h before being co-cultured with BM cells and then treated with the vehicle or 4-IPP at 30 µM. After 72 h, samples were collected, stained with CD45-PE antibody and

DAPI, and analyzed by flow cytometry. After gating selection, percentages of three different populations were quantified; $CD45^+/DAPI^-$ as alive BM cells, $CD45^-/DAPI^-$ as alive LAN-1 cells, and $DAPI^+$ as dead cells (**Figure 22 A**).

In agreement with the MTS assay results, BM cells treated with 4-IPP showed no differences in the $DAPI^+$ population. In contrast, treatment of the LAN-1 cell line with 4-IPP increased percentage of $DAPI^+$ cells with a concomitant decrease in $CD45^-/DAPI^-$ cells. When cultured together, a diminished population of $CD45^-/DAPI^-$ was reported while no differences were observed in the $CD45^+/DAPI^-$ population (**Figure 22 B**). Thus, treatment with 4-IPP was selective for NB cells but not for patient-derived BM primary cells in co-culture *in vitro* models.

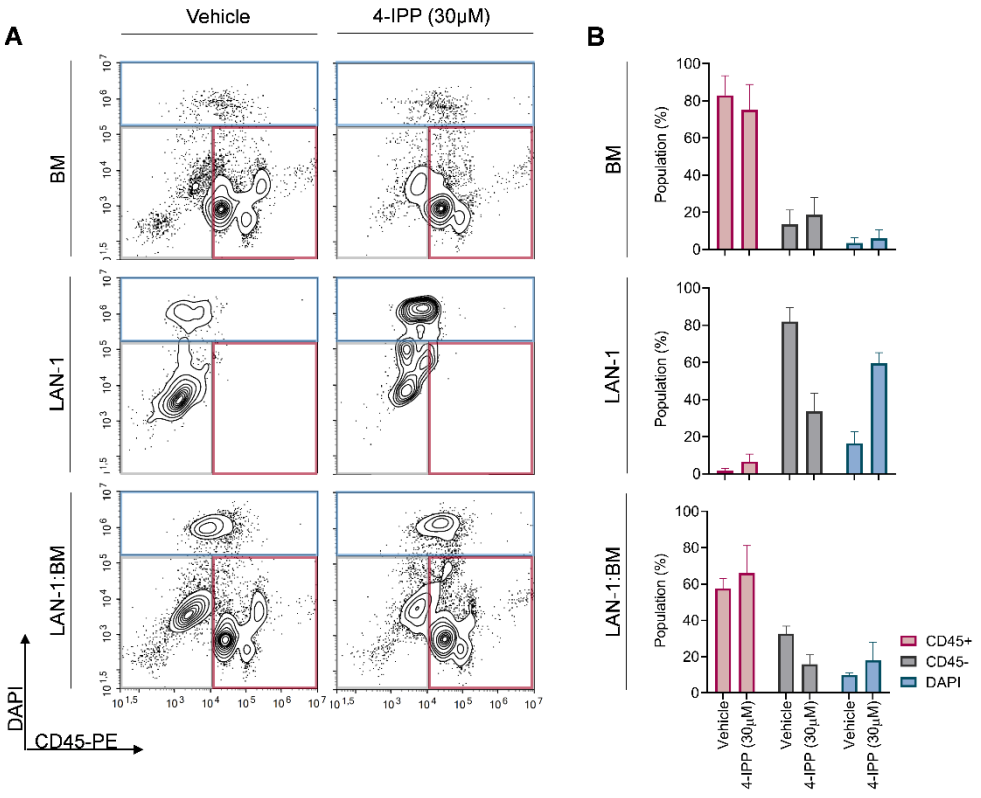

Figure 22: Activity of 4-IPP on LAN-1 and BM co-cultures. **A** Density plots facing CD-45 vs. DAPI signaling. Graphs show single culture of BM and LAN-1 together with co-culture LAN-1:BM ratio (1:10) treated with vehicle or 4-IPP 30 µM, 72 h at regular conditions. **B** Bar graphs showing the percentage of positive population for each experimental condition (n=2).

3.1. MIF inhibition decreases cell viability, migration, chemoattraction and invasion of neuroblastoma cells within the bone marrow niche

Based on our findings and the current knowledge about MIF signaling in cancer (*220, 268, 269*), we proceeded to investigate if the pro-tumorigenic effect of our CM's was related with MIF signaling activity, potentially thought the CXCR4 receptor. To this end, we explored whether treatment with MIF or CXCR4 inhibitors could selectively impair aggressive phenotypes promoted by our BM-model. First, we tested whether AMD3100 or 4-IPP could specifically prevent LAN-1 cell growth when exposed to BM-based model. For cell viability studies, we selected drug concentrations below IC50 values and with minimum activity over cell viability at regular medium conditions; 10 nM of AMD3100 and 5 μM of 4-IPP (**Figure 21 A-B**).

Time-dependent changes in LAN-1 cell viability after treatment with vehicle, AMD3100 or 4-IPP under different CMs and oxygen levels are shown in **Figure 23**. Significant changes were mainly identified at 72 h after treatment (**Figure 23 A**). At this time point, MIF inhibition with 4-IPP decreased LAN-1 cell viability in CM-BM under hypoxia and CM-BM/NB under normoxia and hypoxic conditions (all of them, $P<0.05$). No differences in cell viability were observed when 4-IPP was added in LAN-1 cells cultured in CM-CNT either under normoxia or hypoxia (**Figure 23 B**). Regarding CXCR4 inhibition, AMD3100 did not significantly modify cell viability, even though a minimum trend was observed in the case of CM-BM/NB under normoxia and hypoxia (both, P=0.36) (**Figure 23 B**). Altogether, these results suggested that MIF was critical for NB cell viability in a BM-like environment and such effect could be reverted partially by treatment with 4-IPP.

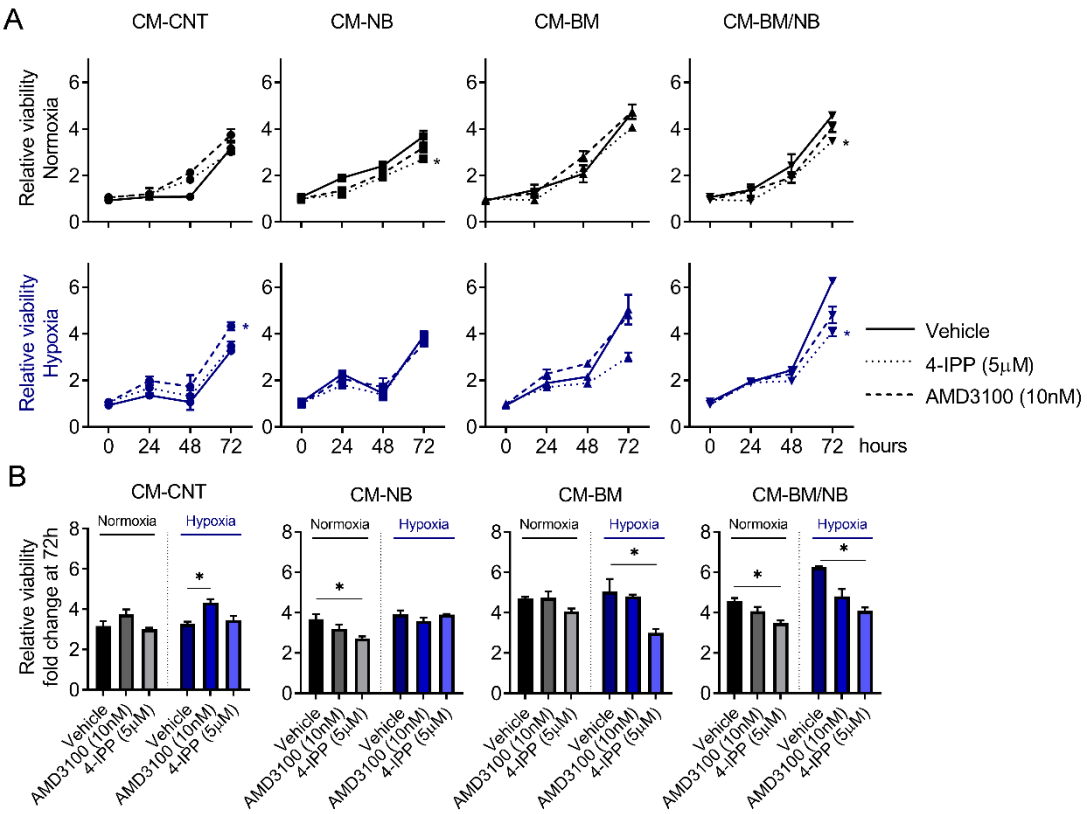

FIGURE 23: **A** Viability of LAN-1 cultured under BM-based model performed over 3 days. Solid line represents vehicle, dot line represents cells treated with 5 μM 4-IPP and hyphen line cells treated with 10 nM AMD-3100. Data are represented as a fold change viability to time 0 (n=3). **B** Bar graphs showing viability differences between treatments at 72 h. Normoxia conditions were represented in black-grey colors, hypoxia conditions in blue range colors. Significances were obtained comparing each CM's vehicle condition with their treatments in One-way Anova Kruskal-Wallis test. (*) *P<0.05*.

Additionally, we tested whether sub-lethal concentrations of CXCR4 or MIF inhibitors could also impair other malignant phenotypes of NB cells. 4-IPP abrogated LAN-1 migration in CM-BM/NB under hypoxia or under normoxia (both, *P<0.05*) whereas the effect of treatment with AMD3100 was less evident (*P=0.35*) (**Figure 24 A-B**). Similar results were obtained with the transwell chamber assay, where 4-IPP treated LAN-1 cells showed a clearly reduced chemoattraction and invasion compared to vehicle-treated control cells (*P<0.05*). AMD3100, treatment showed the same trend even though significance was not reached (*P=0.36*) (**Figure 24 C-D)**.

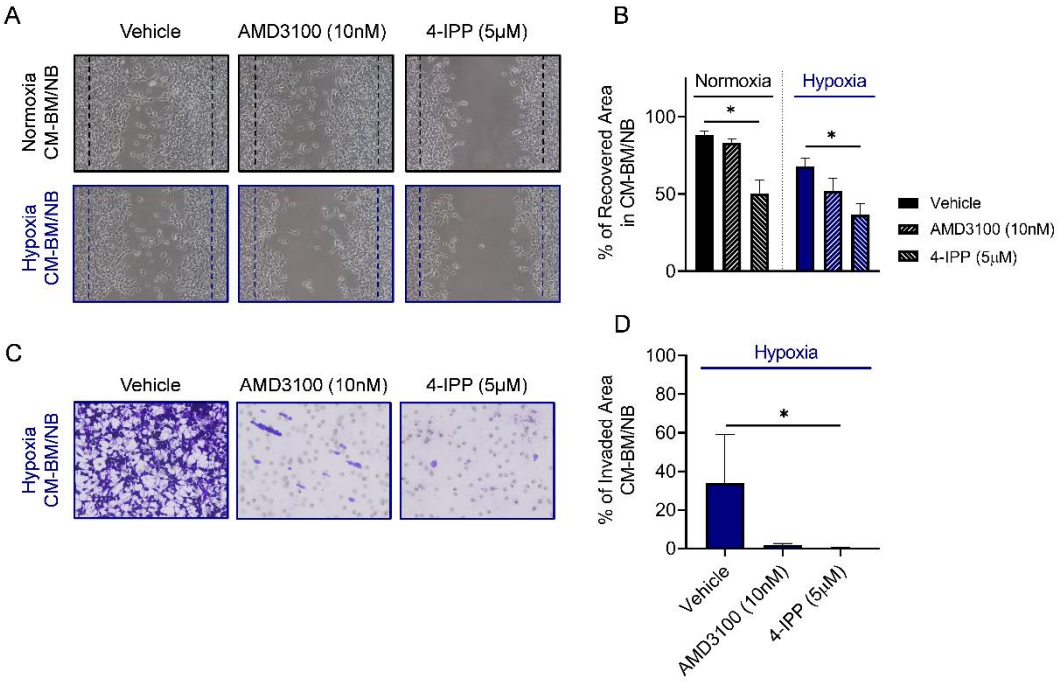

FIGURE 24: Wound healing assay in LAN-1. **A** Wound recovery under CM-BM/NB culture in combination with AMD3100 (10 nM) and 4-IPP (5 µM) at 24 h. Hyphen lines delimitate initial wound edge. **B** Bar graph with recovery quantification. Normoxia (black) and hypoxia (blue). Statistic differences calculated comparing each experimental condition to each Vehicle with One-way Anova Kruskal-Wallis test. (n=3) (*) *P<0.05.* **C** Invaded cells towards hypoxia CM-BM/NB culture together with AMD3100 (10 nM) and 4-IPP (5 µM) at 96h. **D** Bar graph with invasion quantification. Normoxia (black) and hypoxia (blue). Statistic differences calculated comparing each experimental condition to Vehicle with One-way Anova Kruskal-Wallis test (n=3) (*) *P<0.05.*

3.2. MIF inhibition restored chemotherapeutic drug resistance of neuroblastoma cells in the bone marrow niche

MIF inhibitors have been reported to enhance the cytotoxic effects of chemotherapy (*182, 245, 270*). Thus, we aimed to test whether treatment with a MIF inhibitor could modulate drug resistances associated with CM-BM/NB. To this end, a constant concentration of 4-IPP (5 µM) was added to LAN-1 cells exposed to doxorubicin and etoposide (**Figure 25**).

In LAN-1 cells cultured under normoxia, the addition of 4-IPP increased the concentration-dependent cytotoxicity of doxorubicin in CM-BM/NB, reducing significantly cell viability at IC50 values (*P<0.01*) (**Figure 25 C-D**). However, this effect was not observed when the combination was performed in CM-CNT. In hypoxic conditions, 4-IPP did not increase doxorubicin activity neither in CM-CNT or CM-BM/NB (**Figure 25 B and D**). When 4-IPP was combined with etoposide, increased cell cytotoxicity was observed in both normoxia CM-CNT (*P<0.01*) and CM-BM/NB (*P<0.001*) (**Figure 25 E-H**). Moreover, addition of 4-IPP impaired hypoxia-related resistance to etoposide in both CM-CNT and CM-BM/NB (**Figure 25 F and H**).

Overall, our *in vitro* results pointed out that CM-BM/NB along with hypoxia recapitulated NB malignant behavior in the bone marrow niche by promoting cell viability, invasion and drug resistance. In addition, our findings suggested MIF inhibition as an interesting therapeutic strategy to impair NB expansion in the BM niche.

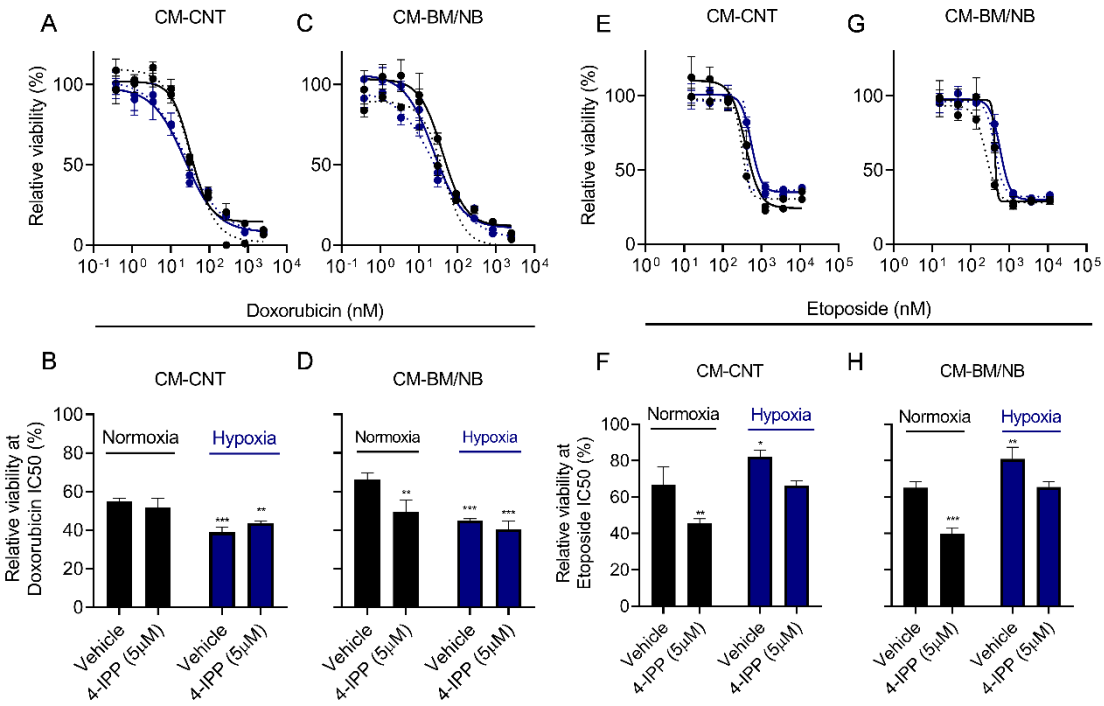

Figure 25: Activity of doxorubicin (**A-D**) and etoposide (**E-H**) together with 5 μM of 4-IPP in LAN-1 cells cultured in BM-based model at 72 h. **A** Doxorubicin cytotoxicity in CM-CNT. **B** Bar graph with relative viability at CM-CNT for doxorubicin IC50. **C** Doxorubicin cytotoxicity in CM-BM/NB. **D** Bar graph with relative viability at CM-BM/NB for doxorubicin IC50 (n=3). **E** Etoposide cytotoxicity in CM-CNT. **F** Bar graph with relative viability at CM-CNT for etoposide IC50. **G** Etoposide cytotoxicity in CM-BM/NB. **H** Bar graph with relative viability at CM-BM/NB for etoposide IC50 (n=3). Normoxia (black) and hypoxia (blue). Differences were calculated comparing each experimental condition to control (Vehicle under normoxia) with Two-way Anova Dunnett's multiple comparison test). (*) P<0.05, (**) P<0.01 and (***) P<0.001.

3.3. MIF inhibition delays neuroblastoma tumor growth in vivo and increases animal survival in a neuroblastoma xenograft model.

Our *in vitro* studies showed that the MIF inhibitor 4-IPP impaired NB growth in the BM niche. Here, we tested the antitumor effect of 4-IPP *in vivo* using LAN-1 cells subcutaneously injected into both flanks (1,5 x 10^6 *per* flank) of athymic nude mice. Based on our findings we reasoned that MIF inhibition could represent a potential approach for the treatment of high-risk NB that have minimal residual disease (MRD) that causes relapse within the BM niche even after therapy. With this aim, we tested the antitumor effect of 4-IPP in a MRD scenario where animal treatments were initiated 7 days after LAN-1 subcutaneous injection.

We further explored the efficacy of 4-IPP when administered in combination with dinutuximab, a chimeric monoclonal antibody that targets the disialoganglioside GD2 antigen on NB cell membrane. Dinutuximab has been approved for second-line treatment for children with high-risk NB (*82*). We approached this combination due to the potential immunostimulatory effects of MIF inhibition describe in previous studies (*271, 272*). Three group treatments were evaluated: Vehicle, 4-IPP 80 mg/kg, Dinutuximab 20 µg/dose and a combination group of 4-IPP plus Dinutuximab (**Figure 26**).

Animals were followed-up and tumor growth was measured every 3-4 days during treatment (4 weeks) until endpoint criteria (**Figure 26 A**). Animals treated with 4-IPP alone or in combination with Dinutuximab showed a tumor growth delay with respect to Dinutuximab or the vehicle group. Moreover, we observed longer survival curves for animals under 4-IPP or combination treatment, with a benefit of 24 days and 31 days respectively (88 days vehicle group vs. 112 days 4-IPP group (*P<0.05)* and vs. 119 days in the combination group (*P<0.05))*. Single treatment with Dinutuximab did not show prolonged survival when compared to vehicle; however, 2 out 5 mice did not develop tumors (**Figure 26 B**). At the experimental endpoint (subcutaneous tumor volume = 2000 mm^3), macroscopic metastatic lesions were observed in all treated groups (2 out of 5 mice, in all three regiments) and (4 out or 7 mice) in the vehicle group (data not show). These metastatic lesions were predominantly located in axillary and retroperitoneal lymph nodes. Importantly, no negative side effects such as physical symptoms, decreased activity or body weight loss were observed for any of the treatment groups (**Figure 26 C**).

Our preliminary results showed that inhibition of MIF affected tumors by delaying initial growth, however, treatment with 4-IPP was not enough to inhibit the invasive behavior of NB cells. These results suggested MIF targeting, alone or in combination treatment, as a potential therapeutic strategy to be further explored for high-risk NB patients with MRD. The pharmacological targeting of MIF, with either 4-IPP or other MIF inhibitors, needs to be further explored in more comprehensive preclinical studies.

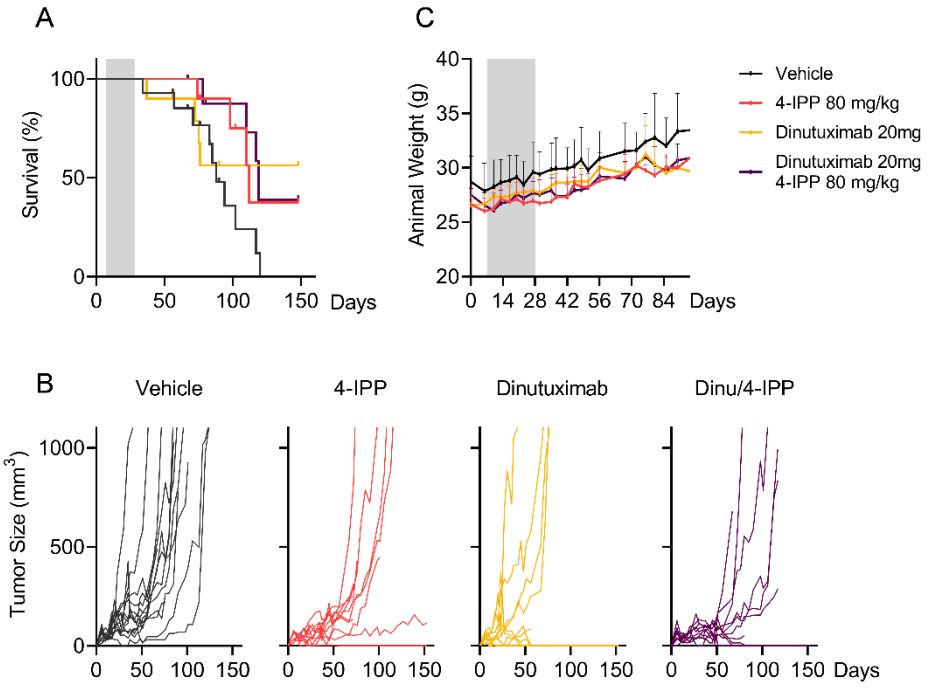

FIGURE 26: *In vivo* efficacy of 4-IPP, Dinutuximab and 4-IPP plus Dinutuximab (Dinu/4-IPP) in sub-cutaneous LAN-1 xenograft. **A** Tumor survival curves for each group. Survival event was reported at 1000 mm^3 tumor size. **B** Plot of individual tumor size for each treatment group. **C** Body weight variation of mice during treatment (grey area) and follow-up.

DISCUSSION:

The unique biological properties of the BM environment make it a preferential niche for aggressive NB cell dissemination. At the moment of diagnosis, 50% of NB patients show disease dissemination to distal sites (*12*). Among these, BM represents the most common site for NB cell dissemination, and its infiltration at diagnosis and relapse is a hallmark of stage 4 disease (*159*). The BM niche is therefore critical for both tumor staging and therapeutic purposes (*77, 78*). NB tumors with disseminated disease still represent a clinical challenge despite advances in treatment strategies. Even though the understanding of the biology underlying NB pathogenesis has grown considerably over the last decade, the mechanisms behind the aggressive behavior of BM disseminated disease are still largely unknown. In this thesis, we focused on the major reservoir of high-risk disseminated NB, the BM, and its role as an oncogenic environment. We aimed to identifying molecular mechanisms that play a critical role in NB survival and tumor progression in the BM niche, and could represent novel therapeutic targets for more tailored NB treatment strategies.

In order to accomplish our primary goal, we first proceeded with the development of an *in vitro* BM model that recapitulated critical features such as the secretome and the low oxygen levels found in the BM microenvironment of NB patients (BM tumor microenvironment (BM-TME). To this end, we combined CMs obtained from patient-derived BM cell cultures with the intrinsic low oxygen levels and NB cells. The strategy of using CM for modelling TME is endorsed by several research articles in the field that reported how CMs improved tumor cell survival and proliferation, similar to the effects obtained with direct contact between tumor and stromal cells (*188*). These effects were mediated by the BM secretome, recapitulated in these studies in the form of CM. Generally, CMs are obtained after purification and expansion of specific stromal cell types such as endothelial cells or MSCs, thus lacking the complex heterogenic cell population present within the BM-TME (*188, 266, 273*). In our study, we obtained CMs from NB patient's BM primary cells directly cultured and expanded *in vitro*. Our strategy permitted to us to mimic more closely the heterogenic and complex cell population of the BM and induce a mesenchymal cell population enrichment (*274*). The analysis of the secretome of CMs showed important similarities with BM patient-derived plasma samples, specifically for cytokines such as MCP-1, IL-1ra, IL-6, IL-8, MIF and PAI-1. Among these, IL-6, IL-8 and PAI-1 are known to affect BM homeostasis

promoting inflammation and osteoclastogenesis, which favor NB progression in this niche (see Introduction Section 4.3) (*161, 186, 275*). CMs obtained from NB cells incubated alone or with BM tumor cells, mimicking an infiltrated BM environment, showed high levels of macrophage migration inhibitory factor (MIF), an inflammatory cytokine. Previous studies have reported expression of MIF in NB cells and similar secretion levels in CMs derived from BM-MSCs (*188*). However, despite MIF is known to be secreted by NB cell lines, its role in maintenance and expansion of NB cells in the BM niche has never been studied (*226, 227*).

Based on our preliminary results, we performed an analysis of the MIF pathway using diverse publicly available gene expression datasets including high-risk NB tumor samples, as well as samples enriched with BM-derived disseminated NB tumors cells. We observed that differential expression of *MIF* and its receptors were significantly associated with NB patient outcome. Specifically, high expression of *MIF* and one of its receptors, *CXCR4,* were associated with poor outcome of patients with high-risk disseminated NB tumors. On the other hand, high expression of CD74, an alternative MIF receptor, CD44 and CXCL12 were found to be associated with low-risk tumors and favorable outcomes. These findings underpinned MIF as a relevant cytokine, potentially involved in NB aggressive behavior.

MIF is a pleiotropic cytokine that plays a key role in several diseases, including cancer (*219*). Previous studies have shown that *MIF* expression is associated with undifferentiated tumors promoting angiogenic signals, *MYCN* gene expression and contributed to immune evasion (*227*). We tested the effect of our BM-model secretome, in the form of CMs, on the malignant behavior of NB cells. Our results showed that CMs were able *per se* to induce an increase of LAN-1 and SH-SY5Y NB cell proliferation. Interestingly, both cells lines are derived from infiltrated BM samples of patients with stage 4 disease (*251*). On the other hand, this response was not observed with IMR5, a cell line derived from a primary abdominal NB tumor mass, and not from a metastatic site (*57*). Borriello L. *et al*. previously observed that metastatic NB cell lines CHLA-255 (origin: brain metastasis) and SK-N-SH (origin: BM dissemination) displayed increased tumorigenicity *in vitro* when exposed to purified BM-MSC secretome (*188*). Our results point to a selective protumorigenic effect of CMs for BM derived NB cells, probably because these cells display, or acquire, a potential for interaction with BM elements. These properties confer to BM disseminated NB cells the potential to respond better to BM microenviroment factors.

Oxygen is a critical component of the BM niche. The hypoxic environment that characterizes the BM niche is considered to be necessary for maintenance of normal physiological function and self-renewal of stem cells. Our *in vitro* model mimicked both secreted molecular factors as well as the hypoxic environment, offering thus a more comprehensive model of the BM, more appropriate to study interactions between NB cells and the BM niche. We observed how CMs and hypoxic conditions promoted cell viability of *MYCN* amplified cells LAN-1 and IMR5, but did not affect the non-amplified SH-SY5Y cell line. *HIF-1α* has been reported preferentially expressed in *MYCN*-amplified NB cell lines and tumors, where it contributes to NB aggressiveness. Our findings support that interplay between MYCN and HIF-1α contributes to NB aggressiveness, particularly in *MYCN* amplified cells (*276*).

In response to our BM-based model, LAN-1 and SH-SY5Y cells increased CXCR4 expression in cell membrane and promoted activation of the PI3K/AKT and MAPK/ERK signaling pathways. The increment of CXCR4 has previously been described in NB cell lines exposed to immortalized MSC secretome (*266*). These results suggest that secretome released by the mesenchymal fraction expanded in our BM culture could be boosting the CXCR4 levels in NB cells. Importantly, Zhang L. *et al.* described that CMs derived from BM and liver stroma cells increased CXCR4 levels in LAN-5 and NUB-7 (both BM-derived NB cell lines), whereas these changes were not observed when using bone, adrenal gland or lung stroma-derived CMs (*277*). Low oxygen levels also trigger CXCR4 expression in several cell types, including NB cell lines (*175, 273, 278*). In normal BM homeostasis, the stabilization of HIF-1α by a hypoxic environment increases CXCR4 levels in HSCs, promoting their retention within the niche (*279, 280*). In our BM-model, hypoxia also up-regulated CXCR4 levels in LAN-1 cells, suggesting that some neuroblastic cells may behave like HSCs upon exposure to the similar environment.

On the other hand, membrane levels of MIF receptor CD74 were not increased by any condition in our BM-based model, suggesting a minor role of this pleiotropic receptor in the NB response to BM environment. However, since CD74 has alternative functions in MIF-related intracellular signaling, its potential role in NB biology cannot be dismissed and needs to be further explored (*281*).

The increment of CXCR4 on the surface of NB cells is widely associated with diverse tumor aggressive properties like cell proliferation, migration and invasion, and usually related to CXCL12 signaling (*166, 167, 170, 266, 277*). In our study, we observed a lack of CXCL12

in the CMs. Nonetheless, the increased levels of CXCR4 induced by our BM-derived CMs improved cell viability and induced colony spread out morphology, suggesting that the aggressive phenotypes were not dependent on the presence of this extracellular cytokine in the environment (*169, 171*). Moreover, LAN-1 cells showed increased migration capacity when exposed to CM-BM/NB, and its combination with hypoxia promoted cellular invasion and chemo-attraction. The enhanced viability, migration and invasion, observed particularly with CM-BM/NB led us to the hypothesis that the aggressive phenotypes could be triggered by MIF signaling through its receptor CXCR4 (*177*).

Different studies reported that ectopic CXCL12 signaling does not attract $CXCR4^+$ NB cell lines by Transwell invasion assays neither in normoxia nor hypoxic conditions (*171, 175, 266*). In line with our hypothesis, we suggest that the reduced cellular motility reported by these studies could be due to the absence of extracellular MIF signaling. In different cancer types, the axis CXCR4/MIF is a critical autocrine pathway linked to tumor progression (*180, 182, 183, 270*). CXCR4/MIF signaling promotes neovascularization, migration and invasion phenotypes in colorectal cancer, non-small cell lung cancer (NSCLC) and glioblastoma (*180, 182, 183*). In fact, exposure of SH-SY5Y cells to exogenous MIF up-regulated genes involved in cell proliferation and migration by increasing BDNF production and AKT signaling (*229, 230, 282*). In a chick developmental model, extracellular MIF has recently been identified as a potent chemoattractant for trunk neural crest cells towards dorsal root ganglia, a plausible locus for neuroblastoma origin (*283, 284*). Altogether, these results support the presence of high extracellular MIF as a potential autocrine mediator promoting aggressive NB behavior in an environment that up-regulates CXCR4 levels in NB cell lines.

In addition to the *in vitro* functional experiments, we also aimed to explore whether BM environment could enhance NB progression *in vivo.* In order to mirror the effects promoted by our BM-derived CMs, we subcutaneously co-injected NB and BM cells preserving the same ratio (1:1) and expansion protocol used to generate CM-BM/NB in an athymic nude mice xenograft model. The presence of BM cells promoted early tumor cell implantation reducing engraftment time, thus correlating with the increased aggressive behavior observed *in vitro*. Borriello L. *et al.* reported similar results *in vivo* by the co-injection of NB cell lines with an increased fraction of stromal cells (NB/BM-MSC ratio 1:4), achieving lower engraftment times and also lower survival rates of the mouse models. Altogether, these results emphasized the importance of the BM-TME facilitating tumor initial adaptation and sustaining the progression of NB tumor growth *in vivo* (*188*). The co-injection of NB cells

with BM cells did not modify LAN-1 metastatic behavior. On this regard, Borriello L*. et al.* did not report any metastatic event in their NB:BM-MSC co-injection study (*188*).

MIF autocrine signaling is known to retain tumor cells in the BM, and its downregulation has been found to promote the development of extramedullary engraftment in multiple myeloma (*270*). Altogether, our result and others suggested that the axis CXCR4/MIF could enhance early NB implantation and invasion while retaining the tumor cells within the BM niche. This pro-tumor and pro-retention signaling would contribute to the progression of the disseminated lesion in the BM niche.

As part of the second objective, we sought to test different pharmacological strategies to target CXCR4/MIF axis using AMD3100 (CXCR4 inhibitor) and ISO-1 and 4-IPP (MIF inhibitors). The compound AMD3100 (Plerixafor) is a well-characterized drug indicated for the autologous transplantation of BM cells in patients with hematologic malignances (*249*). AMD3100 promotes HSC mobilization to peripheral blood by blocking the CXCR4 receptor impairing the signaling CXCR4/CXCL12 (*285*). Unexpectedly, despite high-expression CXCR4 was associated with NB aggressiveness, its inhibition with AMD3100 promoted cell viability in a dose-dependent manner. Similar results have been reported previously in Ewing sarcoma cell lines, where CXCR4 inhibition with AMD3100 activated compensatory signaling cascades involving different tyrosine kinases receptors that promoted malignant proliferation (*267*). These results discourage preclinical studies with Plerixafor, as a single agent against disseminated NB tumors.

We then explored two different MIF inhibition drugs, ISO-1 and 4-IPP. ISO-1 has been formerly tested in NB whereas, to our knowledge, this is the first time that 4-IPP is evaluated as an anticancer drug against NB cells. Hwan Bae S *et al.* demonstrated that, after a hypoxic insult, the neuroprotective effect of MIF over SH-SY5Y cells could be reversed with ISO-1 treatment (*229*). We selected the 4-IPP compound instead of ISO-1 based on the higher cytotoxicity that we observed against NB cells. These cytotoxic differences could be related to the higher MIF inhibition activity achieved by 4-IPP, being 10 times more potent than ISO-1 (*241*).

To approach the potential role of CXCR4/MIF signaling over the aggressive behavior promoted by our BM-model, we used sub-lethal concentrations of 4-IPP and AMD3100. Remarkably, 5 µM of 4-IPP impaired cellular viability specifically enhanced by our BM-based model without affecting the control group. Inhibition of CXCR4 with AMD3100 displayed a

similar trend. We also showed that treatment with sub-lethal concentration of 4-IPP reduced cell migration and abrogated cell invasion when exposed to CM-BM/NB together with hypoxia. Previous studies have demonstrated that 4-IPP decreased the invasive ability of bladder cancer cells and reduced migratory capacity of rhabdomyosarcoma cells (*239, 286*). Altogether, these findings supported our hypothesis that the aggressive behavior of NB cells promoted by BM model was in part mediated by the CXCR4/MIF axis.

In addition to aggressive phenotypes promoted by our BM model, we aimed to explore whether this environment could benefit NB cells in terms of drug response. The BM is known to act as NB reservoir for tumor relapses, being this storage associated with quiescent and chemoresistant tumor clones (*77*). Upon exposure to CM-BM/NB, LAN-1 cells diminished chemotherapy response to doxorubicin and etoposide, both drugs used in NB treatment protocols. The combination with sub-lethal concentrations of 4-IPP treatment reverted LAN-1 drug sensitivity, supporting an important role of MIF over NB chemo-sensitivity. In fact, MIF signaling promotes drug resistance in different tumor types, including NB and other developmental tumors (*182, 228, 239, 270*). In multiple myeloma, combination treatment with 4-IPP enhanced melphalan toxicity, particularly when tumor cells where co-cultured with BM stromal cells (*270*).

In our hands, 4-IPP treatment was found to be selective for NB cells and not cytotoxic against primary BM cells. This finding was relevant, since limited or no treatment-related toxicities would be expected in patients' BM cells, supporting 4-IPP as a compound of interest for targeted inhibition of MIF in the context of NB BM disease.

More than 50% of high-risk patients develop recurrent NB, often from BM-MRD. Overall, our results underpinned MIF as an important mediator in NB progression within the BM niche. Based on these evidences, we explored whether inhibition of MIF with 4-IPP could be therapeutically effective against a MRD xenograft model. Our preliminary data showed that treatment with 4-IPP as a single agent delayed tumor growth and improved survival as compared to vehicle group. These results are consistent with a previous study where single treatment with 4-IPP delayed melanoma tumor growth in a syngeneic murine models, even though 4-IPP did not increase mice survival (*287*). In NB mouse models, SK-N-DZ cells transfected with an antisense *MIF* expression vector reported a strong reduction of tumor growth in a xenograft model in BALB/c nude mice (*225*). Furthermore, the combination of 4-IPP with chemotherapeutic or targeted agents *in vivo* was effective against myeloma

multiple in different studies (*245, 270*). These results reinforced MIF as a critical signaling molecule in NB progression and a targetable protein to be further explored.

MIF has a strong influence over inflammation and immune evasion, therefore we next explored the effect of 4-IPP in combination with the monoclonal antibody dinutuximab that targets GD2, a disialogangloside expressed on the surface of NB cells. Once the antibody recognizes the GD2 antigen, the cells of the immune system are able to lyse the target cells. Dinutuximab is a clinically approved immunotherapeutic approach against MRD in high-risk NB (*268, 288*). In our *in vivo* model the combination treatment with 4-IPP and dinutuximab did not ameliorate the antitumor effect observed in mice treated with 4-IPP alone. In NB, dinutuximab is generally given together with cytokines such as granulocyte macrophage colony-stimulating factor (GM-CSF) and interleukin-2 (IL-2) in order to enhance the patient's immune response. In multiple myeloma, the combination of 4-IPP together with GM-CSF has shown cooperative effects activating antitumor M1-like macrophages in NSG mice (*271*). Since NB immunotherapy protocols include GM-CSF, the addition of this immune stimulatory factor could represent a key stimulatory partner to enhance the antitumor effect of 4-IPP in combination with dinutuximab (*82*). However, more adequate mice models should be considered since our experiment was performed in athymic nude mice, a strain lacking adaptive immunity (T and B cells), which could likely limit the efficacy of the combinatory treatment.

Different limitations are present in this thesis and must be considered. First, the expansion of patient-derived BM cultures and the production of CMs should be ideally performed under hypoxia, as they would better mimic tissue homeostasis. In fact, Nakahara F *et al.* demonstrated that the ability of BM-MSC to maintain HSC niche factors is rapidly impaired *ex vivo* in normoxia. This observation could explain the lack of CXCL12 in our BM-derived CMs (*289*). Secondly, we focused our study on the cytokines released by our CMs; however, additional extracellular mediators such as microvesicles and exosomes are probably present in our CMs and could be linked with NB infiltration in the BM niche (*290-292*). Third, in order to fully demonstrate the importance of CXCR4/MIF signaling in NB biology, we should genetically down-regulate *CXCR4* and *MIF* expression using shRNA or CRISPR techniques and subsequently perform functional studies with our CMs and drug inhibitors. In addition, the administration of exogenous MIF and CXCL12 *in vitro* could better demonstrated its effects over NB cell aggressiveness. Finally, despite its limitations in translational

application, 4-IPP treatment should be tested in a BM orthotopic NB mouse model instead of using MRD or bulk-based subcutaneous tumor models.

In summary, our findings provide new understanding of the contribution of BM microenvironment to high-risk NB aggressive behavior. By using a newly established BM-model, our results suggest that relationship between the BM microenvironment and NB cells is mediated, in part, by the CXCR4/MIF signaling axis. Furthermore, our results suggested that MIF could represent a therapeutic target for the treatment of patients with high-risk NB. However, MIF inhibition needs to be further explored in more adequate and comprehensive preclinical studies.

CONCLUSIONS:

The main conclusions of this study are:

1 Conditioned media generated from NB cell lines and fresh primary patient BM-derived cell cultures together with low O_2 tension provided relevant factors that recapitulated, in part, the BM microenvironment of patients with NB infiltration.

2 This *in vitro* model enabled the identification of the cytokine MIF as a potential mediator for NB survival and progression in the BM niche.

3 Differential gene expression levels of both *MIF* and the receptor *CXCR4* were related with NB patient outcome. High expression of *MIF* was significantly associated with disseminated high-risk NB, being particularly high in disseminated tumors with *MYCN* amplification.

4 The BM-like features of our model obtained from the interaction between BM and NB cells in hypoxic conditions, enhanced cellular viability, migration, invasion and drug resistance of high-risk NB cells.

5 In response to BM microenvironment, the autocrine signaling CXCR4/MIF axis could benefit NB progression in the marrow niche.

6 The pharmacological targeting of MIF and CXCR4 with specific compounds such as 4-IPP and AMD3100, impaired the malignant behavior of NB cell promoted by our *in vitro* BM environment.

7 The pharmacological targeting of MIF with 4-IPP, sensitized BM disseminated NB cells to clinically available chemotherapeutic drugs.

8 Treatment with the MIF inhibitor 4-IPP impaired NB tumor growth in LAN-1 xenograft models by delaying tumor progression and improving survival.

REFERENCES:

1. R. L. Siegel, K. D. Miller, A. Jemal, Cancer statistics, 2015. *CA Cancer J Clin* **65**, 5-29 (2015).
2. E. R. Fearon, B. Vogelstein, A genetic model for colorectal tumorigenesis. *Cell* **61**, 759-767 (1990).
3. M. J., What is a pediatric tumor? *Clinical Oncology in Adolescents and Young Adults* **2**, 9 (2012).
4. P. Kattner *et al.*, Compare and contrast: pediatric cancer versus adult malignancies. *Cancer Metastasis Rev* **38**, 673-682 (2019).
5. R. J. Gilbertson, Mapping cancer origins. *Cell* **145**, 25-29 (2011).
6. D. M. Langenau, A. Sweet-Cordero, R. Wechsler-Reya, M. A. Dyer, Preclinical Models Provide Scientific Justification and Translational Relevance for Moving Novel Therapeutics into Clinical Trials for Pediatric Cancer. *Cancer Res* **75**, 5176-5186 (2015).
7. A. T. Meadows, Pediatric cancer survivorship: research and clinical care. *J Clin Oncol* **24**, 5160-5165 (2006).
8. C. A. Stiller, D. M. Parkin, International variations in the incidence of neuroblastoma. *Int J Cancer* **52**, 538-543 (1992).
9. W. B. London *et al.*, Evidence for an age cutoff greater than 365 days for neuroblastoma risk group stratification in the Children's Oncology Group. *J Clin Oncol* **23**, 6459-6465 (2005).
10. E. Steliarova-Foucher *et al.*, International incidence of childhood cancer, 2001-10: a population-based registry study. *Lancet Oncol* **18**, 719-731 (2017).
11. P. R. E. Peris Bonet R, Muñoz López A, Sayas Sánchez N, Valero Poveda S., paper presented at the X Congreso de la SEHOP, Madrid, May 2017 2017.
12. J. M. Maris, M. D. Hogarty, R. Bagatell, S. L. Cohn, Neuroblastoma. *Lancet* **369**, 2106-2120 (2007).
13. N.-K. V. Cheung, *Neuroblastoma*. Springer-Verlag, Ed., (Springer, Berlin, Heidelberg, Heidelberg, 2005).
14. J. M. Maris, Recent advances in neuroblastoma. *N Engl J Med* **362**, 2202-2211 (2010).
15. B. De Bernardi *et al.*, Epidural compression in neuroblastoma: Diagnostic and therapeutic aspects. *Cancer Lett* **228**, 283-299 (2005).
16. N. R. Mahoney *et al.*, Pediatric horner syndrome: etiologies and roles of imaging and urine studies to detect neuroblastoma and other responsible mass lesions. *Am J Ophthalmol* **142**, 651-659 (2006).
17. B. De Bernardi *et al.*, Neuroblastoma with symptomatic spinal cord compression at diagnosis: treatment and results with 76 cases. *J Clin Oncol* **19**, 183-190 (2001).
18. K. K. Matthay *et al.*, Opsoclonus myoclonus syndrome in neuroblastoma a report from a workshop on the dancing eyes syndrome at the advances in neuroblastoma meeting in Genoa, Italy, 2004. *Cancer Lett* **228**, 275-282 (2005).
19. S. J. Kaplan, C. T. Holbrook, H. G. McDaniel, W. L. Buntain, W. M. Crist, Vasoactive intestinal peptide secreting tumors of childhood. *Am J Dis Child* **134**, 21-24 (1980).
20. G. J. D'Angio, A. E. Evans, C. E. Koop, Special pattern of widespread neuroblastoma with a favourable prognosis. *Lancet* **1**, 1046-1049 (1971).
21. B. Hero, D. H. Hunneman, M. Gahr, F. Berthold, Evaluation of catecholamine metabolites, mIBG scan, and bone marrow cytology as response markers in stage 4 neuroblastoma. *Med Pediatr Oncol* **36**, 220-223 (2001).
22. O. Geatti *et al.*, Iodine-131 metaiodobenzylguanidine scintigraphy for the location of neuroblastoma: preliminary experience in ten cases. *J Nucl Med* **26**, 736-742 (1985).
23. A. Iavarone, A. Lasorella, T. Servidei, R. Riccardi, R. Mastrangelo, Uptake and storage of m-iodobenzylguanidine are frequent neuronal functions of human neuroblastoma cell lines. *Cancer Res* **53**, 304-309 (1993).
24. K. K. Matthay *et al.*, Neuroblastoma. *Nat Rev Dis Primers* **2**, 16078 (2016).
25. J. Mora *et al.*, Results of induction chemotherapy in children older than 18 months with stage-4 neuroblastoma treated with an adaptive-to-response modified N7 protocol (mN7). *Clin Transl Oncol* **17**, 521-529 (2015).
26. J. Stutterheim *et al.*, PHOX2B is a novel and specific marker for minimal residual disease testing in neuroblastoma. *J Clin Oncol* **26**, 5443-5449 (2008).
27. I. Y. Cheung, N. K. Cheung, Quantitation of marrow disease in neuroblastoma by real-time reverse transcription-PCR. *Clin Cancer Res* **7**, 1698-1705 (2001).
28. H. Shimada *et al.*, Histopathologic prognostic factors in neuroblastic tumors: definition of subtypes of ganglioneuroblastoma and an age-linked classification of neuroblastomas. *J Natl Cancer Inst* **73**, 405-416 (1984).
29. H. Shimada *et al.*, The International Neuroblastoma Pathology Classification (the Shimada system). *Cancer* **86**, 364-372 (1999).

30. H. Shimada *et al.*, Terminology and morphologic criteria of neuroblastic tumors: recommendations by the International Neuroblastoma Pathology Committee. *Cancer* **86**, 349-363 (1999).
31. G. M. Brodeur *et al.*, Revisions of the international criteria for neuroblastoma diagnosis, staging, and response to treatment. *J Clin Oncol* **11**, 1466-1477 (1993).
32. T. Monclair *et al.*, The International Neuroblastoma Risk Group (INRG) staging system: an INRG Task Force report. *J Clin Oncol* **27**, 298-303 (2009).
33. S. L. Cohn *et al.*, The International Neuroblastoma Risk Group (INRG) classification system: an INRG Task Force report. *J Clin Oncol* **27**, 289-297 (2009).
34. P. L. Sarnacki S, *Neuroblastoma Clinical and Surgical Management*. (Springer Nature Switzerland, 2020).
35. Z. X. Yue *et al.*, MYCN amplification predicts poor prognosis based on interphase fluorescence in situ hybridization analysis of bone marrow cells in bone marrow metastases of neuroblastoma. *Cancer Cell Int* **17**, 43 (2017).
36. I. M. Morgenstern DA, in *Cancer Genomics from bench to personalized medicine,* G. Dellaire, Ed. (Elsevier, London, 2014), chap. 21.
37. G. M. Brodeur *et al.*, Consistent N-myc copy number in simultaneous or consecutive neuroblastoma samples from sixty individual patients. *Cancer Res* **47**, 4248-4253 (1987).
38. A. P. Berbegall *et al.*, Heterogeneous MYCN amplification in neuroblastoma: a SIOP Europe Neuroblastoma Study. *Br J Cancer* **118**, 1502-1512 (2018).
39. G. M. Brodeur, Neuroblastoma: biological insights into a clinical enigma. *Nat Rev Cancer* **3**, 203-216 (2003).
40. G. M. Brodeur, R. C. Seeger, M. Schwab, H. E. Varmus, J. M. Bishop, Amplification of N-myc in untreated human neuroblastomas correlates with advanced disease stage. *Science* **224**, 1121-1124 (1984).
41. R. C. Seeger *et al.*, Association of multiple copies of the N-myc oncogene with rapid progression of neuroblastomas. *N Engl J Med* **313**, 1111-1116 (1985).
42. N. K. Cheung, M. A. Dyer, Neuroblastoma: developmental biology, cancer genomics and immunotherapy. *Nat Rev Cancer* **13**, 397-411 (2013).
43. S. Zhu *et al.*, Activated ALK collaborates with MYCN in neuroblastoma pathogenesis. *Cancer Cell* **21**, 362-373 (2012).
44. W. A. Weiss, K. Aldape, G. Mohapatra, B. G. Feuerstein, J. M. Bishop, Targeted expression of MYCN causes neuroblastoma in transgenic mice. *EMBO J* **16**, 2985-2995 (1997).
45. A. Faisal *et al.*, The aurora kinase inhibitor CCT137690 downregulates MYCN and sensitizes MYCN-amplified neuroblastoma in vivo. *Mol Cancer Ther* **10**, 2115-2123 (2011).
46. A. Puissant *et al.*, Targeting MYCN in neuroblastoma by BET bromodomain inhibition. *Cancer Discov* **3**, 308-323 (2013).
47. T. J. Pugh *et al.*, The genetic landscape of high-risk neuroblastoma. *Nat Genet* **45**, 279-284 (2013).
48. I. Janoueix-Lerosey *et al.*, Somatic and germline activating mutations of the ALK kinase receptor in neuroblastoma. *Nature* **455**, 967-970 (2008).
49. T. Berry *et al.*, The ALK(F1174L) mutation potentiates the oncogenic activity of MYCN in neuroblastoma. *Cancer Cell* **22**, 117-130 (2012).
50. J. H. Schulte *et al.*, MYCN and ALKF1174L are sufficient to drive neuroblastoma development from neural crest progenitor cells. *Oncogene* **32**, 1059-1065 (2013).
51. G. Schleiermacher *et al.*, Emergence of new ALK mutations at relapse of neuroblastoma. *J Clin Oncol* **32**, 2727-2734 (2014).
52. Y. P. Mosse, Anaplastic Lymphoma Kinase as a Cancer Target in Pediatric Malignancies. *Clin Cancer Res* **22**, 546-552 (2016).
53. J. J. Molenaar *et al.*, LIN28B induces neuroblastoma and enhances MYCN levels via let-7 suppression. *Nat Genet* **44**, 1199-1206 (2012).
54. R. W. Schnepp *et al.*, A LIN28B-RAN-AURKA Signaling Network Promotes Neuroblastoma Tumorigenesis. *Cancer Cell* **28**, 599-609 (2015).
55. N. K. Cheung *et al.*, Association of age at diagnosis and genetic mutations in patients with neuroblastoma. *JAMA* **307**, 1062-1071 (2012).
56. L. J. Valentijn *et al.*, TERT rearrangements are frequent in neuroblastoma and identify aggressive tumors. *Nat Genet* **47**, 1411-1414 (2015).
57. J. J. Tumilowicz, W. W. Nichols, J. J. Cholon, A. E. Greene, Definition of a continuous human cell line derived from neuroblastoma. *Cancer Res* **30**, 2110-2118 (1970).
58. S. Coco *et al.*, Age-dependent accumulation of genomic aberrations and deregulation of cell cycle and telomerase genes in metastatic neuroblastoma. *Int J Cancer* **131**, 1591-1600 (2012).

59. G. Schleiermacher *et al.*, Accumulation of segmental alterations determines progression in neuroblastoma. *J Clin Oncol* **28**, 3122-3130 (2010).
60. C. Lavarino *et al.*, Differential expression of genes mapping to recurrently abnormal chromosomal regions characterize neuroblastic tumours with distinct ploidy status. *BMC Med Genomics* **1**, 36 (2008).
61. E. F. Attiyeh *et al.*, Chromosome 1p and 11q deletions and outcome in neuroblastoma. *N Engl J Med* **353**, 2243-2253 (2005).
62. K. O. Henrich, M. Schwab, F. Westermann, 1p36 tumor suppression--a matter of dosage? *Cancer Res* **72**, 6079-6088 (2012).
63. N. Bown *et al.*, Gain of chromosome arm 17q and adverse outcome in patients with neuroblastoma. *N Engl J Med* **340**, 1954-1961 (1999).
64. K. Adam, J. Lesperance, T. Hunter, P. E. Zage, The Potential Functional Roles of NME1 Histidine Kinase Activity in Neuroblastoma Pathogenesis. *Int J Mol Sci* **21**, (2020).
65. Y. P. Mosse *et al.*, Identification of ALK as a major familial neuroblastoma predisposition gene. *Nature* **455**, 930-935 (2008).
66. B. H. Kushner, F. Gilbert, L. Helson, Familial neuroblastoma. Case reports, literature review, and etiologic considerations. *Cancer* **57**, 1887-1893 (1986).
67. Y. P. Mosse *et al.*, Germline PHOX2B mutation in hereditary neuroblastoma. *Am J Hum Genet* **75**, 727-730 (2004).
68. M. Capasso *et al.*, Common variations in BARD1 influence susceptibility to high-risk neuroblastoma. *Nat Genet* **41**, 718-723 (2009).
69. K. Wang *et al.*, Integrative genomics identifies LMO1 as a neuroblastoma oncogene. *Nature* **469**, 216-220 (2011).
70. K. R. Bosse, J. M. Maris, Advances in the translational genomics of neuroblastoma: From improving risk stratification and revealing novel biology to identifying actionable genomic alterations. *Cancer* **122**, 20-33 (2016).
71. N. R. Pinto *et al.*, Advances in Risk Classification and Treatment Strategies for Neuroblastoma. *J Clin Oncol* **33**, 3008-3017 (2015).
72. V. P. Tolbert, K. K. Matthay, Neuroblastoma: clinical and biological approach to risk stratification and treatment. *Cell Tissue Res* **372**, 195-209 (2018).
73. C. C. Swift, M. J. Eklund, J. M. Kraveka, A. L. Alazraki, Updates in Diagnosis, Management, and Treatment of Neuroblastoma. *Radiographics* **38**, 566-580 (2018).
74. B. H. Kushner *et al.*, Highly effective induction therapy for stage 4 neuroblastoma in children over 1 year of age. *J Clin Oncol* **12**, 2607-2613 (1994).
75. D. A. Haas-Kogan *et al.*, Impact of radiotherapy for high-risk neuroblastoma: a Children's Cancer Group study. *Int J Radiat Oncol Biol Phys* **56**, 28-39 (2003).
76. B. H. Kushner *et al.*, Striking dichotomy in outcome of MYCN-amplified neuroblastoma in the contemporary era. *Cancer* **120**, 2050-2059 (2014).
77. M. R. Abbasi *et al.*, Impact of Disseminated Neuroblastoma Cells on the Identification of the Relapse-Seeding Clone. *Clin Cancer Res* **23**, 4224-4232 (2017).
78. F. Rifatbegovic *et al.*, Neuroblastoma cells undergo transcriptomic alterations upon dissemination into the bone marrow and subsequent tumor progression. *Int J Cancer* **142**, 297-307 (2018).
79. J. R. Park *et al.*, Effect of Tandem Autologous Stem Cell Transplant vs Single Transplant on Event-Free Survival in Patients With High-Risk Neuroblastoma: A Randomized Clinical Trial. *JAMA* **322**, 746-755 (2019).
80. R. E. George *et al.*, High-risk neuroblastoma treated with tandem autologous peripheral-blood stem cell-supported transplantation: long-term survival update. *J Clin Oncol* **24**, 2891-2896 (2006).
81. B. H. Kushner *et al.*, Lack of survival advantage with autologous stem-cell transplantation in high-risk neuroblastoma consolidated by anti-GD2 immunotherapy and isotretinoin. *Oncotarget* **7**, 4155-4166 (2016).
82. J. Mora, Dinutuximab for the treatment of pediatric patients with high-risk neuroblastoma. *Expert Rev Clin Pharmacol* **9**, 647-653 (2016).
83. N. Sidell, Retinoic acid-induced growth inhibition and morphologic differentiation of human neuroblastoma cells in vitro. *J Natl Cancer Inst* **68**, 589-596 (1982).
84. G. Veal, S. Rowbotham, A. Boddy, Pharmacokinetics and pharmacogenetics of 13-cis-retinoic acid in the treatment of neuroblastoma. *Therapie* **62**, 91-93 (2007).
85. K. Dobrenkov, I. Ostrovnaya, J. Gu, I. Y. Cheung, N. K. Cheung, Oncotargets GD2 and GD3 are highly expressed in sarcomas of children, adolescents, and young adults. *Pediatr Blood Cancer* **63**, 1780-1785 (2016).

86. S. Sait, S. Modak, Anti-GD2 immunotherapy for neuroblastoma. *Expert Rev Anticancer Ther* **17**, 889-904 (2017).
87. D. H. Munn, N. K. Cheung, Phagocytosis of tumor cells by human monocytes cultured in recombinant macrophage colony-stimulating factor. *J Exp Med* **172**, 231-237 (1990).
88. R. K. Yang, P. M. Sondel, Anti-GD2 Strategy in the Treatment of Neuroblastoma. *Drugs Future* **35**, 665 (2010).
89. K. L. Osenga *et al.*, A phase I clinical trial of the hu14.18-IL2 (EMD 273063) as a treatment for children with refractory or recurrent neuroblastoma and melanoma: a study of the Children's Oncology Group. *Clin Cancer Res* **12**, 1750-1759 (2006).
90. K. R. Bosse *et al.*, Identification of GPC2 as an Oncoprotein and Candidate Immunotherapeutic Target in High-Risk Neuroblastoma. *Cancer Cell* **32**, 295-309 e212 (2017).
91. H. Du *et al.*, Antitumor Responses in the Absence of Toxicity in Solid Tumors by Targeting B7-H3 via Chimeric Antigen Receptor T Cells. *Cancer Cell* **35**, 221-237 e228 (2019).
92. R. Nguyen *et al.*, Interleukin-15 Enhances Anti-GD2 Antibody-Mediated Cytotoxicity in an Orthotopic PDX Model of Neuroblastoma. *Clin Cancer Res* **25**, 7554-7564 (2019).
93. B. Carlson, *Neural Crest*. (Elsevier, ed. 6th, 2018), pp. 496.
94. C. D. Rogers, C. S. Jayasena, S. Nie, M. E. Bronner, Neural crest specification: tissues, signals, and transcription factors. *Wiley Interdiscip Rev Dev Biol* **1**, 52-68 (2012).
95. D. Hockman *et al.*, A genome-wide assessment of the ancestral neural crest gene regulatory network. *Nat Commun* **10**, 4689 (2019).
96. A. Baggiolini *et al.*, Premigratory and migratory neural crest cells are multipotent in vivo. *Cell Stem Cell* **16**, 314-322 (2015).
97. J. L. Vaglia, B. K. Hall, Regulation of neural crest cell populations: occurrence, distribution and underlying mechanisms. *Int J Dev Biol* **43**, 95-110 (1999).
98. C. T. Gordon, C. Wade, I. Brinas, P. G. Farlie, CXCL14 expression during chick embryonic development. *Int J Dev Biol* **55**, 335-340 (2011).
99. R. K. Baker, P. B. Antin, Ephs and ephrins during early stages of chick embryogenesis. *Dev Dyn* **228**, 128-142 (2003).
100. Q. Schwarz, C. H. Maden, J. M. Vieira, C. Ruhrberg, Neuropilin 1 signaling guides neural crest cells to coordinate pathway choice with cell specification. *Proc Natl Acad Sci U S A* **106**, 6164-6169 (2009).
101. E. Rapizzi *et al.*, A unique neuroendocrine cell model derived from the human foetal neural crest. *J Endocrinol Invest* **43**, 1259-1269 (2020).
102. X. Huang, J. P. Saint-Jeannet, Induction of the neural crest and the opportunities of life on the edge. *Dev Biol* **275**, 1-11 (2004).
103. G. A. Vega-Lopez, S. Cerrizuela, M. J. Aybar, Trunk neural crest cells: formation, migration and beyond. *Int J Dev Biol* **61**, 5-15 (2017).
104. T. Ferronha *et al.*, LMO4 is an essential cofactor in the Snail2-mediated epithelial-to-mesenchymal transition of neuroblastoma and neural crest cells. *J Neurosci* **33**, 2773-2783 (2013).
105. B. Tanno *et al.*, Expression of Slug is regulated by c-Myb and is required for invasion and bone marrow homing of cancer cells of different origin. *J Biol Chem* **285**, 29434-29445 (2010).
106. J. A. Tomolonis, S. Agarwal, J. M. Shohet, Neuroblastoma pathogenesis: deregulation of embryonic neural crest development. *Cell Tissue Res* **372**, 245-262 (2018).
107. H. Rohrer, Transcriptional control of differentiation and neurogenesis in autonomic ganglia. *Eur J Neurosci* **34**, 1563-1573 (2011).
108. M. Simoes-Costa, M. E. Bronner, Establishing neural crest identity: a gene regulatory recipe. *Development* **142**, 242-257 (2015).
109. S. Tsubota, K. Kadomatsu, Origin and initiation mechanisms of neuroblastoma. *Cell Tissue Res* **372**, 211-221 (2018).
110. D. Hanahan, R. A. Weinberg, Hallmarks of cancer: the next generation. *Cell* **144**, 646-674 (2011).
111. S. Liu *et al.*, Cross-talk between Schwann cells and neuroblasts influences the biology of neuroblastoma xenografts. *Am J Pathol* **166**, 891-900 (2005).
112. J. Mora *et al.*, Neuroblastic and Schwannian stromal cells of neuroblastoma are derived from a tumoral progenitor cell. *Cancer Res* **61**, 6892-6898 (2001).
113. T. Vanichapol, S. Chutipongtanate, U. Anurathapan, S. Hongeng, Immune Escape Mechanisms and Future Prospects for Immunotherapy in Neuroblastoma. *Biomed Res Int* **2018**, 1812535 (2018).
114. L. Borriello, R. C. Seeger, S. Asgharzadeh, Y. A. DeClerck, More than the genes, the tumor microenvironment in neuroblastoma. *Cancer Lett* **380**, 304-314 (2016).
115. V. Pistoia *et al.*, Immunosuppressive microenvironment in neuroblastoma. *Front Oncol* **3**, 167 (2013).
116. R. Zeine *et al.*, Presence of cancer-associated fibroblasts inversely correlates with Schwannian stroma in neuroblastoma tumors. *Mod Pathol* **22**, 950-958 (2009).

117. C. F. Chantrain *et al.*, Stromal matrix metalloproteinase-9 regulates the vascular architecture in neuroblastoma by promoting pericyte recruitment. *Cancer Res* **64**, 1675-1686 (2004).
118. G. M. Brodeur *et al.*, Trk receptor expression and inhibition in neuroblastomas. *Clin Cancer Res* **15**, 3244-3250 (2009).
119. M. Hecht, J. H. Schulte, A. Eggert, J. Wilting, L. Schweigerer, The neurotrophin receptor TrkB cooperates with c-Met in enhancing neuroblastoma invasiveness. *Carcinogenesis* **26**, 2105-2115 (2005).
120. V. Pistoia, G. Bianchi, G. Borgonovo, L. Raffaghello, Cytokines in neuroblastoma: from pathogenesis to treatment. *Immunotherapy* **3**, 895-907 (2011).
121. J. H. HaDuong *et al.*, Interaction between bone marrow stromal cells and neuroblastoma cells leads to a VEGFA-mediated osteoblastogenesis. *Int J Cancer* **137**, 797-809 (2015).
122. S. Jodele *et al.*, The contribution of bone marrow-derived cells to the tumor vasculature in neuroblastoma is matrix metalloproteinase-9 dependent. *Cancer Res* **65**, 3200-3208 (2005).
123. F. Morandi *et al.*, CD4(+)CD25(hi)CD127(-) Treg and CD4(+)CD45R0(+)CD49b(+)LAG3(+) Tr1 cells in bone marrow and peripheral blood samples from children with neuroblastoma. *Oncoimmunology* **5**, e1249553 (2016).
124. J. Voeller *et al.*, Combined innate and adaptive immunotherapy overcomes resistance of immunologically cold syngeneic murine neuroblastoma to checkpoint inhibition. *J Immunother Cancer* **7**, 344 (2019).
125. T. Ara *et al.*, Interleukin-6 in the bone marrow microenvironment promotes the growth and survival of neuroblastoma cells. *Cancer Res* **69**, 329-337 (2009).
126. T. Ara *et al.*, Critical role of STAT3 in IL-6-mediated drug resistance in human neuroblastoma. *Cancer Res* **73**, 3852-3864 (2013).
127. L. Song *et al.*, Valpha24-invariant NKT cells mediate antitumor activity via killing of tumor-associated macrophages. *J Clin Invest* **119**, 1524-1536 (2009).
128. L. Song *et al.*, Oncogene MYCN regulates localization of NKT cells to the site of disease in neuroblastoma. *J Clin Invest* **117**, 2702-2712 (2007).
129. S. Asgharzadeh *et al.*, Clinical significance of tumor-associated inflammatory cells in metastatic neuroblastoma. *J Clin Oncol* **30**, 3525-3532 (2012).
130. F. Del Grosso *et al.*, Role of CXCL13-CXCR5 crosstalk between malignant neuroblastoma cells and Schwannian stromal cells in neuroblastic tumors. *Mol Cancer Res* **9**, 815-823 (2011).
131. M. Mina *et al.*, Tumor-infiltrating T lymphocytes improve clinical outcome of therapy-resistant neuroblastoma. *Oncoimmunology* **4**, e1019981 (2015).
132. R. Handgretinger *et al.*, Interferon-gamma upregulates the susceptibility of human neuroblastoma cells to interleukin-2-activated natural killer cells. *Nat Immun Cell Growth Regul* **8**, 189-196 (1989).
133. K. W. Pajtler *et al.*, Expression of NTRK1/TrkA affects immunogenicity of neuroblastoma cells. *Int J Cancer* **133**, 908-919 (2013).
134. A. Birbrair, P. S. Frenette, Niche heterogeneity in the bone marrow. *Ann N Y Acad Sci* **1370**, 82-96 (2016).
135. G. S. Travlos, Normal structure, function, and histology of the bone marrow. *Toxicol Pathol* **34**, 548-565 (2006).
136. K. Yamazaki, T. D. Allen, Ultrastructural morphometric study of efferent nerve terminals on murine bone marrow stromal cells, and the recognition of a novel anatomical unit: the "neuro-reticular complex". *Am J Anat* **187**, 261-276 (1990).
137. E. C. Watson, R. H. Adams, Biology of Bone: The Vasculature of the Skeletal System. *Cold Spring Harb Perspect Med* **8**, (2018).
138. C. Nombela-Arrieta *et al.*, Quantitative imaging of haematopoietic stem and progenitor cell localization and hypoxic status in the bone marrow microenvironment. *Nat Cell Biol* **15**, 533-543 (2013).
139. S. Pinho, P. S. Frenette, Haematopoietic stem cell activity and interactions with the niche. *Nat Rev Mol Cell Biol* **20**, 303-320 (2019).
140. S. J. Morrison, D. T. Scadden, The bone marrow niche for haematopoietic stem cells. *Nature* **505**, 327-334 (2014).
141. S. Mendez-Ferrer *et al.*, Mesenchymal and haematopoietic stem cells form a unique bone marrow niche. *Nature* **466**, 829-834 (2010).
142. P. S. Frenette, S. Pinho, D. Lucas, C. Scheiermann, Mesenchymal stem cell: keystone of the hematopoietic stem cell niche and a stepping-stone for regenerative medicine. *Annu Rev Immunol* **31**, 285-316 (2013).
143. T. Sugiyama, H. Kohara, M. Noda, T. Nagasawa, Maintenance of the hematopoietic stem cell pool by CXCL12-CXCR4 chemokine signaling in bone marrow stromal cell niches. *Immunity* **25**, 977-988 (2006).

144. B. Sacchetti *et al.*, Self-renewing osteoprogenitors in bone marrow sinusoids can organize a hematopoietic microenvironment. *Cell* **131**, 324-336 (2007).
145. Y. R. Zou, A. H. Kottmann, M. Kuroda, I. Taniuchi, D. R. Littman, Function of the chemokine receptor CXCR4 in haematopoiesis and in cerebellar development. *Nature* **393**, 595-599 (1998).
146. M. Ogawa *et al.*, Expression and function of c-kit in hemopoietic progenitor cells. *J Exp Med* **174**, 63-71 (1991).
147. L. Ding, T. L. Saunders, G. Enikolopov, S. J. Morrison, Endothelial and perivascular cells maintain haematopoietic stem cells. *Nature* **481**, 457-462 (2012).
148. A. Greenbaum *et al.*, CXCL12 in early mesenchymal progenitors is required for haematopoietic stem-cell maintenance. *Nature* **495**, 227-230 (2013).
149. F. Ugarte, E. C. Forsberg, Haematopoietic stem cell niches: new insights inspire new questions. *EMBO J* **32**, 2535-2547 (2013).
150. D. Nakada, B. P. Levi, S. J. Morrison, Integrating physiological regulation with stem cell and tissue homeostasis. *Neuron* **70**, 703-718 (2011).
151. S. Mendez-Ferrer, A. Chow, M. Merad, P. S. Frenette, Circadian rhythms influence hematopoietic stem cells. *Curr Opin Hematol* **16**, 235-242 (2009).
152. K. Dus-Szachniewicz *et al.*, Physiological Hypoxia (Physioxia) Impairs the Early Adhesion of Single Lymphoma Cell to Marrow Stromal Cell and Extracellular Matrix. Optical Tweezers Study. *Int J Mol Sci* **19**, (2018).
153. K. Parmar, P. Mauch, J. A. Vergilio, R. Sackstein, J. D. Down, Distribution of hematopoietic stem cells in the bone marrow according to regional hypoxia. *Proc Natl Acad Sci U S A* **104**, 5431-5436 (2007).
154. B. Keith, R. S. Johnson, M. C. Simon, HIF1alpha and HIF2alpha: sibling rivalry in hypoxic tumour growth and progression. *Nat Rev Cancer* **12**, 9-22 (2011).
155. P. A. van Zwieten, Adrenergic and muscarinergic receptors: classification, pathophysiological relevance and drug target. *J Hypertens Suppl* **9**, S18-27 (1991).
156. G. L. Semenza, Life with oxygen. *Science* **318**, 62-64 (2007).
157. J. L. Bonkowsky, J. H. Son, Hypoxia and connectivity in the developing vertebrate nervous system. *Dis Model Mech* **11**, (2018).
158. F. R. Sharp, M. Bernaudin, HIF1 and oxygen sensing in the brain. *Nat Rev Neurosci* **5**, 437-448 (2004).
159. S. G. DuBois *et al.*, Metastatic sites in stage IV and IVS neuroblastoma correlate with age, tumor biology, and survival. *J Pediatr Hematol Oncol* **21**, 181-189 (1999).
160. N. Gross, R. Meier, Chemokines in neuroectodermal cancers: the crucial growth signal from the soil. *Semin Cancer Biol* **19**, 103-110 (2009).
161. L. Raffaghello, C. Cocco, M. V. Corrias, I. Airoldi, V. Pistoia, Chemokines in neuroectodermal tumour progression and metastasis. *Semin Cancer Biol* **19**, 97-102 (2009).
162. I. Airoldi, C. Cocco, F. Morandi, I. Prigione, V. Pistoia, CXCR5 may be involved in the attraction of human metastatic neuroblastoma cells to the bone marrow. *Cancer Immunol Immunother* **57**, 541-548 (2008).
163. L. Goldberg-Bittman *et al.*, Cellular characteristics of neuroblastoma cells: regulation by the ELR--CXC chemokine CXCL10 and expression of a CXCR3-like receptor. *Cytokine* **29**, 105-117 (2005).
164. S. Escot *et al.*, Disruption of CXCR4 signaling in pharyngeal neural crest cells causes DiGeorge syndrome-like malformations. *Development* **143**, 582-588 (2016).
165. H. V. Russell, J. Hicks, M. F. Okcu, J. G. Nuchtern, CXCR4 expression in neuroblastoma primary tumors is associated with clinical presentation of bone and bone marrow metastases. *J Pediatr Surg* **39**, 1506-1511 (2004).
166. A. Muhlethaler-Mottet *et al.*, The CXCR4/CXCR7/CXCL12 Axis Is Involved in a Secondary but Complex Control of Neuroblastoma Metastatic Cell Homing. *PLoS One* **10**, e0125616 (2015).
167. M. Ma, J. Y. Ye, R. Deng, C. M. Dee, G. C. Chan, Mesenchymal stromal cells may enhance metastasis of neuroblastoma via SDF-1/CXCR4 and SDF-1/CXCR7 signaling. *Cancer Lett* **312**, 1-10 (2011).
168. I. Nevo *et al.*, The tumor microenvironment: CXCR4 is associated with distinct protein expression patterns in neuroblastoma cells. *Immunol Lett* **92**, 163-169 (2004).
169. A. J. Carlisle, C. A. Lyttle, R. Y. Carlisle, J. M. Maris, CXCR4 expression heterogeneity in neuroblastoma cells due to ligand-independent regulation. *Mol Cancer* **8**, 126 (2009).
170. J. Liberman *et al.*, Involvement of the CXCR7/CXCR4/CXCL12 axis in the malignant progression of human neuroblastoma. *PLoS One* **7**, e43665 (2012).
171. R. Meier *et al.*, The chemokine receptor CXCR4 strongly promotes neuroblastoma primary tumour and metastatic growth, but not invasion. *PLoS One* **2**, e1016 (2007).
172. R. S. Taichman *et al.*, Use of the stromal cell-derived factor-1/CXCR4 pathway in prostate cancer metastasis to bone. *Cancer Res* **62**, 1832-1837 (2002).

173. J. Shi *et al.*, CXCL12-CXCR4 contributes to the implication of bone marrow in cancer metastasis. *Future Oncol* **10**, 749-759 (2014).
174. H. Geminder *et al.*, A possible role for CXCR4 and its ligand, the CXC chemokine stromal cell-derived factor-1, in the development of bone marrow metastases in neuroblastoma. *J Immunol* **167**, 4747-4757 (2001).
175. I. Airoldi *et al.*, CXCL12 does not attract CXCR4+ human metastatic neuroblastoma cells: clinical implications. *Clin Cancer Res* **12**, 77-82 (2006).
176. J. M. Burns *et al.*, A novel chemokine receptor for SDF-1 and I-TAC involved in cell survival, cell adhesion, and tumor development. *J Exp Med* **203**, 2201-2213 (2006).
177. J. Bernhagen *et al.*, MIF is a noncognate ligand of CXC chemokine receptors in inflammatory and atherogenic cell recruitment. *Nat Med* **13**, 587-596 (2007).
178. S. Alampour-Rajabi *et al.*, MIF interacts with CXCR7 to promote receptor internalization, ERK1/2 and ZAP-70 signaling, and lymphocyte chemotaxis. *FASEB J* **29**, 4497-4511 (2015).
179. M. Tarnowski *et al.*, Macrophage migration inhibitory factor is secreted by rhabdomyosarcoma cells, modulates tumor metastasis by binding to CXCR4 and CXCR7 receptors and inhibits recruitment of cancer-associated fibroblasts. *Mol Cancer Res* **8**, 1328-1343 (2010).
180. X. Guo *et al.*, Macrophage migration inhibitory factor promotes vasculogenic mimicry formation induced by hypoxia via CXCR4/AKT/EMT pathway in human glioblastoma cells. *Oncotarget* **8**, 80358-80372 (2017).
181. H. N. Shin, H. H. Moon, J. L. Ku, Stromal cell-derived factor-1alpha and macrophage migration-inhibitory factor induce metastatic behavior in CXCR4-expressing colon cancer cells. *Int J Mol Med* **30**, 1537-1543 (2012).
182. A. F. Dessein *et al.*, Autocrine induction of invasive and metastatic phenotypes by the MIF-CXCR4 axis in drug-resistant human colon cancer cells. *Cancer Res* **70**, 4644-4654 (2010).
183. B. Jager *et al.*, CXCR4/MIF axis amplifies tumor growth and epithelial-mesenchymal interaction in non-small cell lung cancer. *Cell Signal* **73**, 109672 (2020).
184. S. Rafiei *et al.*, Targeting the MIF/CXCR7/AKT Signaling Pathway in Castration-Resistant Prostate Cancer. *Mol Cancer Res* **17**, 263-276 (2019).
185. Y. Sohara, H. Shimada, Y. A. DeClerck, Mechanisms of bone invasion and metastasis in human neuroblastoma. *Cancer Lett* **228**, 203-209 (2005).
186. T. Ara, Y. A. DeClerck, Mechanisms of invasion and metastasis in human neuroblastoma. *Cancer Metastasis Rev* **25**, 645-657 (2006).
187. M. R. Rutkowski *et al.*, Microbially driven TLR5-dependent signaling governs distal malignant progression through tumor-promoting inflammation. *Cancer Cell* **27**, 27-40 (2015).
188. L. Borriello *et al.*, Cancer-Associated Fibroblasts Share Characteristics and Protumorigenic Activity with Mesenchymal Stromal Cells. *Cancer Res* **77**, 5142-5157 (2017).
189. C. J. Thiele, Z. Li, A. E. McKee, On Trk--the TrkB signal transduction pathway is an increasingly important target in cancer biology. *Clin Cancer Res* **15**, 5962-5967 (2009).
190. J. W. Pollard, Tumour-educated macrophages promote tumour progression and metastasis. *Nat Rev Cancer* **4**, 71-78 (2004).
191. Y. Sohara *et al.*, Bone marrow mesenchymal stem cells provide an alternate pathway of osteoclast activation and bone destruction by cancer cells. *Cancer Res* **65**, 1129-1135 (2005).
192. D. Granchi *et al.*, In vitro blockade of receptor activator of nuclear factor-kappaB ligand prevents osteoclastogenesis induced by neuroblastoma cells. *Int J Cancer* **111**, 829-838 (2004).
193. T. Michigami, M. Ihara-Watanabe, M. Yamazaki, K. Ozono, Receptor activator of nuclear factor kappaB ligand (RANKL) is a key molecule of osteoclast formation for bone metastasis in a newly developed model of human neuroblastoma. *Cancer Res* **61**, 1637-1644 (2001).
194. S. S. Jankauskas, D. W. L. Wong, R. Bucala, S. Djudjaj, P. Boor, Evolving complexity of MIF signaling. *Cell Signal* **57**, 76-88 (2019).
195. M. Takahashi *et al.*, Macrophage migration inhibitory factor as a redox-sensitive cytokine in cardiac myocytes. *Cardiovasc Res* **52**, 438-445 (2001).
196. W. G. Cao *et al.*, Tumour necrosis factor-alpha up-regulates macrophage migration inhibitory factor expression in endometrial stromal cells via the nuclear transcription factor NF-kappaB. *Hum Reprod* **21**, 421-428 (2006).
197. J. Bernhagen *et al.*, MIF is a pituitary-derived cytokine that potentiates lethal endotoxaemia. *Nature* **365**, 756-759 (1993).
198. R. Eickhoff *et al.*, Purification and characterization of macrophage migration inhibitory factor as a secretory protein from rat epididymis: evidences for alternative release and transfer to spermatozoa. *Mol Med* **7**, 27-35 (2001).

199. O. Flieger *et al.*, Regulated secretion of macrophage migration inhibitory factor is mediated by a non-classical pathway involving an ABC transporter. *FEBS Lett* **551**, 78-86 (2003).
200. L. Chen *et al.*, Induction of MIF expression by oxidized LDL via activation of NF-kappaB in vascular smooth muscle cells. *Atherosclerosis* **207**, 428-433 (2009).
201. T. Calandra, T. Roger, Macrophage migration inhibitory factor: a regulator of innate immunity. *Nat Rev Immunol* **3**, 791-800 (2003).
202. N. Dickerhof, L. Schindler, J. Bernhagen, A. J. Kettle, M. B. Hampton, Macrophage migration inhibitory factor (MIF) is rendered enzymatically inactive by myeloperoxidase-derived oxidants but retains its immunomodulatory function. *Free Radic Biol Med* **89**, 498-511 (2015).
203. J. A. Baugh *et al.*, Dual regulation of macrophage migration inhibitory factor (MIF) expression in hypoxia by CREB and HIF-1. *Biochem Biophys Res Commun* **347**, 895-903 (2006).
204. A. Sparkes *et al.*, The non-mammalian MIF superfamily. *Immunobiology* **222**, 473-482 (2017).
205. L. Schindler, N. Dickerhof, M. B. Hampton, J. Bernhagen, Post-translational regulation of macrophage migration inhibitory factor: Basis for functional fine-tuning. *Redox Biol* **15**, 135-142 (2018).
206. J. Bloom, S. Sun, Y. Al-Abed, MIF, a controversial cytokine: a review of structural features, challenges, and opportunities for drug development. *Expert Opin Ther Targets* **20**, 1463-1475 (2016).
207. G. Benedek *et al.*, MIF and D-DT are potential disease severity modifiers in male MS subjects. *Proc Natl Acad Sci U S A* **114**, E8421-E8429 (2017).
208. J. Harris, S. VanPatten, N. S. Deen, Y. Al-Abed, E. F. Morand, Rediscovering MIF: New Tricks for an Old Cytokine. *Trends Immunol* **40**, 447-462 (2019).
209. C. C. Nobre *et al.*, Macrophage Migration Inhibitory Factor (MIF): Biological Activities and Relation with Cancer. *Pathol Oncol Res* **23**, 235-244 (2017).
210. L. Leng *et al.*, MIF signal transduction initiated by binding to CD74. *J Exp Med* **197**, 1467-1476 (2003).
211. X. Shi *et al.*, CD44 is the signaling component of the macrophage migration inhibitory factor-CD74 receptor complex. *Immunity* **25**, 595-606 (2006).
212. F. Momburg *et al.*, Differential expression of Ia and Ia-associated invariant chain in mouse tissues after in vivo treatment with IFN-gamma. *J Immunol* **136**, 940-948 (1986).
213. H. Sternberg *et al.*, Human embryonic stem cell-derived neural crest cells capable of expressing markers of osteochondral or meningeal-choroid plexus differentiation. *Regen Med* **9**, 53-66 (2014).
214. Y. Gore *et al.*, Macrophage migration inhibitory factor induces B cell survival by activation of a CD74-CD44 receptor complex. *J Biol Chem* **283**, 2784-2792 (2008).
215. P. C. Spinosa *et al.*, Short-term cellular memory tunes the signaling responses of the chemokine receptor CXCR4. *Sci Signal* **12**, (2019).
216. V. Schwartz *et al.*, A functional heteromeric MIF receptor formed by CD74 and CXCR4. *FEBS Lett* **583**, 2749-2757 (2009).
217. H. Lue, M. Dewor, L. Leng, R. Bucala, J. Bernhagen, Activation of the JNK signalling pathway by macrophage migration inhibitory factor (MIF) and dependence on CXCR4 and CD74. *Cell Signal* **23**, 135-144 (2011).
218. E. P. van der Vorst, Y. Doring, C. Weber, Chemokines and their receptors in Atherosclerosis. *J Mol Med (Berl)* **93**, 963-971 (2015).
219. T. Kok *et al.*, Small-molecule inhibitors of macrophage migration inhibitory factor (MIF) as an emerging class of therapeutics for immune disorders. *Drug Discov Today* **23**, 1910-1918 (2018).
220. E. Cavalli *et al.*, Emerging Role of the Macrophage Migration Inhibitory Factor Family of Cytokines in Neuroblastoma. Pathogenic Effectors and Novel Therapeutic Targets? *Molecules* **25**, (2020).
221. V. Richard, N. Kindt, S. Saussez, Macrophage migration inhibitory factor involvement in breast cancer (Review). *Int J Oncol* **47**, 1627-1633 (2015).
222. W. M. Tang, X. Gou, Q. X. Liu, [Expression of macrophage migration inhibition factor (MIF) in serum of patients with prostate cancer and its clinical significance]. *Xi Bao Yu Fen Zi Mian Yi Xue Za Zhi* **27**, 97-98 (2011).
223. E. S. White *et al.*, Macrophage migration inhibitory factor and CXC chemokine expression in non-small cell lung cancer: role in angiogenesis and prognosis. *Clin Cancer Res* **9**, 853-860 (2003).
224. C. Wang *et al.*, Macrophage migration inhibitory factor promotes osteosarcoma growth and lung metastasis through activating the RAS/MAPK pathway. *Cancer Lett* **403**, 271-279 (2017).
225. Y. Ren *et al.*, Inhibition of tumor growth and metastasis in vitro and in vivo by targeting macrophage migration inhibitory factor in human neuroblastoma. *Oncogene* **25**, 3501-3508 (2006).
226. Q. Bin, B. D. Johnson, D. W. Schauer, J. T. Casper, R. J. Orentas, Production of macrophage migration inhibitory factor by human and murine neuroblastoma. *Tumour Biol* **23**, 123-129 (2002).
227. Y. Ren *et al.*, Upregulation of macrophage migration inhibitory factor contributes to induced N-Myc expression by the activation of ERK signaling pathway and increased expression of interleukin-8 and VEGF in neuroblastoma. *Oncogene* **23**, 4146-4154 (2004).

228. E. Cavalli *et al.*, Overexpression of Macrophage Migration Inhibitory Factor and Its Homologue D-Dopachrome Tautomerase as Negative Prognostic Factor in Neuroblastoma. *Brain Sci* **9**, (2019).
229. S. H. Bae *et al.*, Brain-derived neurotrophic factor mediates macrophage migration inhibitory factor to protect neurons against oxygen-glucose deprivation. *Neural Regen Res* **15**, 1483-1489 (2020).
230. C. J. Liang *et al.*, Suppression of MIF-induced neuronal apoptosis may underlie the therapeutic effects of effective components of Fufang Danshen in the treatment of Alzheimer's disease. *Acta Pharmacol Sin* **39**, 1421-1438 (2018).
231. J. Fan, Y. Chen, H. M. Chan, P. K. Tam, Y. Ren, Removing intensity effects and identifying significant genes for Affymetrix arrays in macrophage migration inhibitory factor-suppressed neuroblastoma cells. *Proc Natl Acad Sci U S A* **102**, 17751-17756 (2005).
232. G. Liu, Z. Xu, D. Hao, MicroRNA451 inhibits neuroblastoma proliferation, invasion and migration by targeting macrophage migration inhibitory factor. *Mol Med Rep* **13**, 2253-2260 (2016).
233. X. Yan, R. J. Orentas, B. D. Johnson, Tumor-derived macrophage migration inhibitory factor (MIF) inhibits T lymphocyte activation. *Cytokine* **33**, 188-198 (2006).
234. Q. Zhou, X. Yan, J. Gershan, R. J. Orentas, B. D. Johnson, Expression of macrophage migration inhibitory factor by neuroblastoma leads to the inhibition of antitumor T cell reactivity in vivo. *J Immunol* **181**, 1877-1886 (2008).
235. V. Trivedi-Parmar, W. L. Jorgensen, Advances and Insights for Small Molecule Inhibition of Macrophage Migration Inhibitory Factor. *J Med Chem* **61**, 8104-8119 (2018).
236. R. Bertini *et al.*, Effects of chlorpromazine on PMN-mediated activities in vivo and in vitro. *Immunology* **72**, 138-143 (1991).
237. Y. Al-Abed, S. VanPatten, MIF as a disease target: ISO-1 as a proof-of-concept therapeutic. *Future Med Chem* **3**, 45-63 (2011).
238. Y. Song, Y. Sun, Y. Lei, K. Yang, R. Tang, YAP1 promotes multidrug resistance of small cell lung cancer by CD74-related signaling pathways. *Cancer Med* **9**, 259-268 (2020).
239. S. M. Johler, J. Fuchs, G. Seitz, S. Armeanu-Ebinger, Macrophage migration inhibitory factor (MIF) is induced by cytotoxic drugs and is involved in immune escape and migration in childhood rhabdomyosarcoma. *Cancer Immunol Immunother* **65**, 1465-1476 (2016).
240. M. Bacher *et al.*, The role of macrophage migration inhibitory factor in Alzheimer's disease. *Mol Med* **16**, 116-121 (2010).
241. M. Winner *et al.*, A novel, macrophage migration inhibitory factor suicide substrate inhibits motility and growth of lung cancer cells. *Cancer Res* **68**, 7253-7257 (2008).
242. L. Varinelli *et al.*, 4-IPP, a selective MIF inhibitor, causes mitotic catastrophe in thyroid carcinomas. *Endocr Relat Cancer* **22**, 759-775 (2015).
243. N. Kindt *et al.*, Pharmacological inhibition of macrophage migration inhibitory factor interferes with the proliferation and invasiveness of squamous carcinoma cells. *Int J Oncol* **43**, 185-193 (2013).
244. D. Joseph, J. P. Gonsky, S. W. Blain, Macrophage Inhibitory Factor-1 (MIF-1) controls the plasticity of multiple myeloma tumor cells. *PLoS One* **13**, e0206368 (2018).
245. Q. Wang *et al.*, MIF as a biomarker and therapeutic target for overcoming resistance to proteasome inhibitors in human myeloma. *Blood*, (2020).
246. Y. Cho *et al.*, Allosteric inhibition of macrophage migration inhibitory factor revealed by ibudilast. *Proc Natl Acad Sci U S A* **107**, 11313-11318 (2010).
247. J. Schwenkgrub *et al.*, The phosphodiesterase inhibitor, ibudilast, attenuates neuroinflammation in the MPTP model of Parkinson's disease. *PLoS One* **12**, e0182019 (2017).
248. W. Ha *et al.*, Ibudilast sensitizes glioblastoma to temozolomide by targeting Macrophage Migration Inhibitory Factor (MIF). *Sci Rep* **9**, 2905 (2019).
249. E. De Clercq, Mozobil(R) (Plerixafor, AMD3100), 10 years after its approval by the US Food and Drug Administration. *Antivir Chem Chemother* **27**, 2040206619829382 (2019).
250. S. Modak *et al.*, Plerixafor plus granulocyte-colony stimulating factor for autologous hematopoietic stem cell mobilization in patients with metastatic neuroblastoma. *Pediatr Blood Cancer* **58**, 469-471 (2012).
251. C. J. Thiele, Neuroblastoma Cell Lines. *Human Cell Culture* **1**, 32 (1998).
252. S. Gomez *et al.*, DNA methylation fingerprint of neuroblastoma reveals new biological and clinical insights. *Epigenomics* **7**, 1137-1153 (2015).
253. Z. Su *et al.*, An investigation of biomarkers derived from legacy microarray data for their utility in the RNA-seq era. *Genome Biol* **15**, 523 (2014).
254. M. Cardoso-Moreira *et al.*, Gene expression across mammalian organ development. *Nature* **571**, 505-509 (2019).
255. M. W. Alam *et al.*, HIF2alpha contributes to antiestrogen resistance via positive bilateral crosstalk with EGFR in breast cancer cells. *Oncotarget* **7**, 11238-11250 (2016).

256. M. Armoni *et al.*, PAX3/forkhead homolog in rhabdomyosarcoma oncoprotein activates glucose transporter 4 gene expression in vivo and in vitro. *J Clin Endocrinol Metab* **87**, 5312-5324 (2002).
257. M. M. Tomayko, C. P. Reynolds, Determination of subcutaneous tumor size in athymic (nude) mice. *Cancer Chemother Pharmacol* **24**, 148-154 (1989).
258. A. Mohyeldin, T. Garzon-Muvdi, A. Quinones-Hinojosa, Oxygen in stem cell biology: a critical component of the stem cell niche. *Cell Stem Cell* **7**, 150-161 (2010).
259. L. M. Lopez-Sanchez *et al.*, CoCl2, a mimic of hypoxia, induces formation of polyploid giant cells with stem characteristics in colon cancer. *PLoS One* **9**, e99143 (2014).
260. Y. Komada *et al.*, Flow cytometric analysis of peripheral blood and bone marrow for tumor cells in patients with neuroblastoma. *Cancer* **82**, 591-599 (1998).
261. O. Q. J. Contal C, An application of changepoint methods in studying the effect of age on survival in breast cancer.

Computational Statistics & Data Analysis **30**, 7 (1999).
262. H. V. Russell, L. A. Golding, M. N. Suell, J. G. Nuchtern, D. R. Strother, The role of bone marrow evaluation in the staging of patients with otherwise localized, low-risk neuroblastoma. *Pediatr Blood Cancer* **45**, 916-919 (2005).
263. P. Kaczowka *et al.*, The role of N-Myc gene amplification in neuroblastoma childhood tumour - single-centre experience. *Contemp Oncol (Pozn)* **22**, 223-228 (2018).
264. M. Huang, W. A. Weiss, Neuroblastoma and MYCN. *Cold Spring Harb Perspect Med* **3**, a014415 (2013).
265. J. A. Spencer *et al.*, Direct measurement of local oxygen concentration in the bone marrow of live animals. *Nature* **508**, 269-273 (2014).
266. V. Shankar *et al.*, Mesenchymal stromal cell secretome up-regulates 47 kDa CXCR4 expression, and induce invasiveness in neuroblastoma cell lines. *PLoS One* **10**, e0120069 (2015).
267. P. Berning *et al.*, The CXCR4 antagonist plerixafor (AMD3100) promotes proliferation of Ewing sarcoma cell lines in vitro and activates receptor tyrosine kinase signaling. *Cell Commun Signal* **16**, 21 (2018).
268. J. C. Penticuff, B. L. Woolbright, T. M. Sielecki, S. J. Weir, J. A. Taylor, 3rd, MIF family proteins in genitourinary cancer: tumorigenic roles and therapeutic potential. *Nat Rev Urol* **16**, 318-328 (2019).
269. L. Soumoy, N. Kindt, G. Ghanem, S. Saussez, F. Journe, Role of Macrophage Migration Inhibitory Factor (MIF) in Melanoma. *Cancers (Basel)* **11**, (2019).
270. Y. Zheng *et al.*, Role of Myeloma-Derived MIF in Myeloma Cell Adhesion to Bone Marrow and Chemotherapy Response. *J Natl Cancer Inst* **108**, (2016).
271. A. Gutierrez-Gonzalez *et al.*, Evaluation of the potential therapeutic benefits of macrophage reprogramming in multiple myeloma. *Blood* **128**, 2241-2252 (2016).
272. J. A. Chesney, R. A. Mitchell, K. Yaddanapudi, Myeloid-derived suppressor cells-a new therapeutic target to overcome resistance to cancer immunotherapy. *J Leukoc Biol* **102**, 727-740 (2017).
273. B. Das *et al.*, Hypoxia enhances tumor stemness by increasing the invasive and tumorigenic side population fraction. *Stem Cells* **26**, 1818-1830 (2008).
274. M. T. Rojewski, B. M. Weber, H. Schrezenmeier, Phenotypic Characterization of Mesenchymal Stem Cells from Various Tissues. *Transfus Med Hemother* **35**, 168-184 (2008).
275. Y. Sugiura *et al.*, The plasminogen-plasminogen activator (PA) system in neuroblastoma: role of PA inhibitor-1 in metastasis. *Cancer Res* **59**, 1327-1336 (1999).
276. G. Qing *et al.*, Combinatorial regulation of neuroblastoma tumor progression by N-Myc and hypoxia inducible factor HIF-1alpha. *Cancer Res* **70**, 10351-10361 (2010).
277. L. Zhang, H. Yeger, B. Das, M. S. Irwin, S. Baruchel, Tissue microenvironment modulates CXCR4 expression and tumor metastasis in neuroblastoma. *Neoplasia* **9**, 36-46 (2007).
278. T. Schioppa *et al.*, Regulation of the chemokine receptor CXCR4 by hypoxia. *J Exp Med* **198**, 1391-1402 (2003).
279. J. M. Speth, J. Hoggatt, P. Singh, L. M. Pelus, Pharmacologic increase in HIF1alpha enhances hematopoietic stem and progenitor homing and engraftment. *Blood* **123**, 203-207 (2014).
280. C. E. Forristal *et al.*, HIF-1alpha is required for hematopoietic stem cell mobilization and 4-prolyl hydroxylase inhibitors enhance mobilization by stabilizing HIF-1alpha. *Leukemia* **29**, 1366-1378 (2015).
281. B. Schroder, The multifaceted roles of the invariant chain CD74--More than just a chaperone. *Biochim Biophys Acta* **1863**, 1269-1281 (2016).
282. J. Fan, P. Tam, G. Vande Woude, Y. Ren, Normalization and analysis of cDNA microarrays using within-array replications applied to neuroblastoma cell response to a cytokine. *Proc Natl Acad Sci U S A* **101**, 1135-1140 (2004).

283. V. M. Lee *et al.*, Molecular Events Controlling Cessation of Trunk Neural Crest Migration and Onset of Differentiation. *Front Cell Dev Biol* **8**, 199 (2020).
284. J. I. Johnsen, C. Dyberg, M. Wickstrom, Neuroblastoma-A Neural Crest Derived Embryonal Malignancy. *Front Mol Neurosci* **12**, 9 (2019).
285. J. M. Eby *et al.*, Functional and structural consequences of chemokine (C-X-C motif) receptor 4 activation with cognate and non-cognate agonists. *Mol Cell Biochem* **434**, 143-151 (2017).
286. T. Subbannayya *et al.*, Macrophage migration inhibitory factor - a therapeutic target in gallbladder cancer. *BMC Cancer* **15**, 843 (2015).
287. K. Yaddanapudi *et al.*, Control of tumor-associated macrophage alternative activation by macrophage migration inhibitory factor. *J Immunol* **190**, 2984-2993 (2013).
288. S. Dhillon, Dinutuximab: first global approval. *Drugs* **75**, 923-927 (2015).
289. F. Nakahara *et al.*, Engineering a haematopoietic stem cell niche by revitalizing mesenchymal stromal cells. *Nat Cell Biol* **21**, 560-567 (2019).
290. R. Nakata *et al.*, Contribution of neuroblastoma-derived exosomes to the production of pro-tumorigenic signals by bone marrow mesenchymal stromal cells. *J Extracell Vesicles* **6**, 1332941 (2017).
291. M. Colletti *et al.*, Neuroblastoma-secreted exosomes carrying miR-375 promote osteogenic differentiation of bone-marrow mesenchymal stromal cells. *J Extracell Vesicles* **9**, 1774144 (2020).
292. F. Morandi, D. Marimpietri, A. L. Horenstein, M. V. Corrias, F. Malavasi, Microvesicles expressing adenosinergic ectoenzymes and their potential role in modulating bone marrow infiltration by neuroblastoma cells. *Oncoimmunology* **8**, e1574198 (2019).